AD-A269 400

⑷

Final Report

Characterization of Diamond Film Nucleation and Growth Surface

DTIC
S ELECTE
SEP 17 1993
A **D**

Robert J. Nemanich

Department of Physics, Box 8202,

North Carolina State University,

Raleigh, NC 27695-8202

Phone Number: (919) 515-3225

FAX (919) 515-7331

E-Mail Address: Nemanich@pyvax.ncsu.edu

93-21608

93 9 16 084

14988

REPORT DOCUMENTATION PAGE

1. AGENCY USE ONLY *(Leave blank)*	2. REPORT DATE	3. REPORT TYPE AND DATES COVERED
	September 1993	Final Report 4/90-8/91

4. TITLE AND SUBTITLE
Characterization of Diamond Film Nucleation and Growth Surface

5. FUNDING NUMBERS
4145296--01
1114SS
N00179
N66005
43855

6. AUTHOR(S)
Robert J. Nemanich

7. PERFORMING ORGANIZATION NAME(S) AND ADDRESS(ES)
North Carolina State University
Department of Physics
Raleigh, NC 27695-8202

8. PERFORMING ORGANIZATION REPORT NUMBER
N00014-90-J-1707

9. SPONSORING/MONITORING AGENCY NAMES(S) AND ADDRESS(ES)
Sponsoring: ONR, 800 N. Quincy, Arlington, VA 22217-5000
Monitoring: Office of Naval Research Resider
The Ohio State University Research Center
1960 Kenny Road
Columbus, OH 43210-1063

10. SPONSORING/MONITORING AGENCY REPORT NUMBER

11. SUPPLEMENTARY NOTES

12a. DISTRIBUTION/AVAILABILITY STATEMENT

Approved for Public Release; Distribution Unlimited

12b. DISTRIBUTION CODE

13. ABSTRACT *(Maximum 200 words)*

The project has involved advanced studies of diamond nucleation and the diamond growth surface utilizing scanning tunneling microscopy. For diamond growth on Si substrates, diamond nucleation was observed at scratches on the surface. These results were the first reports of nuclei with dimensions less than 100 Å. While nucleation was apparently random many nuclei exhibited growth surfaces which paralleled the substrate. Nuclei which exhibited a nearly hemispherical structure were considered to exhibit 3-dimensional type growth. It was found that both flat or 2 dimensional and three dimensional nucleation were observed on the same sample. Scanning tunneling spectroscopy was applied to the nuclei. It was found that the nuclei exhibited characteristics similar to that expected for diamond. In contrast, the substrate showed electronic structure similar to graphite, thus indicating that graphitic layers form on the surface prior to nucleation. The interface of a continuous film was examined by etch removal of the Si, and electronic features characteristic of SiC were observed. A detailed analysis of the STS from diamond surfaces indicated Fowler-Nordheim tunneling. The effect indicated that the valence band minimum was essentially coincident with the vacuum level. The results are consistent with a negative electron affinity for diamond.

14. SUBJECT TERMS
diamond surface, diamond nucleation, scanning tunneling microscopy

15. NUMBER OF PAGES

16. PRICE CODE

17. SECURITY CLASSIFICATION OF REPORT	18. SECURITY CLASSIFICATION OF THIS PAGE	19. SECURITY CLASSIFICATION OF ABSTRACT	20. LIMITATION OF ABSTRACT
UNCLAS	UNCLAS	UNCLAS	SAR

I Introduction

This report describes the results of ONR grant N00014-90-J-1707 on "Characterization of Diamond Film Nucleation and Growth Surface." The report includes a list of publications and presentations which documented the research results. The details of the research are described in section III. This section is essentially the Ph.D. thesis of Kevin F. Turner.

The project involved the application of scanning tunneling microscopy (STM) and scanning tunneling spectroscopy (STS) to examine the nucleation of diamond on Si and to explore the growth surface of diamond films. The application of the two complimentary techniques allowed correlation of surface morphology (obtained from STM) with surface electronic states obtained with STS. These results in many instances represent the first application to diamond films.

DTIC QUALITY INSPECTED 4

Accesion For		
NTIS CRA&I	N	
DTIC TAB	☐	
U a o: ced	☐	
Justification		
By		
Distribution /		
Availability Codes		
Dist	Avai : a.o 'or Special	
A-1		

II. Publications

Papers Published in Refereed Journals:

Y.H. Lee, K.J. Bachmann, J.T. Glass, Y.M. LeGrice, and R.J. Nemanich. "Vapor deposition of diamond thin films on various substrates," Appl. Phys. Lett. 57, 1916-1918 (1990).

R. J. Nemanich, L. Bergman, Y. M. LeGrice, K. F. Turner, and T. P. Humphreys. "Microstructures and Domain Size Effects in Diamond Films Characterized by Raman Spectroscopy," SPIE Symp. Proc. Vol. 1437:2, (1991).

T.P. Humphreys, R.J. Nemanich, J.B. Posthill, R.A. Rudder, D.P. Malta, R.J Markunas and N.R. Parikh, "High Temperature Rectifying Contacts Using Heteroepitaxial Ni Films on Semiconducting Diamond", Jap. J. Appl. Phys. 30, L1409-L1411, (1991).

J.B. Posthill, R.A. Rudder, S.V. Hattangady, G.G. Fountain, T.P. Humphreys, R.J. Nemanich, N.R. Parikh, and R.J. Markunas, "Heteroepitaxial $C_x Si_{1-x}/Si$ (100) Metastable Alloys," Mat. Res. Soc. Symp. Proc., Vol. **198**, 497-502 (1991).

K.F. Turner, Y.M. LeGrice, B.R. Stoner, J.T. Glass, and R.J. Nemanich, "Surface Topography and Nucleation of CVD Diamond Films on Silicon by Scanning Tunneling Microscopy," J. Vac. Sci. Technol. B9, 914-919 (1991).

K.F. Turner, B.R. Stoner, L. Bergman, J.T. Glass, and R.J. Nemanich, "Nucleation and Growth Between Domains of Diamond Films on Silicon Scanning Tunneling Microscopy," Proceedings of the Second International Conference on the New Diamond Science and Technology, published by Materials Research Society, 607-612 (1991).

R.A. Rudder, J.B. Posthill, G.C. Hudson, D. Malta, R.E. Thomas, R.J. Markunas, T.P. Humphreys, and R.J. Nemanich. "Selected-Area Homoepitaxial Growth and Overgrowth on Si Patterned Diamond Substrates," Proceedings of the Second International Conference on the New Diamond Science and Technology, published by Materials Research Society, 425 (1991).

R.J. Nemanich, L. Bergman, Y.M. LeGrice, and R.E. Shroder, "Raman Characterization of Diamond Film Growth," Proceedings of the Second International Conference on the New Diamond Science and Technology, published by Materials Research Society, 741 (1991).

K.F. Turner, B.R. Stoner, L. Bergman, J.T. Glass, and R.J. Nemanich, "Observation of surface modification and nucleation during deposition of diamond on silicon by scanning tunneling microscopy," Journal of Applied Physics, 69:6400-6405 (1991).

R.A. Rudder, G.C. Hudson, J.B. Posthill, R.E. Thomas, R.J. Markunas, R.J. Nemanich, Y.M. LeGrice, and T.P. Humphreys, "Acetylene Production in a Diamond-Producing Low Pressure rf-Plasma Assisted Chemical Vapor Deposition Environment," Electrochemical Society, Vol. 91-8, p. 209 (1991).

J.B. Posthill, R.A. Rudder, G.C. Hudson, D.P. Malta, R.E. Thomas, R.J. Markunas, T.P. Humphreys, R.J. Nemanich, and D. Black, "Substrate Effects and the Growth of Homoepitaxial Diamond (100) Layers Using Low Pressure rf Plasma-Enhanced Chemical Vapor Deposition," Electrochemical Society, Vol. 91-8, p. 274 (1991).

T. P. Humphreys, H. Jeon, J. V. LaBrasca, K. F. Turner, R. J. Nemanich, K. Das, and J. B. Posthill, "Characterization of Titanium Silicide Contacts Deposited on Semiconducting Diamond Substrates," Applications of Diamond Films and Related Materials, edited by Y. Tzeng, M. Yoshikawa, M. Murakawa, and A. Feldman, 73:353-358 (1991).

J. VanderWeide and R.J. Nemanich. "Interface Reactions of Titanium on Single Crystal and Thin Film Diamond Analyzed by Ultraviolet Photoemission Spectroscopy," Applications of Diamond Films and Related Materials, edited by Y. Tzeng, M. Yoshikawa, M. Murakawa, and A. Feldman, 73:359-364 (1991).

T. P. Humphreys, J. V. LaBrasca, R. J. Nemanich, K. Das, and J. B. Posthill, "Titanium Silicide Contacts on Semiconducting Diamond Substrates," Electronic Letters 27:1515-1516 (1991).

R. A. Rudder, G. C. Hudson, J. B. Posthill, R. E. Thomas, M. J. Mantini, D. Malta, R. J. Markunas, T. P. Humphreys, and R. J. Nemanich. "Chemical Vapor Deposition of Diamond Films from Water Vapor RF-Plasma Discharges," Appl. Phys. Lett., 60(3), 329-331 (1992).

T. P. Humphreys, J. V. LaBrasca, K. F. Turner, R. J. Nemanich, K. Das, J. B. Posthill, J.D. Hunn and N.R. Parikh, "Growth and Characterization of Titanium Silicide Films on Natural Diamond (001) Substrates," J. Appl. Phys. Vol. 31, pp. 2369-2373 (Part 1) (1992).

Books or Chapters Published

"Growth and Characterization of Diamond Thin Films," Annual Rev. Mat. Sci. 21, 535 (1991). R. J. Nemanich.

"Surface Characterization," Analytical Chemistry Application Reviews 63, 99R (1991). M.A. Ray. G.E. McGuire, I.H. Musselman, R.J. Nemanich, and D.R. Chopra.

Invited Presentations at Workshops or Prof. Society Meetings:

R. Nemanich and J.T. Glass, *Characterization of Diamond Thin Films* Mat. Res. Soc. Short Course, presented at the Spring '91 meeting of the Mat. Res. Soc., Anaheim, California.

R.J. Nemanich, L. Bergman, Y.M. LeGrice, K.F. Turner and T.P. Humphreys, "Microstructures and Domain Size Effects in Diamond Films Characterized by Raman Spectroscopy," presented at the SPIE Symposium on Applied Spectroscopy in Materials Science. January 20-January 25, 1991, Los Angeles, California.

Presentations at Workshops or Prof. Society Meetings:

T.P. Humphreys, R.J. Nemanich, J.B. Posthill, R.A. Rudder, R.J. Markunas, N.R. Parikh, "Growth and Characterization of Heteroepitaxial Nickel Films on Diamond Substrates," presented at the Fall 90 meeting of the Mat. Res. Soc., 11/26/91, Boston, MA.

C. Wang, G. Lucovsky, and R.J. Nemanich, "Deposition of Amorphous and Microcrystalline Si,C Alloy Thin Films by Remote Plasma-Enhanced Chemical-Vapor Deposition Process," presented at the Materials Research Society Symposium. April 29-May 3, 1991. Anaheim, California.

L.M. Spellman R.C. Glass, R.F. Davis, T.P. Humphreys, H. Jeon, R.J. Nemanich, S. Chevacharoenkul, and N.R. Parikh, "Heteroepitaxial Growth and Characterization of Titanium Films on Alpha (6H)Silicon Carbide," presented at the Materials Research Society Symposium. April 29-May 3, 1991, Anaheim, California.

J.B. Posthill, R A. Rudder, G.C. Hudson, D.P. Malta, R.E. Thomas, R.J. Markunas, T.P. Humphreys, R.J. Nemanich, and D. Black, "Substrate Effects and the Growth of Homoepitaxial Diamond (100) Lay Using Low Pressure rf Plasma-Enhanced Chemical Vapor Deposition," presented at the Electrochemical Society Meeting. May 26-31, 1991, Washington, DC.

K.F. Turner, B.R. Stoner, L. Bergman, J.T. Glass, and R.J. Nemanich, "Scanning Tunneling Microscopy/Spectroscopy Investigation of the Nucleation of Diamond," presented at 6th International STM Conference. August 12-16. 1991, Interlaken. Switzerland.

J.V. LaBrasca, K.F. Turner, T.P. Humphreys, and R.J. Nemanich, "Scanning Tunneling Microscopy and Spectroscopy of Metal and Metal-Silicide Contacts to Natural Semiconducting Diamond," presented at 6th International STM Conference. August 12-16, 1991, Interlaken, Switzerland.

J. VanderWeide and R.J. Nemanich, "Interface Reactions of Titanium on Single Crystal and Thin Film Diamond Analyzed by Ultraviolet Photoemission Spectroscopy," presented at the Applied Diamond Conference. August 20-21, 1991, Auburn, Alabama.

T. P. Humphreys, H. Jeon, J. V. LaBrasca, K. F. Turner, R. J. Nemanich, K. Das, and J. B. Posthill, "Characterization of Titanium Silicide Contacts Deposited on Semiconducting Diamond Substrates," presented at the Applied Diamond Conference. August 20-21, 1991, Auburn, Alabama.

III   Research Results

A Study of the Nucleation and Growth of Diamond on Silicon
by Scanning Tunneling Microscopy and Spectroscopy

Kevin F. Turner

Contents

Figures

Abbreviations

SEM	Scanning Electron Microscope (Microscopy)
TEM	Transmission Electron Microscope (Microscopy)
STM	Scanning Tunneling Microscope (Microscopy)
TS	Tunneling Spectroscopy
STS	Scanning Tunneling Spectroscopy
CITS	Current Imaging Tunneling Spectroscopy
CVD	Chemical Vapor Deposition
RMS	Root Mean Square
PVD	Peak to Valley Displacement
I/V or I-V	Current - Voltage (Spectrum)

Symbols

Å	ångstroms (10^{-10} meters)
nm	nanometers (10^{-9} meters)
μm	microns (10^{-6} meters)
V	Volts
eV	electron volt(1.602×10^{-19} Joules)
V_B	Bias Voltage
A	Amperes
nA	nanoamperes (10^{-9} Amperes)
C	carbon
Si	silicon
SiC	silicon carbide
Ge	germanium
Cu	copper
HOPG	highly-oriented pyrolithic graphite
W	tungsten
Pt	Platinum
Ir	Iridium

1.0 Introduction

The focus of this thesis is the use of Scanning Tunneling Microscopy (STM) and related techniques to examine the nucleation and growth of diamond on silicon by chemical vapor deposition (CVD). There are many techniques that have been utilized to better understand the growth of diamond. Some of these experimental procedures are Raman spectroscopy [1], X-ray photoelectron spectroscopy (XPS) [2], scanning electron microscopy (SEM) [3], Auger electron spectroscopy (AES) [4], transmission electron microscopy (TEM) [5],, photoluminescence (PL) [6], and electron energy loss spectroscopy (EELS) [7]. None of these techniques has the ultimate resolution of STM and none allow for the characterization of the electronic structure of diamond on an atomic scale. It might be said that, for insulators such as diamond, the dependence of STM on conductivity makes it unsuitable as experimental tool in the examination of the growth process of diamond. It was this conclusion that kept others from attempting what we were able to accomplish first, namely the imaging of undoped diamond nuclei. As will be shown in later chapters, it was the ability to tunnel to undoped diamond, that was an anomaly, that led to other discoveries about the growth process.

It is factual to say that this work could not have been done 10 years ago. Technology now permits the growth of diamond thin films of good quality. [8] The ability to grow diamond from the gas phase was first demonstrated by W. G. Eversole [9] at the Union Carbide Corporation during the period of 1949 through 1953. This first work involved the continuous growth of low-pressure diamond on preexisting diamond nuclei. This work was followed by successful research by J. C. Angus [10] in the United States and B. V. Derjaguin et al [11] in the Soviet Union. This work was greeted with skepticism until the early in the

1980's when Japanese scientists confirmed the experiments of Derjaguin and others. [12,13] These scientists showed that diamond could be synthesized at rates of several μm per hour with the use of seed crystals.

The development of STM has occurred over a similar period of time. The invention of STM by Binnig, Rohrer, and co-workers [14], in 1982, allowed for the first time the direct imaging of geometric and electronic surface structures with atomic resolution. It is interesting that some of the first imaging experiments that utilized quantum mechanical tunneling at the National Bureau of Standards (NBS) preceded the development of the STM by more than ten years [15]. The device developed at NBS, however, never achieved the resolution necessary to image atomic positions. It was the resolution of the structure of the reconstruction of the Si(111) surface [16] that demonstrated the value of the STM as a legitimate surface science tool. These findings were followed by results that showed the atomic positions of the (1 x 2) reconstruction of the Au(110). [17]

Since then there have been five STM conferences, more than 10 conferences focusing on diamond growth technology, and countless symposia in many other meetings and conferences. Diamond growth has been accomplished by thermally assisted CVD [18], plasma assisted CVD [19], reactive vapor deposition [20], and combinations of these techniques. STM has spawned techniques such as scanning tunneling spectroscopy (STS) [21], atomic force microscopy (AFM) [22], and ballistic electron emission microscopy (BEEM) [23], to name just a few.

It is the aim of this research, by drawing on this vast experience and knowledge, to characterize the formation and development of diamond nuclei on silicon and identify the growth surface that allows for this nucleation.

The presentation of this research has been divided into four parts: the nucleation of diamond on silicon (§3.1), the development of complete diamond films and the investigation of the interfacial structure (§4.0), current-voltage spectroscopy applied to diamond nucleation (§5.0), and comparison with nucleation on other substrates (§6.0).

References

1   S. A. Solin and A. K. Ramdas, Phys. Rev. B **1**, 1687 (1970).

2   D. N. Belton, S. J. Harris, S. J. Schmieg, A. M. Weiner and T. A. Perry, Appl. Phys. Lett. **54**, 416 (1989).

3   S. Matsumoto and Y. Matsui, J. Mater. Sci. **18**, 1785 (1983).

4   B. R. Stoner, G. H. M. Ma, S. D. Wolter and J. T. Glass, Phys. Rev., B **45**, 11067 (1992).

5   B. E. Williams and J. T. Glass, J. Mater. Res. **4**, 373 (1989).

6   J. A. Freitas, J. E. Butler, S. G. Bishop, W. A. Carrington, and U. Strom, Mat. Res. Soc. Symp. Proc. **162**, 237 (1990).

7   D. N. Belton and S. J. Schmieg, J. Vac. Sci. Technol. A **8**, 2352 (1990).

8   M. Frenklach, W. Howard, D. Huang. J. Yuan. K. E. Spear and R. Koba, Appl. Phys. Lett. 59, 546 (1991).

9   W. G. Eversole, U. S. Patent 3,030,188 (1961).

10   J. C. Angus, H. A. Will, and W. S. Stanko, J. Appl. Phys. **39**, 2915 (1968).

11   B. V. Spitsyn, L. L. Bouilov, B. V. Derjaguin, J. Cryst. Growth **53**, 219 (1981).

12   S. Matsumoto, Y. Sato, M. Kamo, N. Setaka, Jpn. J. Appl. Phys. pt 2 **21**, 183 (1982).

13   Y. Matsui, S. Matsumoto, N. Setaka, J. Mater. Sci. Lett. **2**, 532 (1983).

14   G. Binnig, H. Rohrer, Ch. Gerber, E. Weibel, Appl. Phys. Lett. **40**, 178 (1982).

15   R. Young, J. Ward, and F. Scire, Phys. Rev. Lett. **27**, 922 (1971).

16   G. Binnig, H. Rohrer, Ch. Gerber, E. Weibel, Appl. Phys. Lett. **50**, 120 (1983).

17   G. Binnig, H. Rohrer, Ch. Gerber, E. Weibel, Surf. Sci. **131**, L379 (1983).

18   Y. Saito, K. Sato, H. Tanaka, K. Fujita, and S. Matsuda, J. Mater. Sci. **23**, 842 (1988).

19   T. Kawato and K. Kondo, Jpn. J. Appl. Phys. **26**, 1429 (1987).

20   L. M. Hanssen, W. A. Carrington, J. E. Butler, K. A. Snail, Mater. Lett. **7**, 289 (1988).

201   R. J. Hamers, R. M. Tromp, and J. E. Demuth, Phys. Rev. Lett. **56**, 1972 (1986).

22   G. Binnig, C. F. Quate, and Ch. Gerber, Phys. Rev. Lett. **56**, 930 (1986).

23   W. J. Kaiser and L. D. Bell, Phys. Rev. Lett. **60**, 1406 (1988).

2.0 The Theories of STM/STS and Nucleation of Diamond

As described above, the techniques of STM and STS, and low temperature and low pressure CVD diamond growth are relatively new. In the short space of time from the development of each process, until each was accepted, the theories governing each have developed rapidly. The following two sections present overviews of the theories and issues involved, and specific results as they apply to this thesis.

2.1 The Theory of Scanning Tunneling Microscopy and Scanning Tunneling Spectroscopy

Scanning Tunneling Microscopy is a technique for imaging, with potential atomic scale resolution, the surface of a conductor or semiconductor. STM utilizes a chemically or mechanically etched metal wire, in the case of the research presented here Tungsten or platinum iridium, with a tip radius of a few angstroms, mounted at the end of a piezoelectric transducer (PZT) assembly. This PZT moves the tip both perpendicular to the surface (the z-direction) and parallel to and above the surface (the x- and y-directions) [fig. 1.1].

A coarse positioning system is used to bring the tip close enough to the surface so that it is in the operable range of the PZT. A bias voltage is applied between the sample and the tip, so that the net flow of tunneling will not be zero. Electrons tunnel through the potential barrier presented by that gap, establishing an electric current between tip and sample. A feedback circuit uses the current to control the distance between the tip and the sample and maintains that same distance. The value of the current maintained is called the setpoint current. When this value is made larger, the tip to sample distance
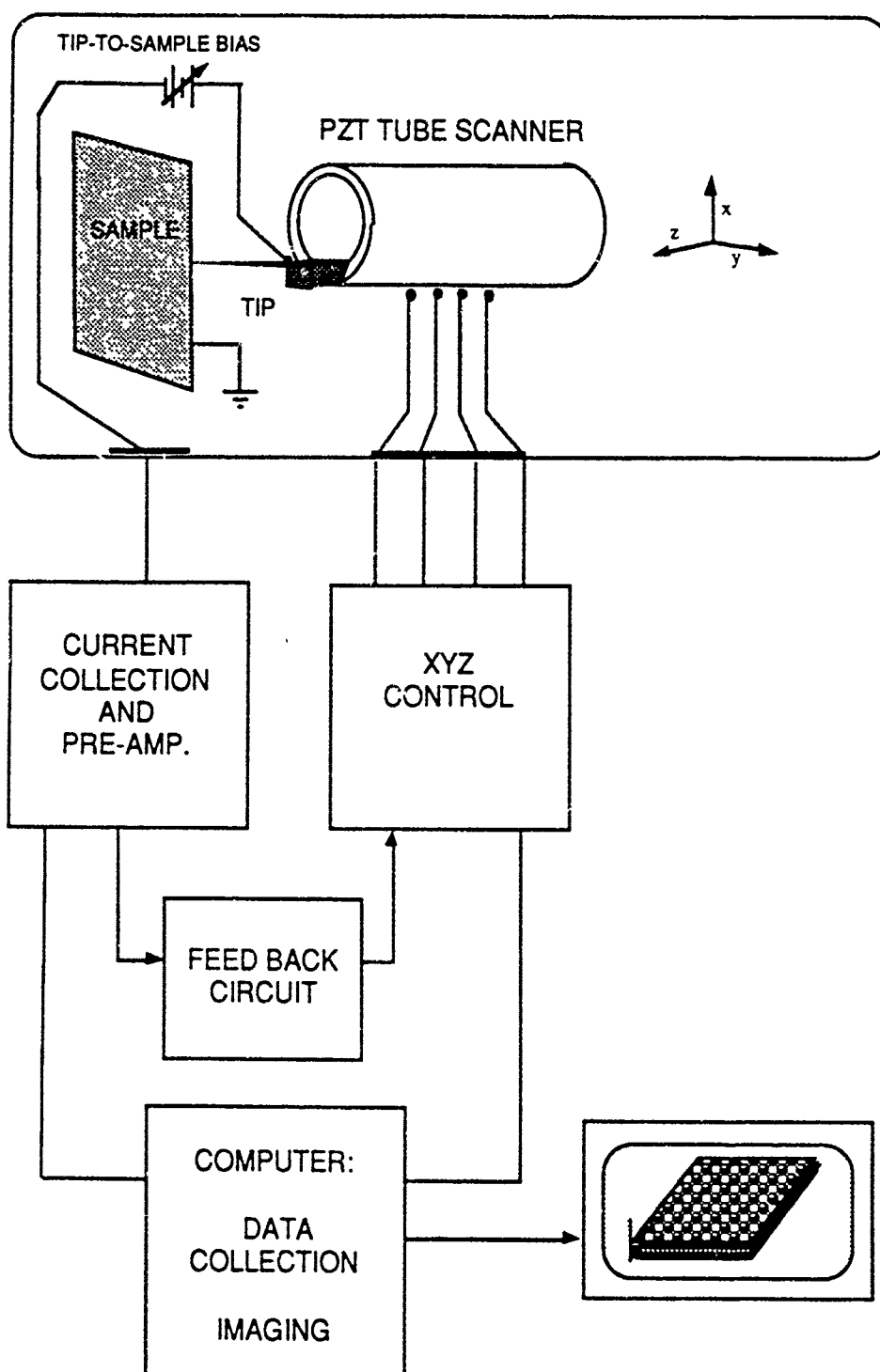
Figure. 2.1

Basic STM schematic. The tip is brought close to the sample, until a current can be detected. That current is then used to maintain the distance between the tip and the sample. The tube is scanned in the X and Y directions, the tip follows the topography of the surface by maintaining a constant current.

decreases. In this study the setpoint current was always selected to obtain the clearest image, even when taking spectroscopic data. To image the surface, the tip is scanned over the surface while maintaining a constant current, thus tracing the topography of the sample.

For negative bias voltages applied to the tip, the net tunneling current comes from electrons that tunnel from occupied states in the tip to unoccupied states in the sample. For positive bias voltages applied to the tip, electron originate from occupied states of the sample into unoccupied states of the tip. For each case, as the tip is scanned over the surface, it follows a contour which is related to the spatial distribution of occupied or unoccupied states of the sample.

To determine the functional dependence of the current on the sample-tip separation, the WKB theory for planar tunneling must be used. Using this theory:

$$I = \int_0^{eV} \rho_s(r,E)\rho_t(r,-eV+E)T(E,eV,r)dE \tag{2.1}$$

where

$$T(E,eV) = \exp(- \frac{2z\sqrt{2m}}{\hbar} \sqrt{\frac{\phi_s+\phi_t}{2}+\frac{eV}{2}-E}) \tag{2.2}$$

where $\rho_s(r,E)$ and $\rho_t(r,E)$ are density of states of the sample and tip at location r and the energy E, measured with respect to their respective Fermi levels, $T(E,eV)$ is the transmission probability for electrons, z is the tip-sample separation, ϕ_s and ϕ_t are the barrier heights of the sample and the tip, respectively, m is the mass of the tunneling particle, and V is the bias voltage.

Quantum Mechanical Tunneling
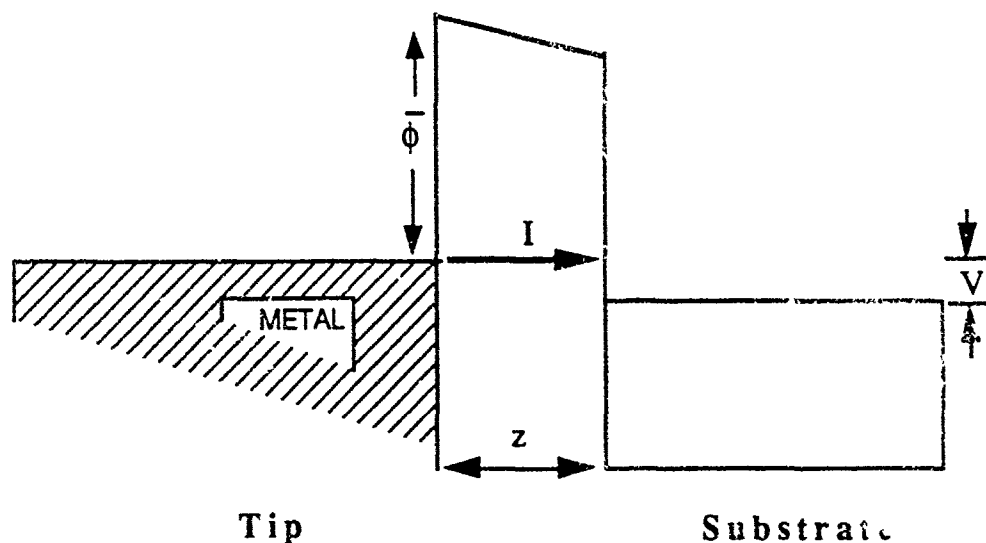
$$I \; \alpha \; e^{-2Kz} \qquad (2.3)$$

where

$$K = \frac{1}{h} \sqrt{2m\overline{\phi}} \quad (2.4)$$

For metals, $\overline{\phi}$ is typically about 3 or 4 eV, so K is approximately 1 (Å)$^{-1}$. For z = 10 Å, $\Delta d = 1$ Å yields a tenfold change in I (ΔI x 10). Thus, if the current can be sensed to within 10% , then the gap distance can be measured with 0.1Å resolution.

Figure. 2.2
Schematic of quantum mechanical tunneling at the STS tip-interface junction.

For these equations, the nomenclature of Hamers [1] and Tersoff and Hamann [2,3] has been utilized.

By inspection, we see that for eV < 0, T(E,eV) has a maximum for E = 0, which means that electrons at the Fermi level of the sample have the greatest transmission probability. For eV > 0, T(E,eV) has a maximum at E = eV or that the electrons at the Fermi level of the tip have the greatest transmission probability. Therefore, the tunneling probability is greatest for electrons at the Fermi level of either the tip or the sample, whichever is negatively biased.

If $\bar{\phi}$, the average barrier height, is defined as $\bar{\phi} = (\phi s + \phi t)/2$, then for smoothly varying density of states for both the tip and the sample, and $V < \bar{\phi}$, a simple treatment of the tunneling effect is allowable. This approximation is given in Figure 2.2. This relation illustrates the source of the resolution of STM and the chief dependence of the current on the tip-sample separation.

For $V > \bar{\phi}$, the situation is illustrated in Figure 2.3. In this case, there is field-emission of electrons into the well formed between the tip and the sample. In this region, there are resonances which can be observed in the conductivity as the bias voltage is increased, and each successive energy level is accessed. [4-7] The relationship between the current and the tip-sample separation also changes for $V > \bar{\phi}$. In this regime, the relation is given by the Fowler-Nordheim equation [8],

$$I \propto \exp(-B(\bar{\phi})^{3/2}(\frac{Z}{V})).$$
(2.5)

It should be noted that the (1/V) term in the exponential will increase rapidly with increasing bias voltage once the bias voltage exceeds the average local barrier
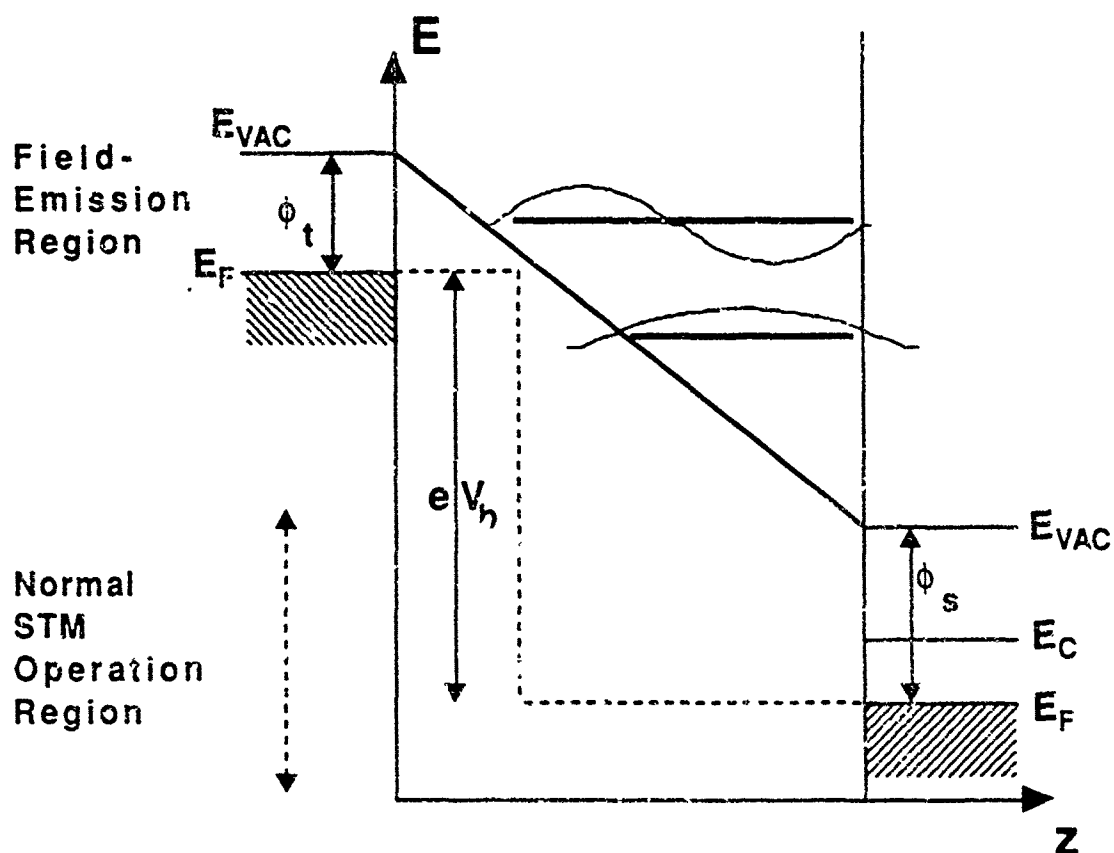
Figure. 2.3

Schematic of band diagrams showing field emission and tunneling processes. E_{VAC}, E_F, and E_C are the energy levels of the vacuum level, the Fermi level, and the conduction band edge. ϕ_t and ϕ_s are the barrier heights of the tip and sample and V_B is the bias voltage
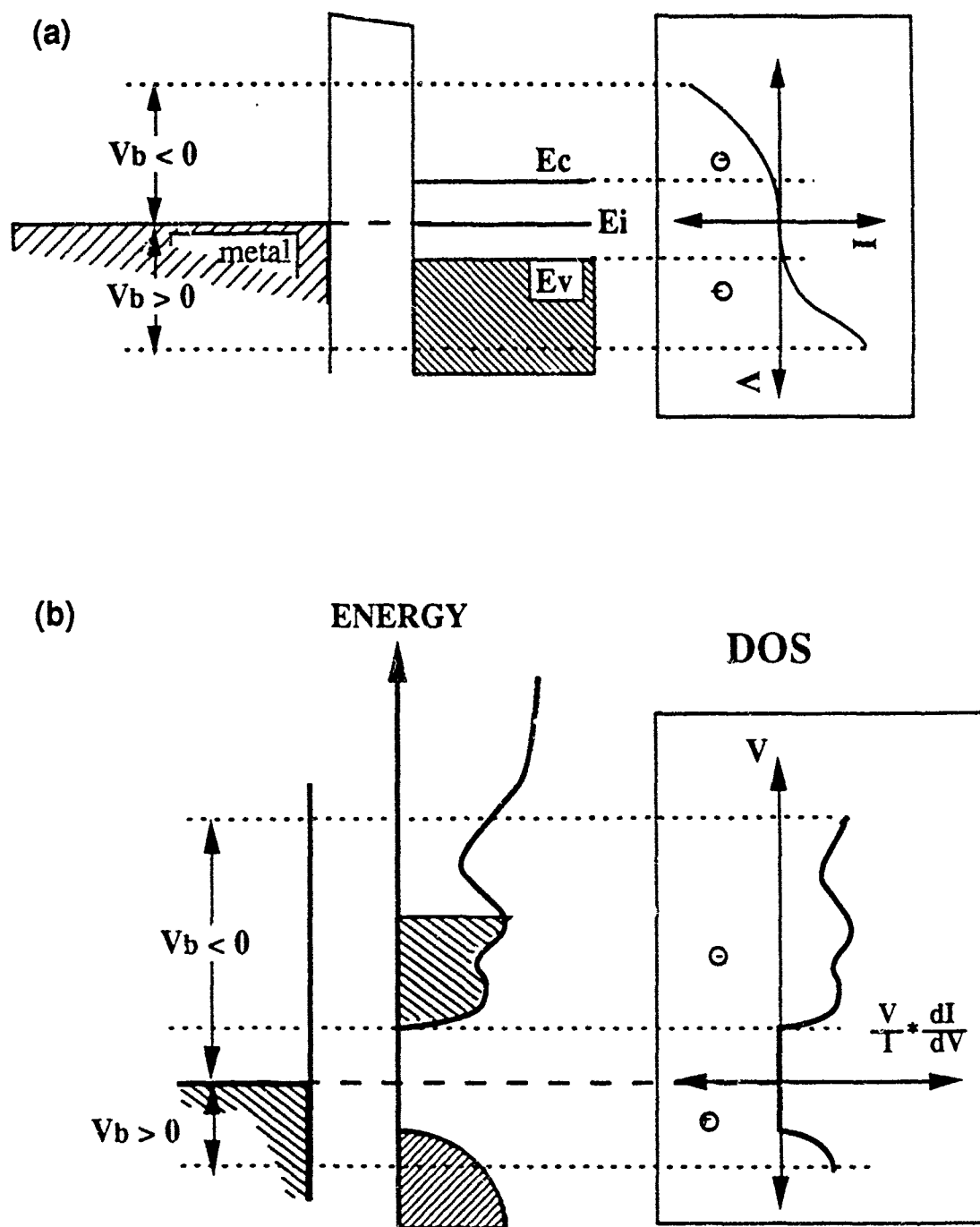
Figure. 2.4

Tunneling spectroscopy and relationship to DOS. (a) The relationship between band structure and I-V curves. (b) The relationship between the energy surface density of states and the ratio of the differential conductivity to the conductivity.

height. A new observation of this effect will be detailed later (§5.0), as it is a distinguishing feature in the surface density of states of diamond.

Scanning tunneling spectroscopy (STS) is a form of potentiometry making use of the capabilities of the STM. In this case, when the tip is scanned, the applied voltage between the tip and sample is ramped between two values and the tunneling current recorded as a function of bias. The z-direction feedback loop is turned off momentarily, so that the loop does not compensate for the change in bias voltage, but not so long as to allow the gap between tip and sample to vary due to drift. The spectra obtained contain information about the density of states at the surface of the sample.

This relationship between the I-V curve obtained from STS and the electronic structure of the sample is illustrated in Figure 2.4. With a bias voltage applied to the tip, a positive bias voltage raises the Fermi level of the metal tip and electrons tunnel from the tip to the sample. This is also referred to as probing empty states of the sample. When the bias voltage applied to the tip is negative, electrons tunnel form the sample to the tip and this is also referred to as the probing of filled states. Figure 2.4 (a) shows an I-V curve that results from STS performed on the band structure to its left. As the Fermi level reaches either the conduction or valence band edges, a large increase in the current is observed.

While the electronic structure of the sample is most often the focus of an STS investigation, it must be recognized that the density of states of the tip also affects the results This effect can be lessened if the same tip is used to compare different regions of a surface, and changes from point to point are noted. In this case the constant density of states of the tip acts as a kind of background to the

DOS measurements. This effect can also be reduced by insuring that all results are reproducible with several different tips [9].

Analysis of STS results can be difficult of the bias voltage dependence of the tunneling probability. (See (2.2)) Most often, the exact relationship between the bias voltage and the tunneling probability is hot known not known explicitly. Often, if the data is presented in the form of a normalized differential conductivity, the dependence of the tunneling probability on the bias voltage does not need to be known. From (2.1),

$$\frac{dI/dV}{I/V} = \frac{\rho s(eV)\rho t(0) + \int_0^{eV} \frac{\rho s(E)\rho t(-eV+E)}{T(eV,eV)} \frac{dT(E,eV)}{dV} dE}{\int_0^{eV} \rho s(E)\rho t(-eV+E) \frac{T(E,eV)}{T(eV,eV)} dE}. \quad (2.6)$$

Feenstra and co-workers [6] were the first to suggest that in many cases, the transmission coefficient terms tend to cancel and it can be approximated as:

$$\frac{dI/dV}{I/V} = \frac{d(\log I)}{d(\log V)} = \frac{\rho s(eV)\rho t(0) + A(V)}{B(V)} \quad (2.7)$$

If one assumes that $A(V)$ and $B(V)$ are slowly varying functions in voltage, then (2.7) simply represents the density of states of the tip and sample. This is shown in a schematic in Figure 2.4 (b). It should be noted, however, that $A(V)$ and $B(V)$ vary rapidly at the band edges and the numerator of (2.6) goes to zero at the band edges.

There are several limitations to the above theory. The first is that the WKB theory is for planar tunneling. A tip used to image the surface should have a small radius of curvature, and this causes effects that are not dealt with in WKB theory of planar tunneling. Secondly, the correlation between the theory

and experiment breaks down if the tunneling is occurring between more than two atoms. For a tip with a large radius of curvature, other effects, due to tunneling from more than one point on the tip, can be observed. One of these effects is tip imaging, which is explored in Appendix A. The specific case of STS as applied to the characterization of diamond films and interfaces is dealt with in §5.0.

2.1 Issues of Nucleation of Diamond

The growth of any material by CVD is a complicated process. All of the particles and films studied here were grown by either hot filament or microwave plasma CVD processes. The source of the deposited materials is usually gaseous mixtures containing hydrogen and carbon and the most widely used source gas is methane. These gas mixtures must be excited by some form of energy, such as thermal or electromagnetic, to create active species containing hydrogen and carbon. These radicals, excited molecules, ions, atomic hydrogen, etc. must be in a concentration greater than their concentration at equilibrium with the growth environment in order for sustained growth to occur. The substrate is usually heated to allow for surface diffusion and surface reactions to occur and facilitate growth.

The growth of polycrystalline diamond films by CVD is possible over a wide range of parameters. Diamond deposition is possible with methane to hydrogen ratios of 0.1% to over 10% [10-13], with substrate temperatures between 600 and 1100° C [14,15], and at total pressures of 0.1 to 800 Torr [10,11]. Growth at temperatures greater than 1127° C or below 400° C results in graphite [16] or amorphous carbon [17].

The difficulty in forming a theory of diamond nucleation is that there are a large number of factors which affect the growth process. First, it is not known absolutely whether diamond nucleation occurs from the gas phase or on the substrate. Nucleation from the gas is possible [18], but cannot account for the high densities of nuclei observed during the growth process. Therefore, it is generally accepted that the nucleation occurs on the surface.

A second difficulty in forming a theory of diamond nucleation is that it is not known what species gives rise to nucleation of diamond on the surface. Several species have been suggested for this precursor that leads to nucleation [19]. Pederson and others examined theoretically the interactions of dangling bonds on the surface and several gaseous radicals. They found [19] that the acetylenic radical $\{C_2H\}$, the methyl radical $\{CH_3\}$, and the acetylene molecule $\{C_2H_2\}$ were all capable of binding to the surface and all three may contribute to nucleation of diamond. The presence of several growth species makes comparisons between the modeling of nucleation by a certain radical or molecule and the observed experimental results more difficult. It is also through these initial interactions between the growth species and the substrate that a non-diamond carbon or a Si-C structures can form on the surface.

This possible change in the chemical constituency of the surface provides another source of difficulty. This difficulty is that it is not known what the diamond is nucleating on. Diamond may be nucleated on a pristine silicon surface, but this is only observed for very low nucleation densities [20]. Often the surface of the substrate is abraded in order to enhance nucleation. It has been postulated that nucleation may occur preferentially on areas of high surface-defect density [21]. Diamond grit is most often used, but abrasion by cubic boron nitride [22] and silicon carbide [23] have produced enhancements

in nucleation densities. Nucleation enhancement can also occur by predeposition of diamondlike carbon (DLC) layers [24,25] and by biasing techniques [26,27]. It has been shown [29] that diamond nucleation can occur on small diamond particles left over from the abrading process. However, since nucleation can occur without abrasion by diamond grit, it has been proposed that "homoepitaxial nucleation" is not the only nucleation process occurring during growth.

There have been many scientific investigations that have supported the role of a stable carbonaceous precursor layers in the nucleation of diamond [28-31]. This precursor layer would form on the surface prior to and during nucleation and the precursor layer has been postulated to be made up of a carbide, a graphitic carbon, a DLC layer or some form of hydrocarbon. It is this lack of knowledge of the interfacial properties that makes exact theoretical treatments difficult. A general theory of nucleation can, however, be outlined and compared with experimental results.

Several authors [32-36] have attempted to understand nucleation from both thermodynamic and kinetic approaches. The steps involved in the nucleation on a surface are shown in Figure 2.5. During the CVD process, species of carbon and hydrogen, from the vapor phase, interact with the substrate. For typical growth temperatures, these species can diffuse over the surface, be re-evaporated, or remain bonded to the surface. Clusters form from stable species that do not diffuse or re evaporate, and increase or decrease their size in a statistical manner. Once a cluster has reached a critical size, where it is statistically more likely to grow than shrink, it becomes a stable site for further growth and is referred to as a nucleus.

This situation for nucleation of diamond can be more complicated, because of a number of factors. The first is that the surface of the substrate can be hydrogen terminated and that hydrogen affects the growth. This termination is caused by the large density of hydrogen in the plasma and the pressure and temperature during growth. The species which arrive on the surface must interact with the hydrogen and the diamond which nucleates is also hydrogen terminated. [37] This hydrogen terminated diamond surface affects the subsequent growth of diamond on the nuclei and complicates the simple model of nucleation and growth described above. The large density of hydrogen is also thought to reduce the relative amounts of sp^2 bonded material in the diamond, as described below.

It has been shown that if oxygen is present in the growth gases, that the quality of diamond grown is affected [38]. It has also been shown that the type of carbon source for CVD, such as different types of alcohol, also affects the nucleation and growth of diamond on silicon [39].

A second complication is that radicals and/or molecules that arrive at the surface do not have to bond with other species to form diamond. Rather, because diamond is known to be thermodynamically unstable relative to graphite, it would be assumed that the carbon would bond into a graphitic structure. It is believed that hydrogen plays a role in the preferred growth of diamond. It has been theorized that there is an enhanced etching of graphitic regions by hydrogen relative to diamond [40]. In this view, the growth of diamond is kinetically stable relative to the growth of graphite. Another view is that hydrogen stabilizes the surface of the diamond and prevents the diamond surface from reconstructing [41,42]. In this case, it is believed that the diamond

surface is thermodynamically stable relative to the surfaces of graphite for the conditions of growth.

A third complication to the simple theory of nucleation is the interfacial properties between the diamond and the substrate. The growth mode of the diamond depends strongly on the free energies of the substrate and the material being deposited and the interface energy. The mode will be either Volmer-Weber (3d), layer by layer (2d), or Stranski-Krastanov (2d followed by 3d) (see Fig. 2.6). It is, therefore, possible that a material may have two different modes of growth, under the same growth conditions, for two different substrates. This is important if there is a precursor involved with growth, i. e. nucleation does not occur on a pristine substrate. In that case, the nucleation would occur on some other deposited material and the resulting growth mode would be different. Without a better understanding of the effect and composition of the precursor(s), a complete understanding of the nucleation process is not possible.

In relation to the theory of nucleation, the structure of the nuclei will be dealt with in §3.0 and §4.0. The nature of the growth surface and interfacial layers will be covered in §3.0 and §5.0. Secondary nucleation, nucleation which occurs on top of other nuclei, will be discussed in §4.0. The issue of finding a critical nucleus size will be discussed in §5.0. A comparison of growth on different substrates is given in §6.0.
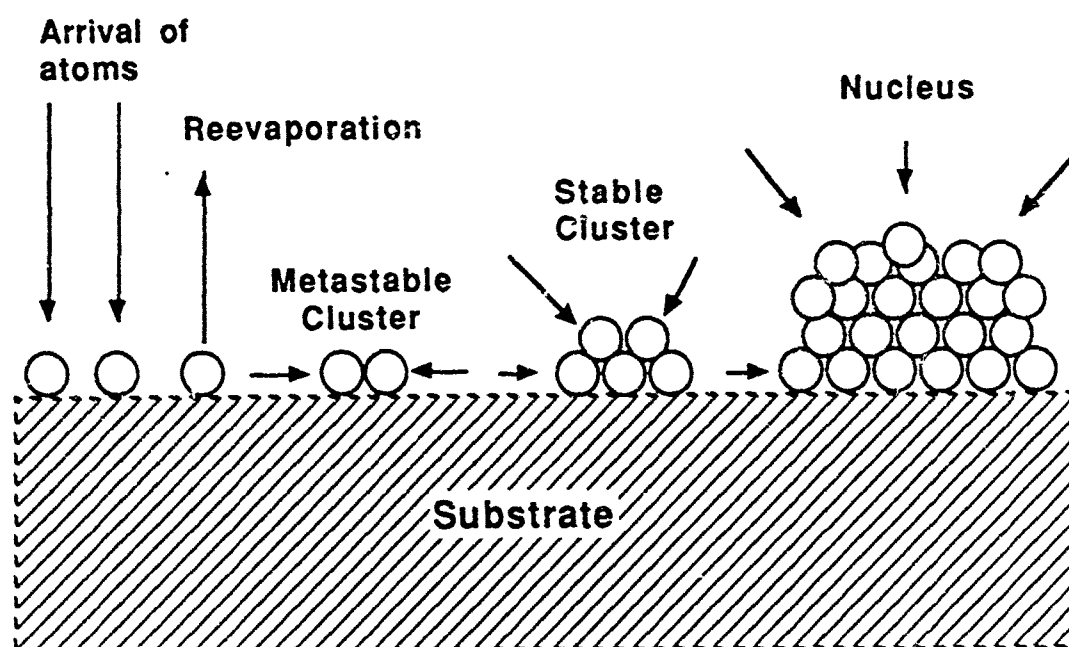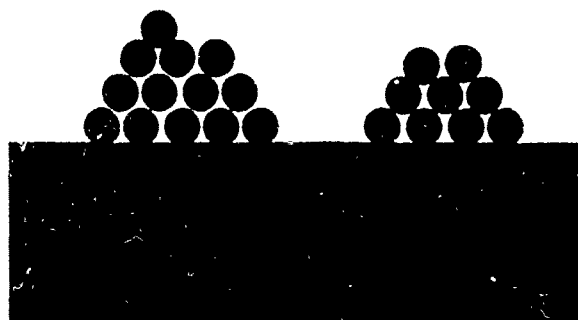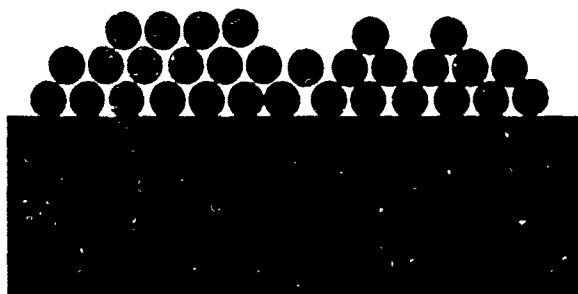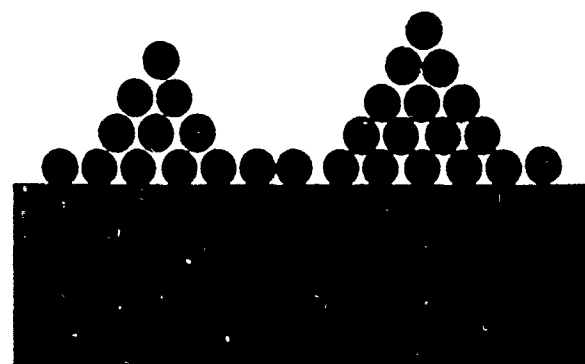
Figure. 2.5
Schematic of the process of surface nucleation. Atoms impinge on the surface, diffuse over the surface, cluster together, and may form into a stable nucleus

(a) Island growth (Volmer Weber)

(b) Layer by layer growth

(c) Layer + island (Stranski-Krastanov)

Figure. 2.6

Comparison of growth modes.

References

1   R. J. Hamers, R. M. Tromp, and J. E. Demuth, Phys. Rev. Lett. **56**, 1972 (1986).

2   J. Tersoff and D. R, Hamann, Phys. Rev. Lett. **50**, 1998 (1983).

3   J. Tersoff and D. R, Hamann, Phys. Rev. B **31**, 805 (1985).

4   G. Binnig and H. Rohrer, Helv. Phys. Acta **55**, 726 (1982).

5   R. S. Becker, J. A. Golovchenko, and B. S. Swartzentruber, Phys. Rev. Lett. **55**, 987 (1985).

6   R. M. Feenstra, J. A. Stroscio and A. P. Fein, Surf. Sci. **181**, 295 (1987).

7   J. H. Coombs and J. K. Gimzewski, J. Microscopy **152**, 841 (1988).

8   R. H. Fowler and L. Nordheim, Proc. Roy. Soc. London A **119**, 173 (1928).

9   J. P. Pelz, Phys. Rev., B. **43**, 6746 (1991).

10   K. E. Spear, M. Freklch, A. Badzain, T. Badzian, and R. Messier, Ceram. Eng. Sci. Proc. **9**, 1095 (1988).

11   S. Matsumoto, J. Mater. Sci. Lett. **4**, 600 (1985).

12   S. Matsumoto, M. Hino, and T. Kobayashi, Appl. Phys. Lett. **51**, 737 (1987).

13   S. Matsumoto, in *Diamond and Diamond-Like Materials Synthesis*, edited by G. H. Johnson, A. R. Badzian, and M. W. Geis (Materials Research Society, Pittsburgh, 1988), p.99.

14   K. Suzuki, A. Sawabe, H. Yasuda, and T. Inuzuka, Appl. Phys. Lett. **50**, 728 (1987).

15   P. K. Bachmann, G. Gartner, and H. Lydtin, Mater. Res. Soc. Bull. **13**, 52 (1988).

16   K. Suzuki, A. Sawabe, H. Yasuda, and T. Inuzuka, Appl. Phys. Lett. **50**, 728 (1987).

17   Y. Liou, A. Inspektor, R. Weimer, D. Knight, and R. Messier, J. Mater. Res. **5**, 2305 (1990).

1 8   W. Howard, D. Huang, J. Yuan, M. Frenklach, K. E. Spear, R. Koba, and A. W. Phelps, J. Appl. Phys. **68**, 1247 (1990).

1 9   M. R. Pederson, K. A. Jackson and W. E. Pickett, in *Proceedings of the Second International Conference on the New Diamond Science and Technology*, edited by R. Messier and J. T. Glass (Japan New Diamond Forum, Washington, D.C., 1990), p.29.

2 0   P. K. Bachmann, W. Drawl, D. Knight, R. Weimer, and R. F. Messier, in *Diamond and Diamond-Like Materials Synthesis*, edited by G. H. Johnson, A. R. Badzian, and M. W. Geis (Materials Research Society, Pittsburgh, 1988), p.99.

2 1   S. Yugo and T. Kimura, in *First International Conference on the New Diamond Science and Technology, Program and Abstracts* (JNDF, Tokyo, 1988), p.130.

22   K. Suzuki, A. Sawabe, H. Yasuda, and T. Inuzaka, Appl. Phys. Lett. **50**, 728 (1987).

23   A. Sawabe and T. Inuzuka, Thin Solid Films **137**, 89 (1986).

24   K. V. Ravi and C. A. Koch, Appl. Phys. Lett. **57**, 348 (1990).

25   J. J. Dubray, C. G. Pantano, M. Meloncelli and E. Bertran, J. Vac. Sci. Technol., A. **9**, 3012 (1991).

26   S. Yugo, T. Kanai, T. Kimura and T. Muto, Appl. Phys. Lett. **58**, 1036 (1991).

27   B. R. Stoner, G. H. M. Ma, S. D. Wolter and J. T. Glass, Phys. Rev., B **45**, 11067 (1992).

28   S. Iijima, Y. Aikawa, and K. Baba, J. Mater. Res. **6**, 1491 (1991).

29   K. V. Ravi, C. A. Koch, H. S. Hu. and A. Joshi, J. Mate. Res. **5**, 2356 (1990).

30   S. Yugo, T. Kimura and T. Muto, Vacuum **41**, 1364 (1990).

31   D. E. Meyer, R. O. Dillon, and J. A. Woollam, J. Vac. Sci. Tecnol. A. **7**, 2325 (1989).

32   *Growth and Properties of Metal Clusters*, edited by J. Bourdon (Elsevier, Amsterdam, 1980), pp. 15-33.

33   M. Avrami, J. Chem. Phys. **7**, 1103 (1939).

34   R. J. H. Voorhoeve, Surf. Sci. **28**, 145 (1971).

35   J. L. Robins, Appl. Surf. Sci. **33/34**, 379 (1988).

36   M. Tomellini, R. Polini and V. Sessa, J. Appl. Phys. **70**, 7573 (1991).

37   D. W. Brenner, Phys. Rev. B **42**, 9458 (1990).

38   T. Kawato and K. Kondo, Jap. J. Appl. Phys. **26**, 1429 (1987).

39   R. A. Rudder, G. C. Hudson, J. B. Posthill, R. E. Thomas, and R. J. Markunas, Appl. Phys. Lett. **59**, 791 (1991).

40   M. Sommer, K. Mui, and F. W. Smith, in *Final Program and Abstr. Third Annual SDi/OST Diamond Symposium*, Crystal City, VA, July 1988.

41   W. A. Yarbrough and R. Roy, in *Diamond and Diamond-Like Materials Synthesis*, edited by G. H. Johnson, A. R. Badzian, M. W. Geis (Materials Research Society, Pittsburgh PA, 1988). pp. 33-38

42   B. B. Pate, Surface Sci. **165**, 83 (1986).

3.0 A Note of Preface

The following paper was published in the *Journal of Applied Physics.*, volume 69, 9th issue, 1991. Since the time of it publishing, other results have been established. These results involve photoluminescence from diamond nuclei and other information regarding the ability to image undoped diamond with a scanning tunneling microscope. These additions are presented in Section 3.2.

3.1

Observation of surface modification and nucleation during deposition of diamond on silicon by scanning tunneling microscopy

K.F. Turner, B.R. Stoner, L. Bergman, J.T. Glass, R.J. Nemanich,

Department of Physics and Department of Materials Science and Engineering

North Carolina State University

Raleigh, NC 27695-8202

Abstract

The surface topography of silicon substrates after the initial stages of diamond growth, by microwave plasma enhanced chemical vapor deposition (PECVD), has been observed by scanning tunneling microscopy. The initial surfaces were polished with diamond paste before deposition to enhance nucleation, and the scratches were examined. After one half hour growth, the surface showed additional topography over all regions, and widely spaced faceted structures were detected which were attributed to diamond nuclei. The surface between nuclei showed increased roughness with increased deposition time. The faceted nuclei were found along the scratches. The nuclei showed facets which were smooth to within 5Å. Finger-like ridge structures were found extending from and in-between some of the nuclei. These structures indicate a mechanism of the lateral diamond growth. The electronic properties of the surface were probed by local I-V measurements, and characteristics attributable to SiC were observed.

I. Introduction

The large thermal conductivity, high electron and hole mobilities and radiation hardness make diamond a potential new material of choice for high temperature or high power electronic applications. Growth of diamond thin films by chemical vapor deposition (CVD) has been accomplished by many research groups [1-4], and this advancement offers the possibility of a wide range of technological applications. The typical CVD processes employ excitation of a mixture of methane (or other gaseous hydrocarbons) and hydrogen and deposition onto substrates heated to between 500 to 1000°C.[5] In order to initiate the growth of diamond, the substrates are often scratched with diamond paste to increase the nucleation density.[6] The faceted diamond structures have been observed to nucleate preferentially along these scratches and then grow together to form a complete film.[6] TEM examinations of the films have indicated that for some conditions, a SiC layer forms at the interface of the Si and diamond.[7]

In this study, we will examine the surface at the initial stages of diamond nucleation on Si substrates. The diamond growth is obtained using microwave plasma enhanced CVD. The issues include the structure of the surface before diamond nucleation, the formation of diamond nuclei and the lateral growth mechanisms. The major technique that will be employed is scanning tunneling microscopy, and micro-Raman spectroscopy will also be used to verify the presence of diamond.

Scanning tunneling microscopy (STM) is a useful characterization technique in part because it provides a direct method for observing surfaces. The graphite form of carbon has proved the standard for demonstration of atomic resolution by STM in air, and the technique has been used in the

examination of other forms of sp^2 bonded carbon.[8] While the most common characterization technique for diamond films is scanning electron microscopy (SEM) [7,9], STM can provide greater resolution than SEM and also provides information on the local surface electronic structure.

II. Experiment

All the films to be discussed were prepared by microwave plasma CVD on 1 inch diameter n-type Si<111> substrates. The substrates were polished with 0.25 μm diamond powder for 5 minutes and then solvent cleaned. The samples examined were grown for 30 and 60 minutes as well as a reference sample on which no growth occurred but which was prepared in the same fashion as the others. A 30 minute hydrogen plasma etch was performed before growth. In both cases, the growth occurred at a pressure of 25 Torr, a methane to hydrogen ration of 0.5% with a total flow rate of 1000 sccm and an average substrate temperature of ~760°C. No intentional dopant was used in the growth process. These are the same parameters that have been used to grow thicker diamond films in this and many similar systems. [7,10] SEM micrographs were taken of the surfaces to show the surface topography on a large scale and to provide an estimate of the nucleation density.

The STM analysis of the surface was done over a wide range of parameters. All of the analysis was performed using an RHK ATM-500 scanning tunneling microscope.   This system required that the samples be cleaved to a size measuring ~2 x 3mm so that they could be accommodated to the sample holder of this microscope. The scans of the surface covered scan ranges between 20 – 8000Å. All of the scans were preformed with tip velocities between 200 - 10,000 nm/s and with tunneling currents ranging between 0 2nA

to 3nA. Positive biases between 0.05 - 2 volts and negative biases between 0.05 - 3 volts were used during examinations of the surface. With the STM used, a positive bias corresponds to a voltage applied to the tip that is positive relative to the sample. All of the STM images presented in this paper come from scans preformed with a negative bias of two volts which yielded the most stable images. At biases less than one volt, it is assumed that current is due to electrons tunneling into surface states or defect or impurity states within the band gap of the substrate material. Current-voltage measurements were also made using the STM with a process that is called tunneling spectroscopy. In these measurements, the bias was ramped between -9 and +9 volts and currents between ±10 nA were measured.

In some regions of the samples, there was a great deal of instability in the STM measurements which was attributed to the high resistance of the samples. The tip would pull back from the surface with time in order to maintain the same tunneling current. One possibility is that this is due to charging of the surface. The as-prepared Si substrate, with no deposition, required an etch with a $HF:H_2O$ solution before the surface could be imaged. and even then the response of the STM was extremely unstable.

III. Results and Discussion

The results of the investigation of the surface will be divided into three topics: modification of the surface which occurs before complete diamond coverage, observation and analysis of the nuclei formed, and the electronic properties of the nuclei and the surface modified by deposition. Figure 3.1 shows the surface structure of some of the particles as viewed by SEM. It
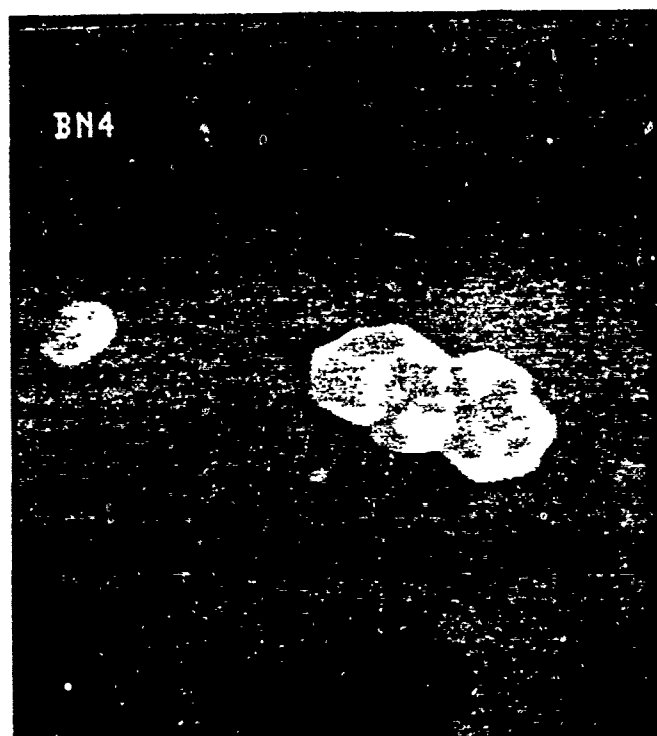
0.5 μm

Figure 3.1
SEM micrograph of early nucleation of diamond on
silicon after 60 min of growth showing the faceting
of the individual nuclei.

should be noted that the nuclei varied widely in their dimensions as well as their spacing from other nuclei. The SEM micrograph shows well faceted, multiply twinned particles, approximately 0.25 μm in size, which are commonly observed for CVD diamond. [6,10]

Changes in the surface can be observed for different samples with different deposition times. Figures 3.2 (a) and 3.2 (b) show STM images of the surface after 30 minutes and 60 minutes of growth respectively. The scratches which can be seen on the surface are remnants of the pre-seeding polish with diamond paste. These scratches are measured to be between 75 - 100Å deep and varying in width from 200 - 1000Å. The radii of the tip was found to be approximately 25μm. The STM tips were prepared by mechanical polishing of etched tungsten wire. On a micron scale, the end of the tip is very blunt with only a few jagged protrusions at the surface. It is likely, from examination of SEM micrographs of the tips, that the tunneling is occurring between one of these protrusions and the surface. The protrusions were generally greater than 100nm in scale. Therefore, the actual depths of the scratches may be larger than those observed, because of tip geometry.

The 60 minute and 30 minute growth samples can also be examined in terms of their surface roughnesses. One of the options available on the RHK STM system is to show the "Z" range and the standard deviation of the "Z" range values. In each case, a plane subtraction was performed on the data to remove the tilt due to the orientation of the sample. The "Z" ranges and the standard deviations were determined from the corrected Z values. The 60 minute sample had a "Z" range of 550Å with a standard deviation of ~65Å and the 30 minute sample had a "Z" range of 302Å with a standard deviation of ~33Å. As a film forms on the silicon substrate, the surface should be more rough. The surface

(a)

Figure 3.2

STM images of the surface after (a) 30 and (b) 60 min. The scratches from the polishing of the silicon before deposition can be seen in both pictures.
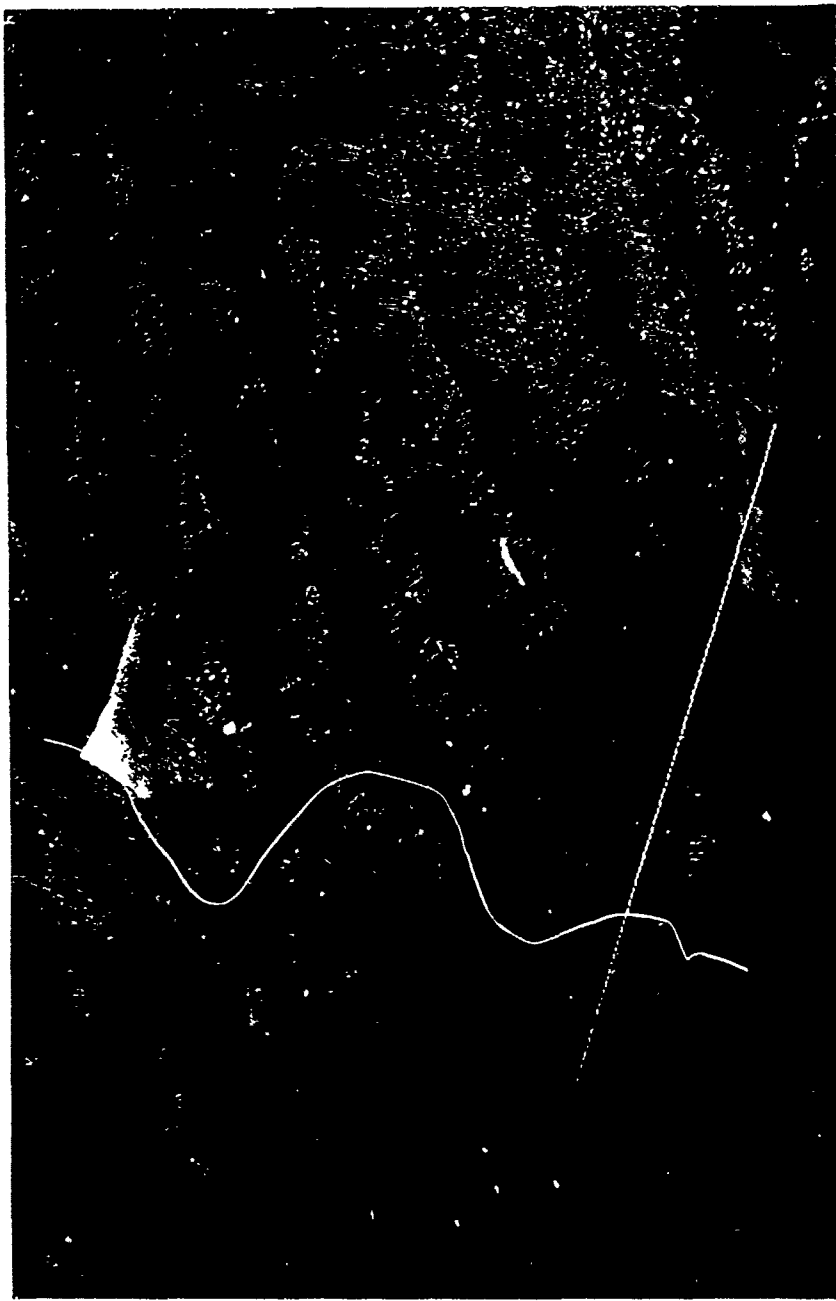
Figure 3.2 (Continued)

(b)

or the 60 minute sample shows increased roughness from the 30 minute sample. This indicates a film formation or growth of a surface layer.

The observed change in surface roughness may be due to the growth of a surface silicon carbide layer. Williams et al. [10] have observed a silicon carbide layer that exists between the silicon substrate and the diamond by cross-sectional TEM in thicker diamond films. Also, other studies [11,12], have shown the existence of a carbide before the presence of diamond can be detected. Tunneling spectroscopy measurements, which are presented below, also suggest that this layer is silicon carbide.

Results from the micro-Raman analysis, shown in Fig. 3.3, demonstrate that the nuclei on the surface are diamond. For the spectra shown, the micro-Raman probe, with a spot size of ~5μm, was focused on different areas of the surface. Curve (a) corresponds to a spectra resulting from sampling an area where there was a large density of nuclei on the surface, and curve (b) is a result of sampling an area containing few nuclei. For (a) the laser spot contained approximately 20 particles and for (b) the laser spot contained less than 5 particles. The peak observed at 1332 cm^{-1} is an indication of the presence of diamond.

The STM was used to display aspects of the topography of the nuclei including the faceting of the nuclei. Figure 4 (a), which shows a single nucleus, illustrates the faceting of the nuclei that were observed. It is apparent that the growth has occurred along the edge of a scratch on the surface. The plane which forms the top of the nucleus is within 4° of parallel to the plane of the substrate. This observation may be understood either if nucleation occurs near the top of the scratch or if the lateral growth of the diamond is conforming to the substrate. The planes of the longest sides are at 153° ± 4° relative to the "top"
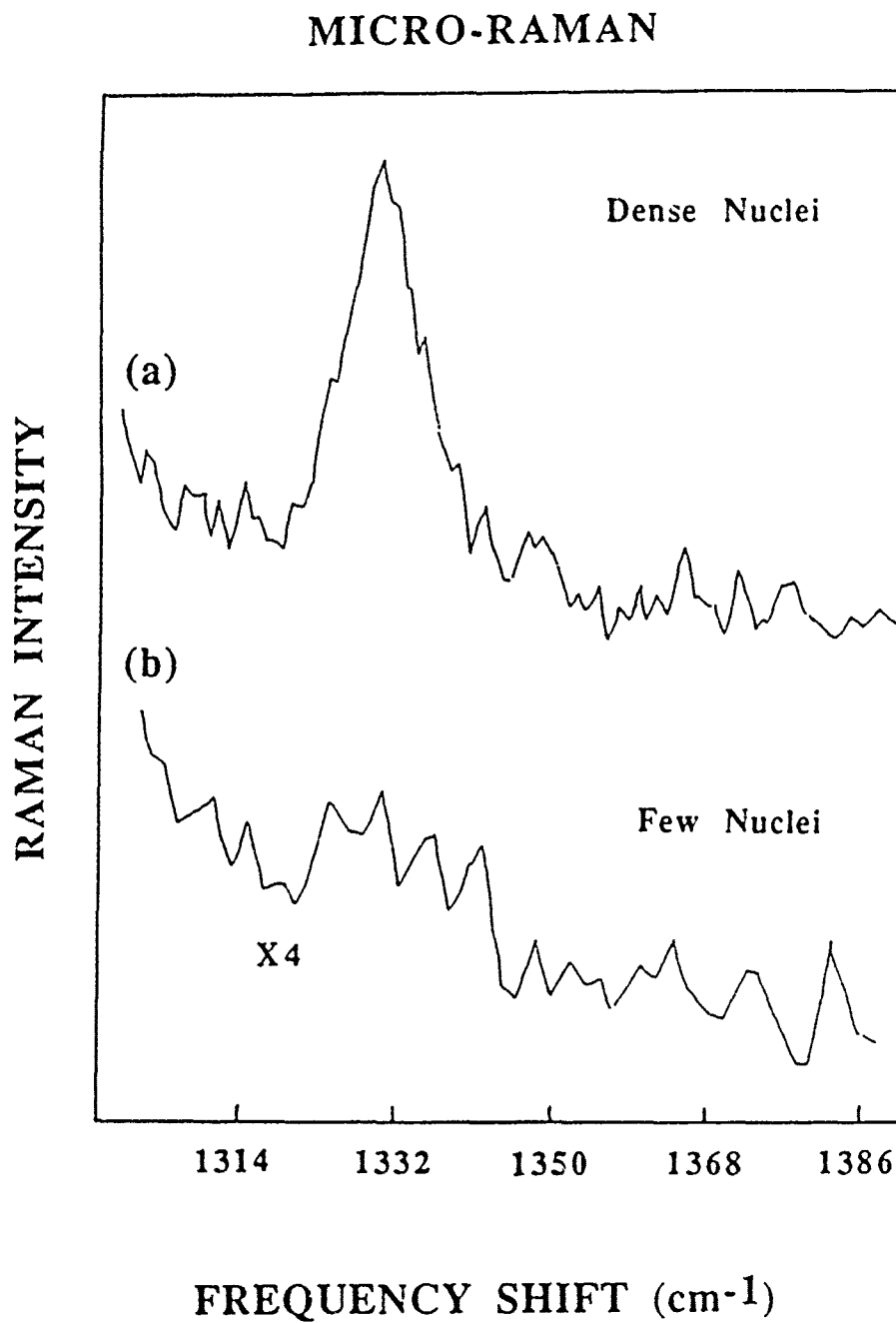
MICRO-RAMAN

Figure 3.3

Results from micro-Raman spectroscopy of the 60 minute growth sample. The curve (a) is the result of examining an area of high concentration of nuclei and in the curve (b) is from an area of low concentration of nuclei

Figure 3.4

STM images showing: (a) A single diamond nucleus. (b) A closer view of this same nucleus. (c) A cross-section showing the difference in roughness of the nucleus and the modified surface between A and B.

1838 Å

1855 Å

198.9 Å

(b)

Figure 3.4 (Continued)

(c)

Figure 3.4 (Continued)

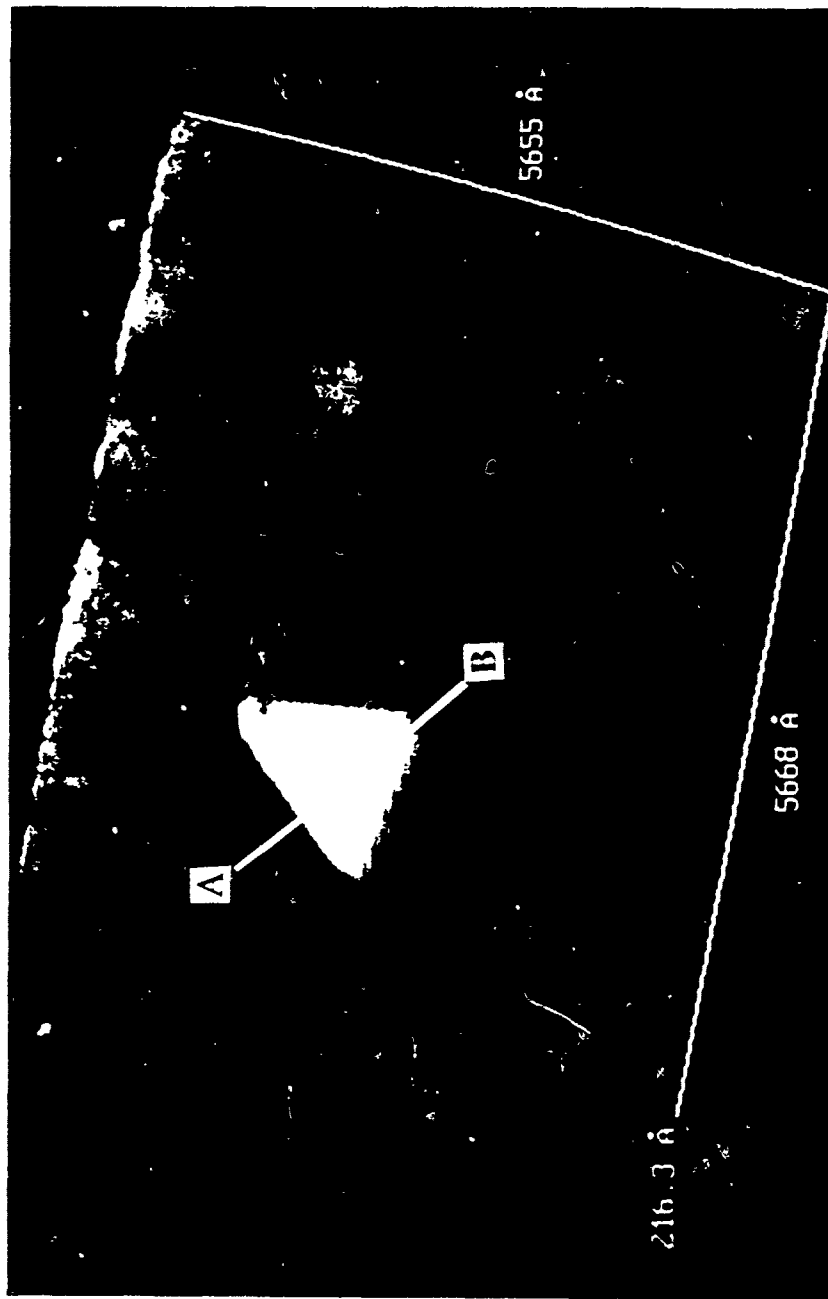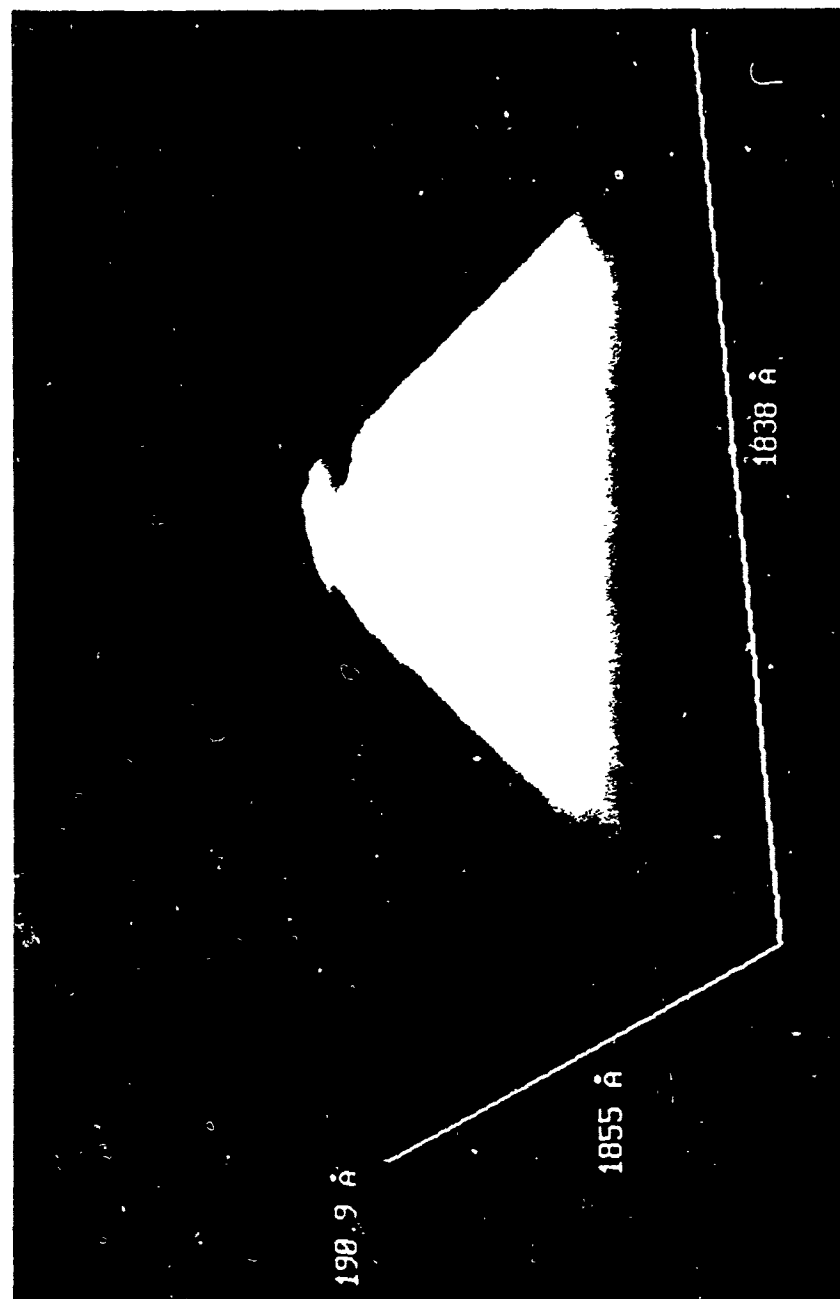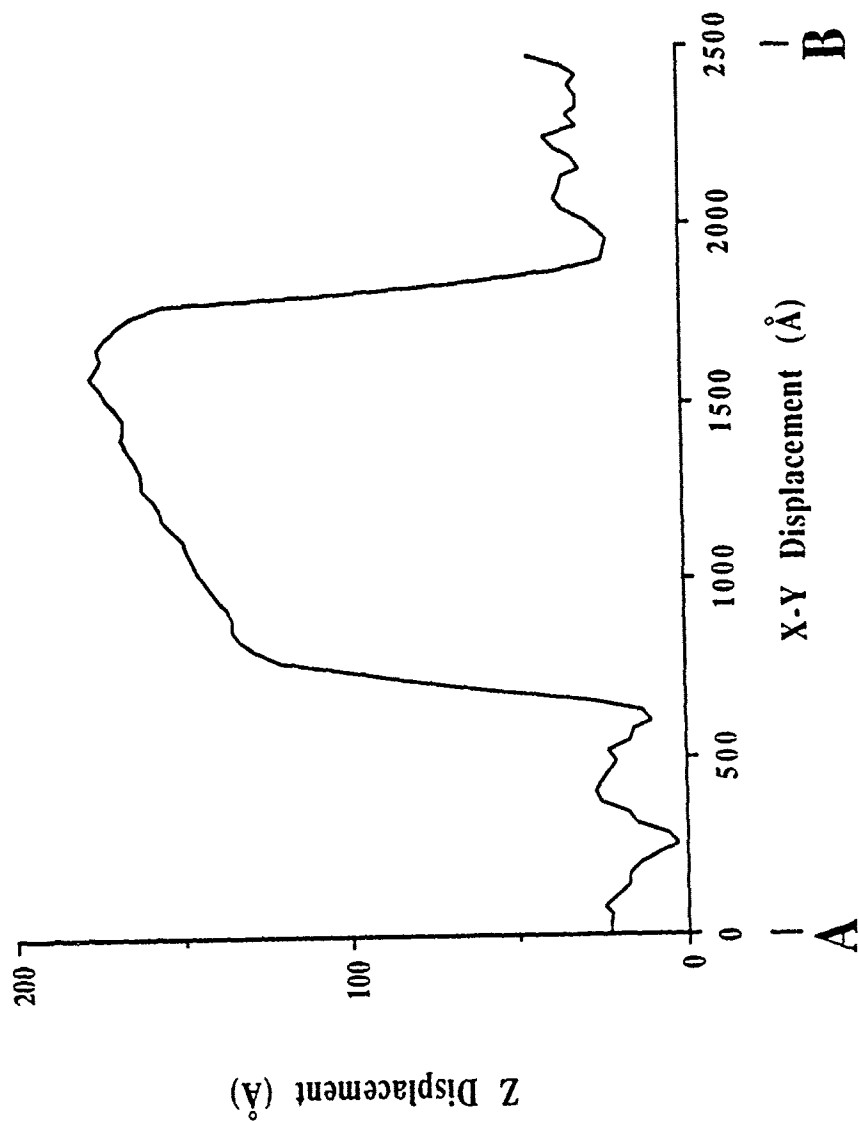of the nucleus. The structure is nearly triangular as can be seen from Fig. 4 (b). The edges which meet to form corners are terminated by planes which are at angles between 130° to 160° relative to the plane of the "top" of the nucleus. This suggests that these are the planes which grow at a faster rate and have "grown themselves out of existence". Measured at the base of each facet, the longer sides are 1350Å, 1450Å, and 1700Å in length. The shorter sides are each between 1/5 to 1/4 of the length of the longer sides with lengths between 300 and 350Å.

Because of the large band gap of diamond, it would be impossible to detect a tunneling current through a 10nm particle at the tunneling bias used. One possibility to account for the observations is that the nuclei have a sufficient number of defects which allow for conduction to occur. This is also consistent with inability to tunnel to thicker diamond films since the number of defects decreases as the thickness increases.[10]

It can be observed that there is a difference between the structure of the modified surface of the silicon and the diamond nuclei. Fig. 3.4 (a) shows the change in topography between a nucleus and the modified surface. In Fig. 3.4 (c), the cross-sectional view shows the difference in the fluctuations in the z direction, with displacements in the scanning directions, between the two surfaces. The diamond appears smoother than the other layer on the silicon. It is possible that the differences in the conductivities of the two regions may affect the measured roughness. If the tunneling current measured when the tip is over the diamond region has less signal-to-noise than when it is over the other region, then this will affect the roughness measured. In this case, however, the observed differences in the signal-to noise ratios of the tunneling current when the tip was over the different regions were negligible. The change in roughness

Figure 3.5

(a) STM images of nuclei with growth structures between them. (b) The surface topography along the line joining points C and D. (c) A STM image illustrating the structures growing in the area between two nuclei.
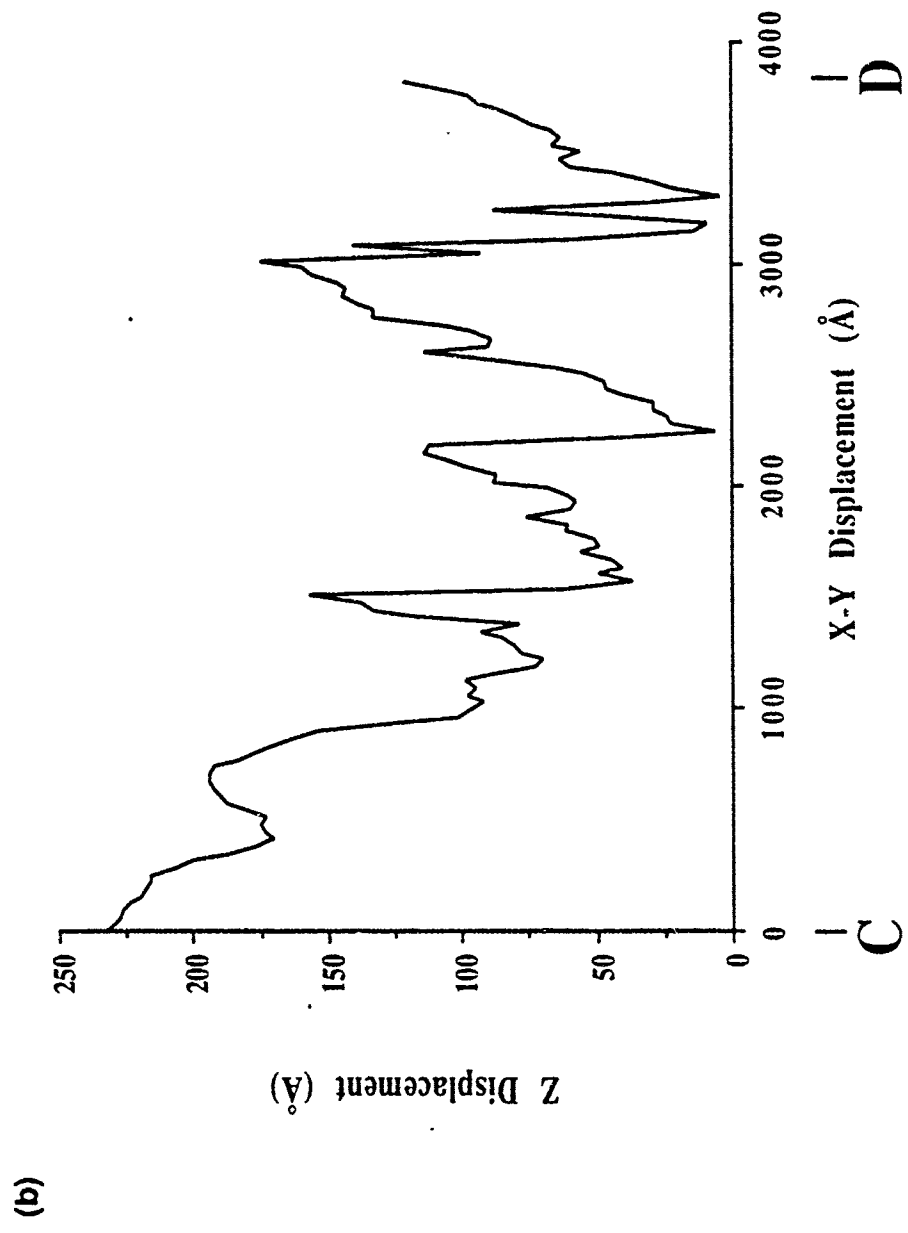
Labels in image: C, D, 484.2 Å, 6481 Å, 6458 Å, (a)

Figure 3.5 (Continued)

(b)

Figure 3.5 (Continued)

(c)

between the two regions was more than an order of magnitude. If this difference was due to the differences in conductivities of the two regions, then there should have been an observable difference in the signal-to-noise ratios of the tunneling current.

In Figure 3.5 (a), two nuclei are displayed with structures extending between them. Figure 3.5 (b) shows a cross-sectional view of this area. The structures fan out radially from the nucleus on the side facing the other nucleus. The structures are ~100Å in height and 100-200Å in width. These changes in the surface may be indicative of how the nucleus spreads laterally to connect with other nuclei. This would be consistent with results reported by Kawarada et al. [13] that the growth occurs over an interlayer of SiC. Another example of the elongated ridge structures can be seen in Figure 3.5 (c) with the same height and width dimensions. The structures observed to occur between the nuclei are similar to other structures that have been observed by STM between facets of thicker diamond films. [14]

In both Figures 3.5 (a) and 3.5 (c), evidence of faceting is also observed. The surfaces are at different angles relative to the substrate and from a top down view, the angles are close to those observed from SEM micrographs. The bases of the facets lie along the scratches. In other cases, (Fig. 3.6 (a)) the nuclei are more elongated. In the same picture, there is an example of the structure which occurs when two planes of the facets meet at what appears to be a plateau. When examined in greater detail, this region is not flat, but is a "V" shaped valley. This type of structure is often attributed to re-emergent planes of adjoining domains. [15] A cross-sectional view of the twined structure is shown in Fig. 3.6 (b). The planes of the smaller inner facets and the plane of the facets on the right of the cross-section are all at ~15° to the plane of the scan. The
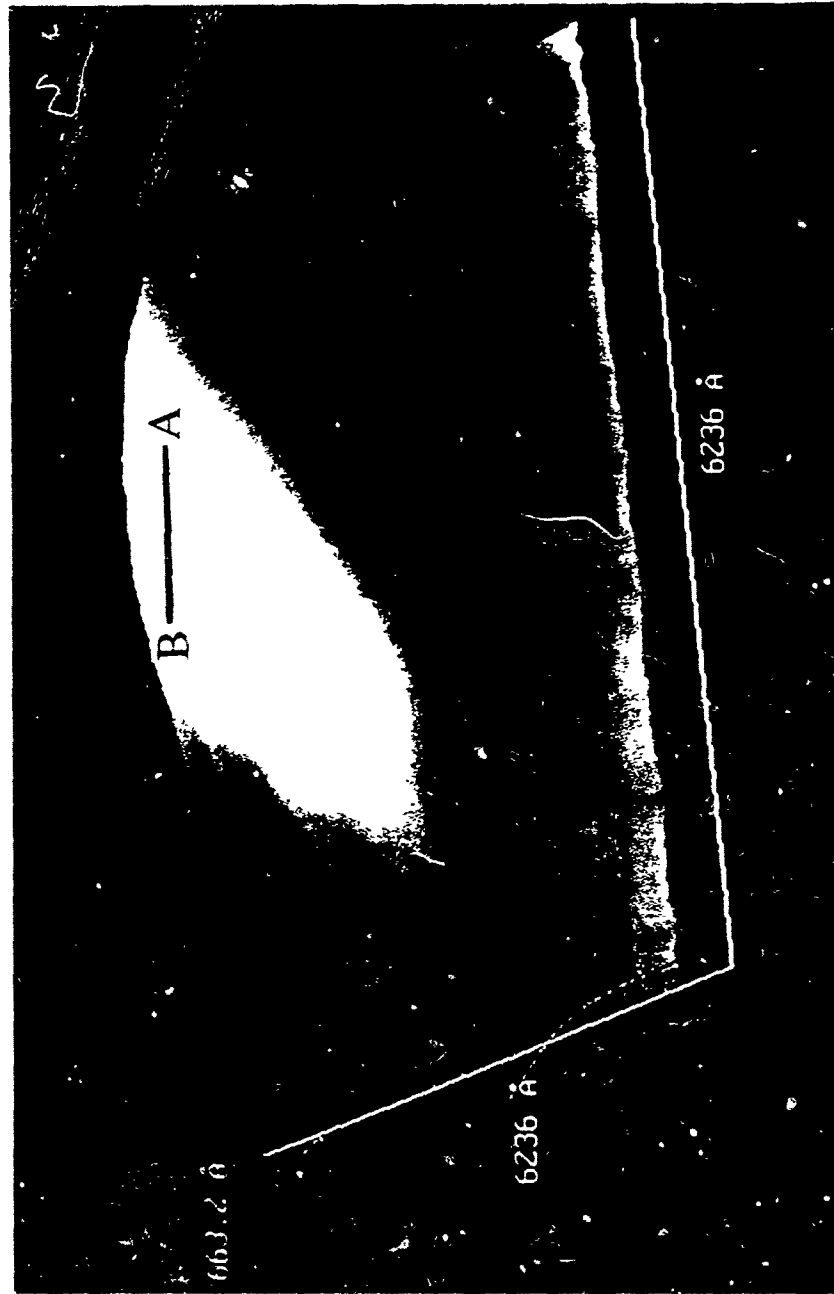
Figure 3.6

(a) A STM image of a twinned structure on a nucleus. (b) A cross-section showing
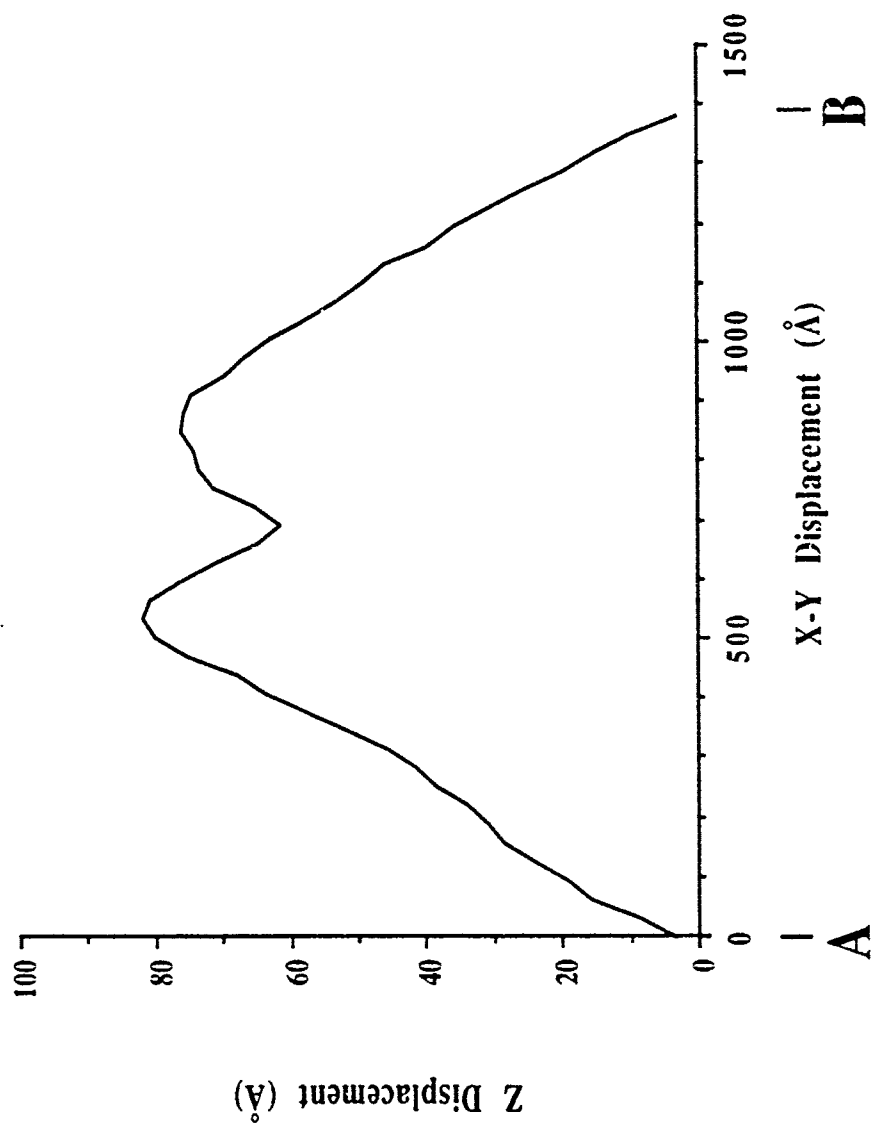the topography of the area between A and B.

(a)

X-Y Displacement (Å)

Z Displacement (Å)

A   B

(b)

Figure 3.6 (Continued)

angle between the inner two facets is 148° ± 1°. The plane of the facet on the left of the cross-section is at an angle of ~8° relative to the plane of the scan.

The electronic structure of the surface can also be measured by using the STM for tunneling spectroscopy [16-19]. Usually, the feedback loop controls the position of the tip while scanning, so that in topographic mode, the distance between the sample and the tip is held constant. The tunneling spectroscopy technique involves switching off the feedback loop, ramping the bias voltage and then switching the feedback loop back on. This process is preformed quickly so that the tip does not drift. The resulting current values are used to form an I-V curve. Since the tip can be positioned over different areas of the surface, I-V curves can be obtained for different regions observed by the STM.

The positive bias voltage side of the I-V curves represents electrons tunneling from the sample into the tip, and with a negative bias voltage, electrons tunnel from the tip to the sample. The magnitude of the tunneling current is dependent on the availability of states that the electrons can tunnel from or to. For a semiconductor, the increased current is indicative of tunneling to states above the conduction band edge or from states below the valence band edge. This is because there are an increasing number of states available for tunneling of the electrons. The voltage difference between the different onsets of the current for the two bias polarities is the band gap of the semiconductor.

Examples of curves obtained from this method are shown in Fig. 3.7. The curves were taken at different points on the surface. The curves were repeatable at a single point and consistent at many different points. No spectra were obtained from the surfaces of the nuclei. In the graphs, the voltage separating the onsets of the currents is 2.5 V, approximately the band gap of
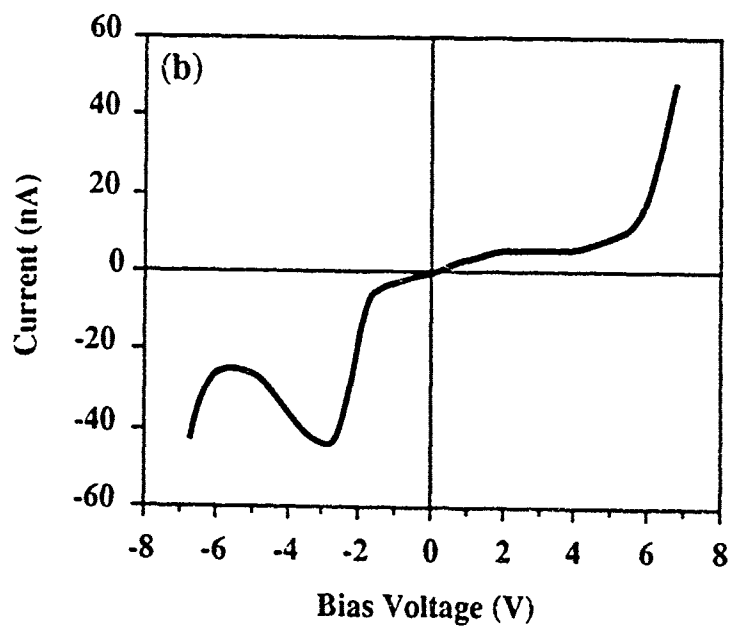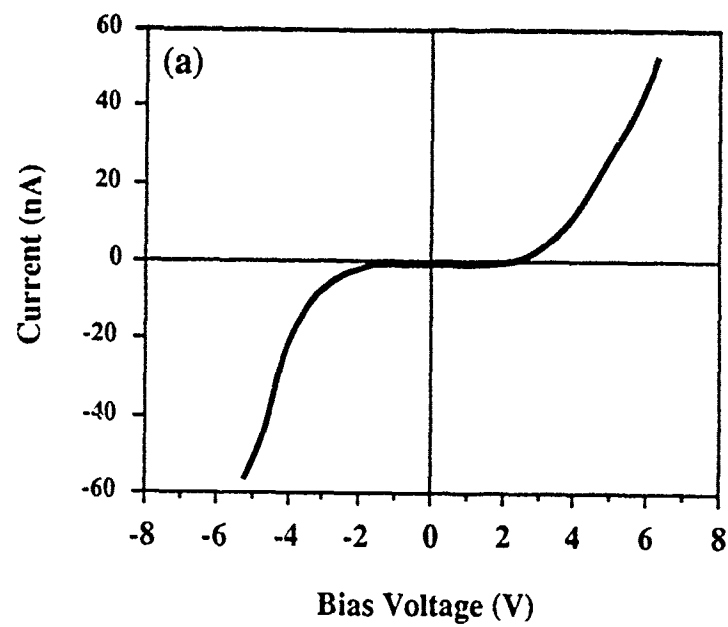
Figure 3.7
Tunneling spectroscopy I-V curves (a) and (b) showing the electronic structure at different points on the surface.

silicon carbide. The spectra shown in (a) was found at a majority of the points examined on the surface. The curve in (b) shows a different effect that was observed less often. A drop off in the current occurs at ~4 volts and starts to increase again at ~6.5 volts.

It must be noted that the tip used for the spectroscopic investigations was tungsten that was chemically etched. We have neglected the electronic structure of the tip in the interpretation of the STS results. Often, in metal-insulator-semiconductor tunnel diodes, negative differential resistance (NDR) can occur.[20] This effect can be observed in I-V curves when the slope of the curve becomes negative over a short range of the voltage. The feature in Fig. 7(b), in the voltage region between ~4 volts and ~6.5 volts, exhibits the characteristics of NDR. This feature may be explained in terms of double barrier tunneling. If the tip is over an area that is SiC, then the silicon and the silicon carbide form one junction and the tunneling gap and the metallic tip form the other junction. It should be noted that other mechanisms may also be possible.[21,22]

IV. Summary and Conclusions

The results presented here demonstrated the application of STM to explore the initial stages of diamond growth. An increase in the surface roughness of the modified surface of the silicon with growth was observed. The STM showed a difference in the roughness of the diamond nuclei and the modified surface layer with the diamond nuclei appearing much more smooth. Nucleation of diamond was observed, and the growth was found to occur along the scratches. The growth of the nuclei was observed to occur parallel to the surface. With the nucleation occurring in the scratches, this would imply that the

lateral growth of the nuclei conforms to the surface. Inspection of the nuclei revealed that they exhibited faceting and twinning. Most of the facets were found to be smooth to within the limit of the electrical noise. Other structures were found between some of the nuclei that may be precursors to intergrowth of the nuclei later on in the growth process. Through tunneling spectroscopy, changes in the surface were examined. The electronic properties of the modified surface show characteristics typical of the band gap of SiC.

Acknowledgments

References

1   Y. Saito and M. Kamo, Surf. Coat. Tech. **39/40**, 183 (1989).

2   T. Kawato, K. Kondo, Jpn. J. Appl. Phys. Lett. **26**, 1429 (1987).

3   L. M. Hanssen, W. A. Carrington, J. E. Butler, K. A. Snail, Mat. Lett. **7**, 289 (1988).

4   C.-P. Chang, D. L. Flamm, D. E. Ibbotson, J. A. Mucha, J. Appl. Phys. **63**, 1744 (1988).

5   S. Matsumoto, Y. Sato, M. Kamo, N. Setaka, Jpn. J. Appl. Phys. Lett. **21**, L183 (1982).

6   K. Kobashi, K. Nishimura, Y. Kawate, T. Horuchi, Phys. Rev. B **38**, 4067 (1988).

7   J. T. Glass, B. E. Williams, R. F. Davis, SPIE **877** (Micro-Optoelectronic Materials), 56 (1988).

8   V. Elings and F. Wudl, J. Vac. Sci.Tech. A **6(2)**, 412 (1988).

9   S. Matsumoto and Y. Matsui, J. Mater. Sci. **18**, 1785 (1983).

10   B. E. Willaims and J. T. Glass, J. Mater. Res. **4(2)**, 373 (1989).

11   B. E. Williams, B. R. Stoner, Ashbury, and J. T. Glass, Proc. of NATO Adv. Study Inst. on Diamond and Diamond-Like Films and Coatings, (1990).

12   D. N. Belton, S. J. Harris, S. J. Schmeig, A. M. Weiner and T. A. Perry, Appl. Phys. Lett. **54** (5), (1989).

13   H. Kawarada, K. S. Mar, J. Suzuki, T. Ito, H. Mori, H. Fujita, A. Hiraki, Jpn. J. Appl. Phys. Lett. **26**, L1903 (1987).

14   K. F. Turner, Y. M. LeGrice, R. J. Nemanich, to be published.

15   W. Zhu, A. R. Badzian, and R. Messier, J. Mater. Res. **4(3)**, 659 (1989).

16   R.J. Hamers, R.M. Tromp, J.E. Demuth, Phys. Rev. Lett. **56** 1972 (1986)

17   R.M. Feenstra, W.A. Thompson, and A.P. Fein, Phys. Rev. Lett. **56** 608 (1986)

18   P. Muralt, H. Meier, D.W, Pohl, and H.W.M. Salemink, Appl. Phys. Lett. **50** 1357 (1987)

19   R.M. Feenstra, J.A. Stroscio, and A.P. Fein, Surf. Sci. **181** 1668 (1987)

20   S.M. Sze, in <u>Physics of Semiconductor Devices 2nd Edition</u> (John Wiley & Sons, New York, 1981), p. 546

21   I. Lyo and P. Avouris, Science **245** 1369 (1989)

22   M. G. Youngquist and J. D. Baldeschwieller, to be published.

3.2 Photoluminescence of and Tunneling to Undoped Diamond

The ability to carry out tunneling experiments from undoped diamond regions is in itself unique since diamond has such a high electrical resistivity. When the results described in §3.1 were first presented there was no proven mechanism for conduction through undoped diamond. Since that time, the defect and impurity properties of undoped nuclei have been examined. This was accomplished through micro-photoluminescence (μ-PL) of the undoped nuclei. Some of these results were published elsewhere [1] and others are to be published [2]. A complete description of the apparatus is given in [1].

Results as they pertain to this thesis are presented in Figure 3.8. The curves in (a) and (b) were obtained from the 60 minute growth sample used in the nucleation study described in §3.1. In (a), the μ-PL was taken from a region with no obvious nuclei. The spectrum is relatively flat, showing the absence of optically active defects that region. The spectrum in (b) was taken from a region with nuclei present. A peak in the spectrum is observed at ~1.68eV. The curves in (c) and (d) were obtained from the 90 minute growth sample and are analogous to (a) and (b), with (c) obtained from a non-nucleated region and (d) from a region showing nucleation. Again in this case, a peak is observed at ~1.68eV for curve (d). It can also be discerned from the graph, the curves in (b) and (d) each show a Raman peak at 1332 cm^{-1}, which is attributed to diamond structure. The largest peak on all of the spectra is at ~550 cm^{-1}, and is signature of the Si substrate.

The peaks at ~1.68eV in curves (b) and (d) are at an energy near to that of the 1.674 eV GR1 peak found in photoluminescence (PL) spectra of single crystal diamond, which is due the presence of neutral vacancies. It has been

suggested that the 1.68eV feature in polycrystalline films is due to a complex involving silicon and/or nitrogen. [3,4] From a comparison of the curves (b) and (d), the relative intensity of the 1.68eV peak to the Raman diamond peak is greater in (d) than in (b). It has been shown that the relative intensity of this peak increases until after 7 hours of growth [1] and the absolute intensity increases more slowly for subsequent growth. This leveling off of the increase in the 1.68eV emission occurs at the same time that most of the silicon substrate has been covered by diamond. This result, taken in concert with evidence that Si is etched in the presence of atomic hydrogen, suggests that the peak is due to the incorporation of Si that has been etched from the substrate.

We suggest that the presence of the Si in the diamond lowers the resistivity of the diamond and therefore allow for conduction of tunneled electrons. This assertion is supported by results presented in §5.0, showing the presence of states in the gap, as shown in the density of states measurement. Results form §6.0, examining nucleation of diamond on other substrates, also substantiate this interpretation. For nucleation on Ge and Cu, μ-PL results show a peak at 1.68eV, but at a substantially reduced intensity relative to the Raman diamond peak. This is consistent since the etching of Ge and Cu by atomic hydrogen is less and therefore, there is less Ge and Cu incorporated into the diamond.

These results provide a basis for understanding tunneling experiments in undoped diamond. They also provide a rational for the difficulty found in imaging of undoped diamond grown on Ge and Cu. Since Ge and Cu are etched less by the presence of the plasma during the CVD process, and less of these atoms are incorporated into the diamond lattice, fewer impurities would

available to aid in the conduction of tunneled electrons. As proposed in §7.2, the growth of doped diamond nuclei on Si, Ge, or Cu substrates would allow for a comparison of the relative growth modes on each substrate.

It also provides a justification for the result that undoped diamond nuclei can be imaged at a greater variety of bias voltages than doped diamond nuclei can be imaged at. As shown in §5.0, there are more mid-gap states in the surface density of states of the undoped diamond, than in the surface density of states of the doped diamond. Excluding higher bias voltages that allow for tunneling into the conduction or valence band, there are more states that can be tunneled into for undoped diamond than for doped diamond This last result will be discussed more fully in §4.0.

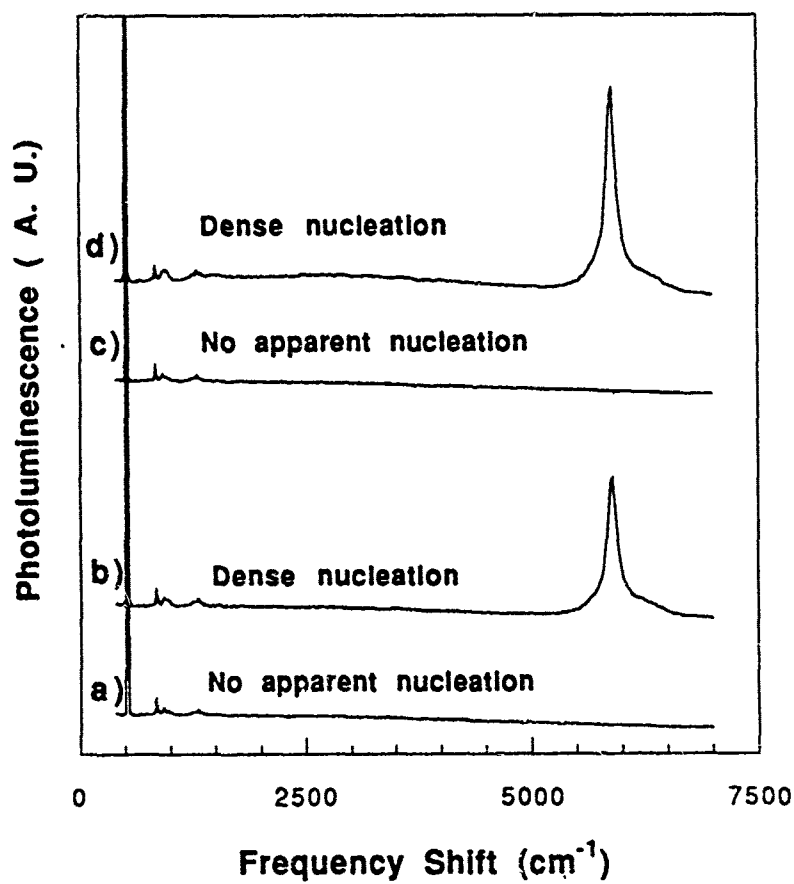**Figure 3.8**
Micro-Raman/photoluminescence of the 60 and 90 min growth samples. The curves (a) and (b) show the spectra for two points on the 60 min growth sample and curves (c) and (d) show the spectra for two points on the 90 min growth sample.

References

1   R. J. Nemanich, L. Bergman, K. F. Turner, J. van der Weide, and T. P. Humphreys, in *Proceedings of the 7th Trieste Semiconductor Symposium on Wide-Band-Gap Semiconductors*, edited by C. G. van de Walle, to be published.

2   L. Bergman, B. R. Stoner, J. T. Glass, and R. J. Nemanich, to be published.

3   A. T. Collins, M. Kamo, and Y. Sato, J. Mater. Res. 5, 2507 (1990).

4   J. A. Freitas, J. E. Butler, and U. Strom, J. Mater. Res. 5, 2503 (1990).

4.0 Examination of Further Growth: From Nucleation to the Formation of
Complete Films

I. Introduction.

The focus of this study is to investigate the nucleation and growth of CVD
diamond into a complete film. In §3.1, nucleation of undoped nuclei were
examined. As described in §3.2, for undoped films, the density of impurities,
that allow for tunneling characterization to occur, decreases with increasing film
thickness. Not enough samples have been examined to give the limiting
diamond film thickness for which STM investigations are not feasible. However,
for most samples, the analysis of undoped films by STM can include only the
nucleation stage of growth. To study the full development of the films with STM,
the material must be doped.

The analysis presented in this chapter can be broken down into three
areas: the nucleation of doped diamond on silicon and development of nearly
complete films, the effects of further growth on top of polycrystalline diamond,
and characterization of the interface between the diamond and the silicon. The
effects of the topography of the substrate and interaction between the substrate
and the diamond have on nucleation structure, and how the initial topography of
the diamond nuclei affect the final topography of the film will discussed in
section III. Secondary nucleation and growth structures that result from further
growth of diamond on top of complete diamond films will be examined in
section IV. The interfacial structure of a diamond film grown on silicon and the
evolution of the domain size will be considered in section V.

II. Experiment

The samples used to study the nucleation of diamond were prepared by microwave plasma CVD on 1 inch diameter p-type Si<100> substrates with resistivities between 0.005 and 0.02 Ω-cm. The substrates were polished with 0.25 μm diamond powder for 5 minutes and then solvent cleaned. The samples were exposed to conditions that lead to the growth of complete polycrystalline diamond films for 0.5, 1, 1.5, 5, 6 hours. In all cases, the growth occurred at a pressure of 35 Torr, a methane to hydrogen ratio of 0.5% with a total flow rate of 1000 sccm and an average substrate temperature of 800°C. Diborane was included in the gas mixture at a level of 10.0 ppm. SEM micrographs of the surfaces were obtained to provide an estimate of the nucleation density.

The complete films deposited on silicon were prepared by hot filament CVD on Si<100> substrates. The substrates were pre-seeded with diamond powder, and the gas flow of hydrogen, methane, and oxygen were controlled to obtain diamond growth. The thicknesses of the films were between 1μm and 2 μm. Diborane was introduced into the gas flow to dope the samples to the desired levels. The films were doped with gas phase concentrations corresponding to 6×10^{19}, 9×10^{18}, and 1.8×10^{18} per cm^3. The boron incorporation efficiency was determined to be approximately 20% by SIMS analysis.

The freestanding film used in the exploration of interfacial properties was originally grown on an n-type Si<100> substrate. The substrate was polished with 0.25 μm diamond powder and then solvent cleaned. The sample was grown for 27 hours. The growth occurred at a pressure of 90 Torr, a methane to hydrogen ration of 0.5% with a total flow rate of 100 sccm and an average substrate temperature of 900°C. Diborane was included in the gas mixture to dope the film and a dopant concentration of ~1000 atom/cm^3 was subsequently

measured by SIMS. The silicon substrate was removed by chemically etching using a solution of nitric and hydrofluoric acid.

Raman spectroscopy was employed to verify the presence of diamond in all of the samples and determine the relative presence of diamond and graphitic structures. Photoluminescence was also employed to examine the defect structures of the samples.

The STM analysis of the surface was done using a wide range of parameters with both a Park Scientific Instruments STM-SA1 or an RHK ATM-500 STM. The scans of the surface covered ranges between 100Å - 10μm. The tip was scanned at rates corresponding to between 0.08 to 2 Hz and tunneling currents ranging between 0.2nA to 4nA. The tip bias was optimized for each of the samples in order to enhance imaging of that particular film and substrate.

III. Characterization of Doped Nuclei and Incomplete Films

It follows that the early nucleation structure affects the properties of the completed film. If, for example, the growth of two-dimensional platelet nuclei could be enhanced, then larger grain polycrystalline films could be achieved with better quality electrical properties. By following the development of nuclei into a complete film, it may be possible to change growth conditions to enhance or retard certain factors which control the final properties of the film.

Many of the same results obtained for undoped nuclei (§3.1), also hold true for nucleation of doped diamond. These results include observation of the growth of a carbon layer on the surface as a function of time, of faceted nuclei in or near scratches used to enhance nucleation, and observation of both two-dimensional and three-dimensional growth. Examples of these different growth modes are shown in Figure 4.1. Both topographs show diamond nuclei after
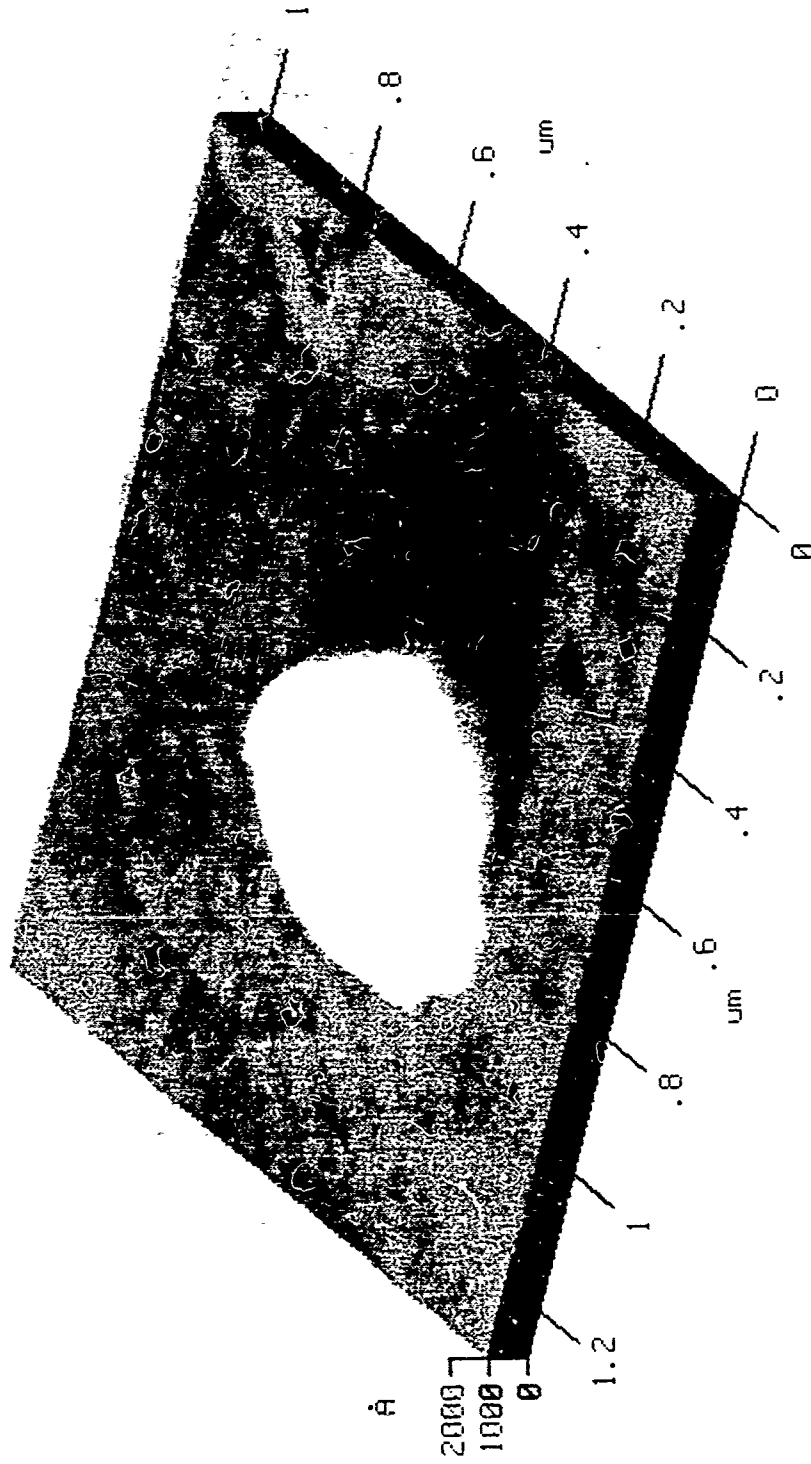
Figure 4.1

An STM image of a single diamond nucleus on silicon(a), and several nuclei (b) both after one hour of growth. Both images were obtained from the same sample.
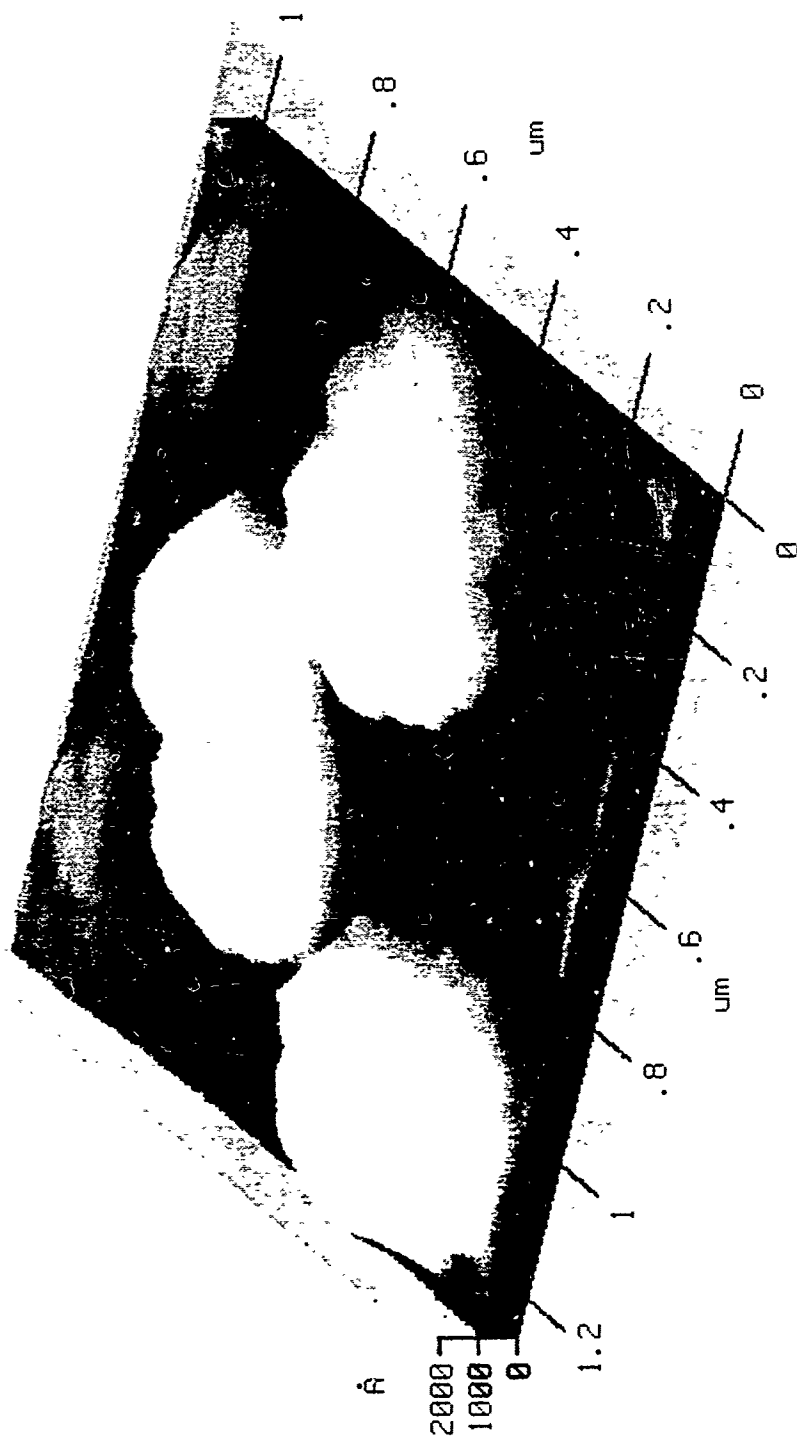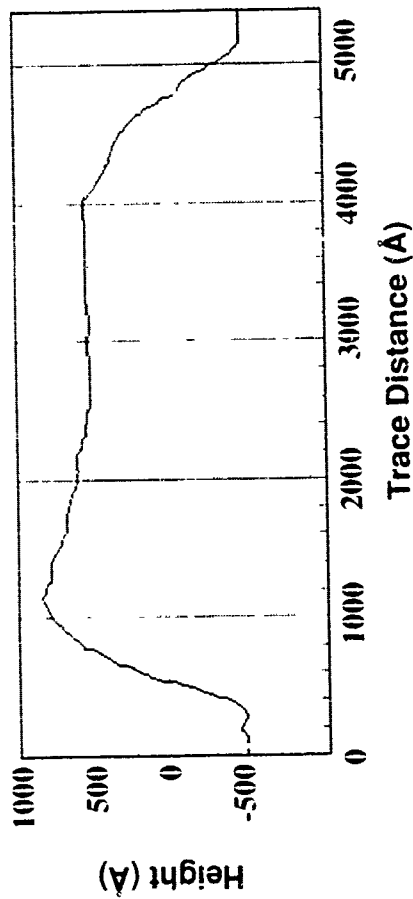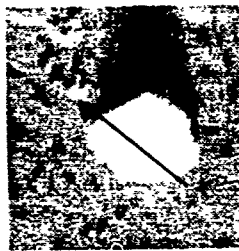
(b)

Figure 4.1 (Continued)

one hour of growth. The nucleus shown in Figure 4.1 (a) is flat on "top" and most of its growth has been parallel to the substrate. In contrast, Figure 4.1 (b) shows nuclei that appear to have grown three-dimensionally. As all the nuclei were grown on the same substrate, under the same growth conditions, for the same period of growth, there must be some effect that is causing the different nucleation morphologies.

A majority of the nuclei, ~80-90%, observed on the surface were three-dimensional and it is not fully understood why a minority of them exhibit two-dimensional growth. This result is inexact as only approximately 200 nuclei were examined to arrive at the 80-90% figure. It is most likely that the two types of topography seen for the diamond nuclei represent different modes of growth. Angus et al [1] have speculated that hexagonally shaped platelets, similar to what has been observed here, can arise from the growth of nuclei with two or more parallel twin planes. It would appear, therefore, that for the growth conditions of this study, the conditions that produce nuclei with two or more parallel twin planes are less favorable, and this would explain the minority status of the two-dimensional nuclei.

Figure 4.2 shows cross-sections taken of diamond nuclei presented in Figure 4.1. Each graph shows the height relative to the displacement along the arrow shown on the image to its left. The top graph shows the structure of the flat, two-dimensional nucleus. The surface of the top of the nucleus is flat except at the beginning of the cross-section. This rise is probably due to the fact that the nucleus was imaged from left to right, and is a result of the response of the STM. This response is often observed when material the STM is tunneling to changes conductivity rapidly. A similar effect, though not as drastic, is observed in delineation of pn junctions by STM [2]. The lower graph shows the

(a)

Height (Å)

1000　500　0　-500

0　1000　2000　3000　4000　5000

Trace Distance (Å)

(b)

Height (Å)

1000　500　0　-500　-1000

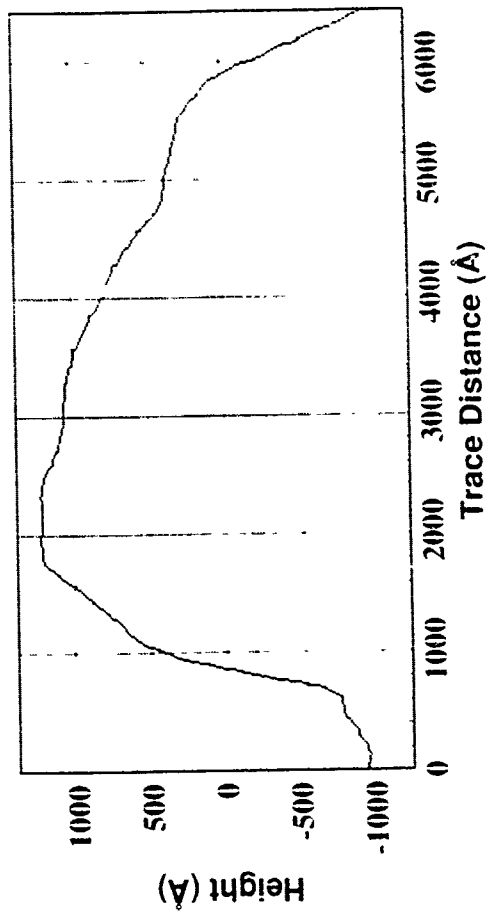0　1000　2000　3000　4000　5000　6000

Trace Distance (Å)

Figure 4.2

Cross-sections showing the surface topography of diamond nuclei. The cross-sections were obtained along the directions of the arrows shown in images to the left of each graph.

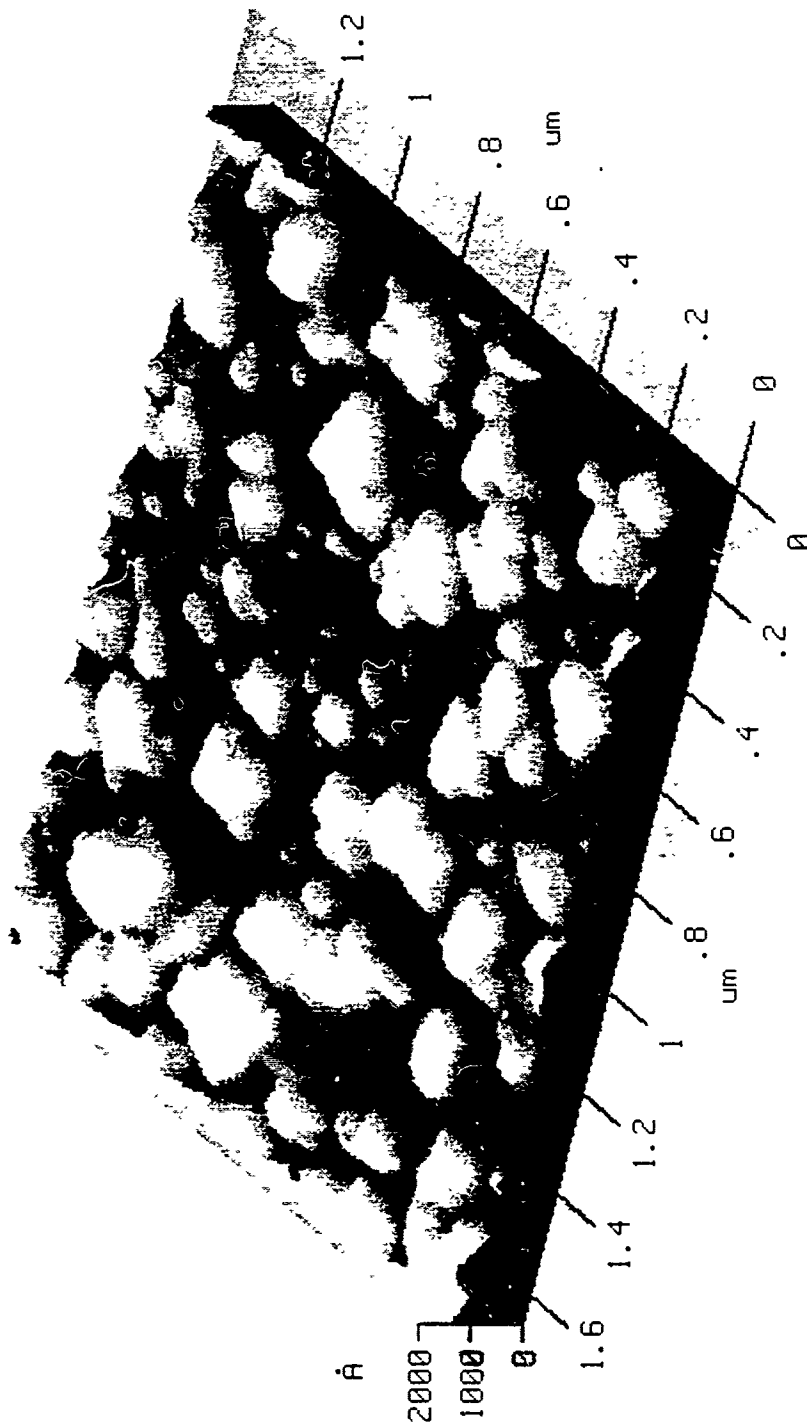**Figure 4.3**

(a) STM image of dense nucleation at the intersection of two scratches and (b) a higher resolution image of the same region. Note the variations in the sizes of the nuclei.
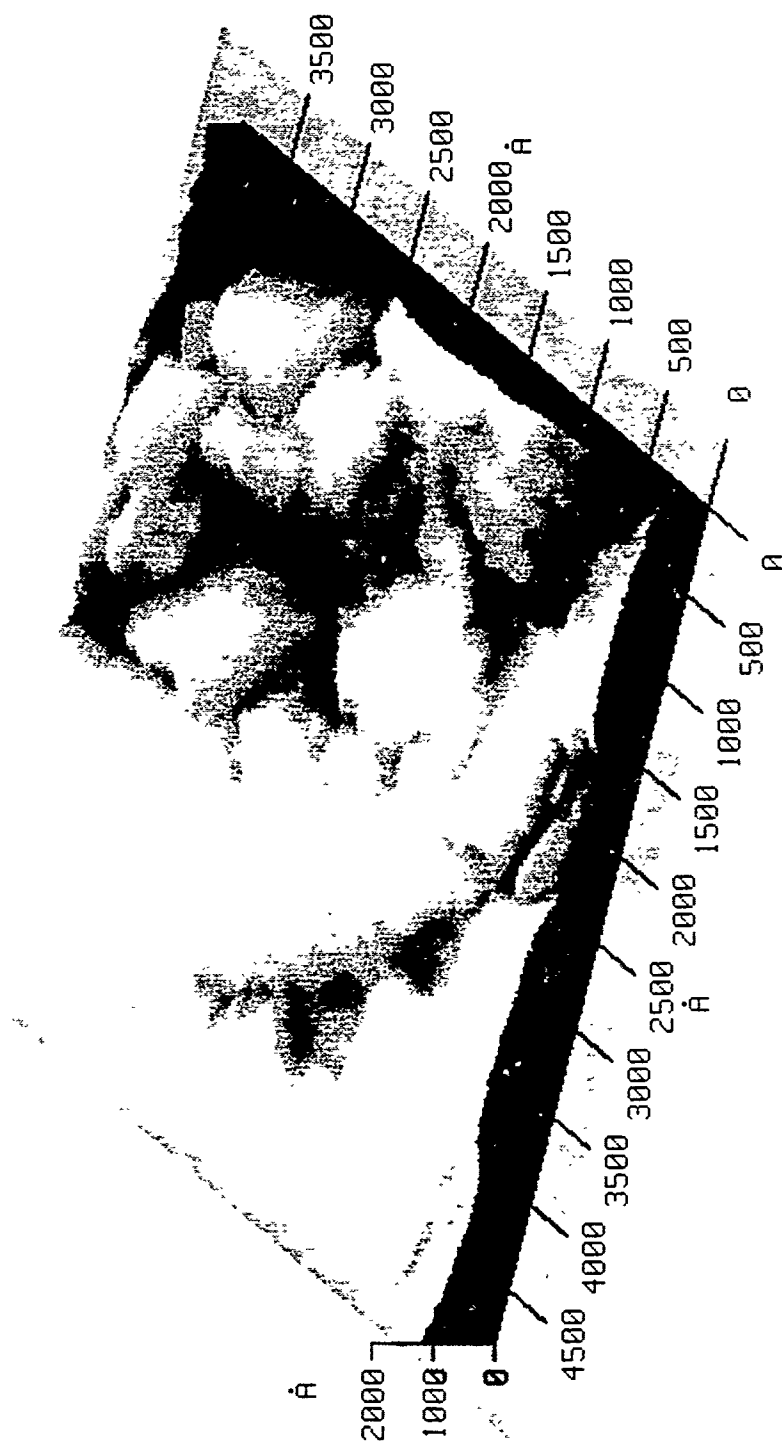
Figure 4.3 (Continued)

(b)

cross-section of the three-dimensional nucleus. This cross-section shows more regions of distinct slope relative to the plane of the substrate. This is consistent with its three-dimensional growth.

The scratches made on the silicon to increase nucleation were observed for the case of doped diamond nucleation also. They were found to be consistent with those found on the substrates used for undoped growth. The scratches were measured to be between 80 - 100Å deep and varying in width from 250 - 1200Å.

As the growth process continues, the nuclei eventually grow together. At the scratches, where the nucleation density is approximately ten times greater than elsewhere on the substrate, this process occurs sooner. Figure 4.3 (a) shows an area where several scratches intersected, and the nuclei have grown together. The image in Figure 4.3 (b) shows this region in greater detail. The structure is similar to that of more complete films that will be discussed in section V, with the exception of the smaller size of the particles. It should also be noted that there is evidence of secondary nucleation in this region even though the growth has only progressed for one and a half hours.

In the center of the image in Figure 4.3 (b), many overlapping triangular planes were observed. There are two possible explanations for this observation. The first is that these are the growth planes of diamond which have nucleated on the side of a scratch, which is at an angle relative to the plane of the substrate. This is consistent if the nuclei are conforming to the surface of the scratch. On the surface, this type of growth would appear to be inconsistent with the model given in §3.1. It is consistent if the conformal growth in the scratches occurs for scratches of large depth and width. As reported above, the topography of the scratches on the silicon the same for both doped

and undoped experiments. Examination of Figure 4.3 (b) suggests that the particles have nucleated at the meeting of scratches of very large topography. Then, in this case, the structure of the scratch is the topography that the growth of the original nucleus conforms to.

A second possible explanation for the observed triangular planes is that they are due to the overgrowth of other diamond nuclei. In this hypothesis, the diamond nucleates in a scratch and conforms to the planer surface near the scratch, as suggested in §3.1. Because the density of nuclei is high in the area near the scratch, the nuclei begin to grow together. Eventually, there can be growth between the domains of different nuclei, as detailed in section V of this chapter, and overgrowth occurs. Examination of Figure 4.3 (b) suggests that the observed triangular planes are the overlapping each other, supporting this hypothesis. Without the actual dimensions of the scratches, which are hidden by the nucleation of the diamond, it cannot be determined which explanation is correct.

After five hours of growth, most of the silicon surface is covered with diamond. Figure 4.4 shows the surface of the film including many regions where no nuclei could be observed. It is likely that these regions are "pinholes" in the incomplete diamond film. The image in Figure 4.4 (b) shows the structure of the nuclei that cover the surface, as shown in Figure 4.4 (a). The surface is still smooth and the average observable grain size is ~850Å. The average roughness of the surface, taken from the image shown in Figure 4.4 (a), was 212Å with a peak to peak range of 2528Å. When compared with the surface after six hours of growth, as shown in Figure 4.5, the density of pinholes decreased 60%, with only minor changes in the observable grain size. This figure, of 60%, is only approximate because it is not possible to determine if an

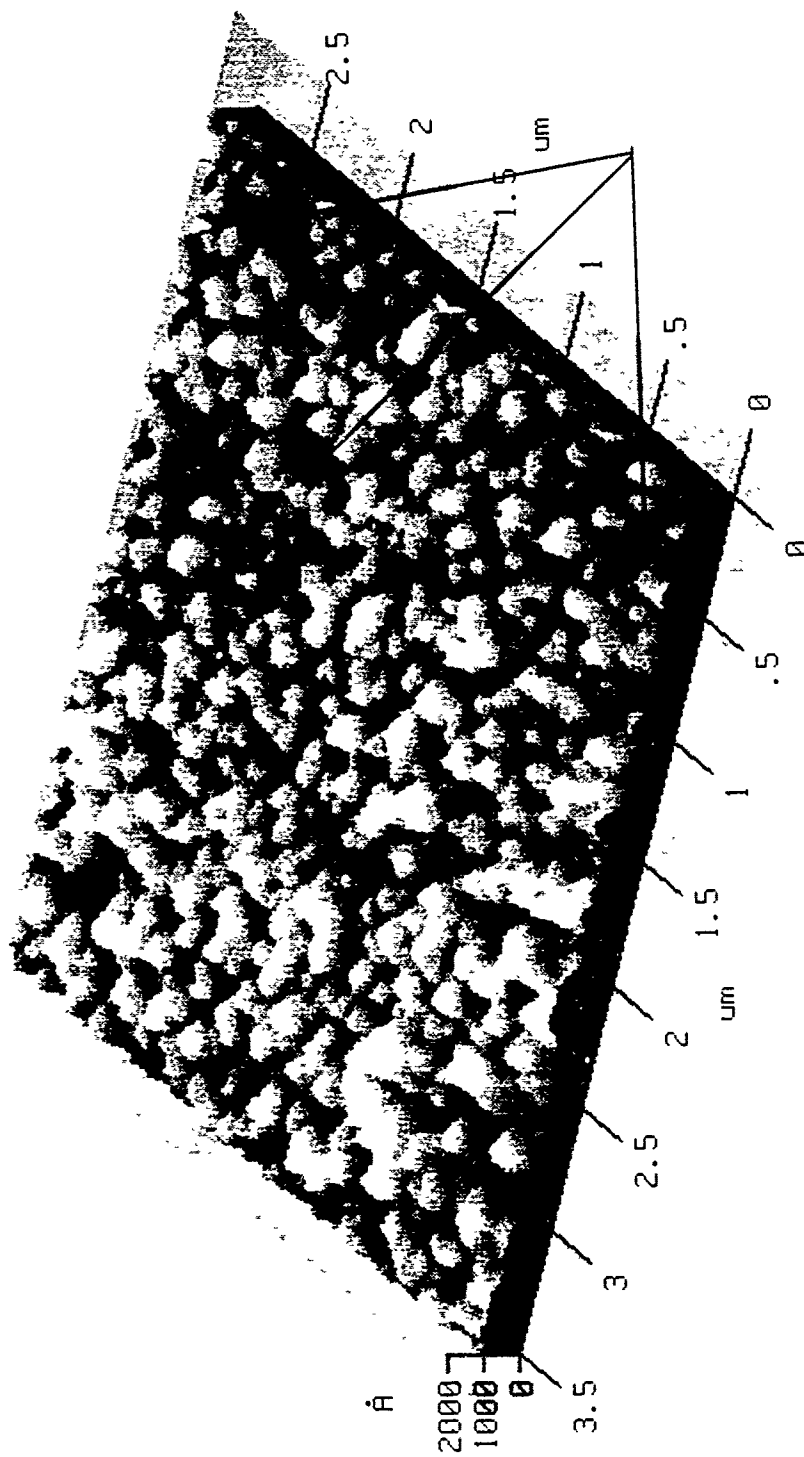**Figure 4.4**

STM image of a diamond covered surface of silicon after exposure to growth conditions for 5 hours. Note the visible "pinholes" in the film. The image in (b) shows the size of the grains.
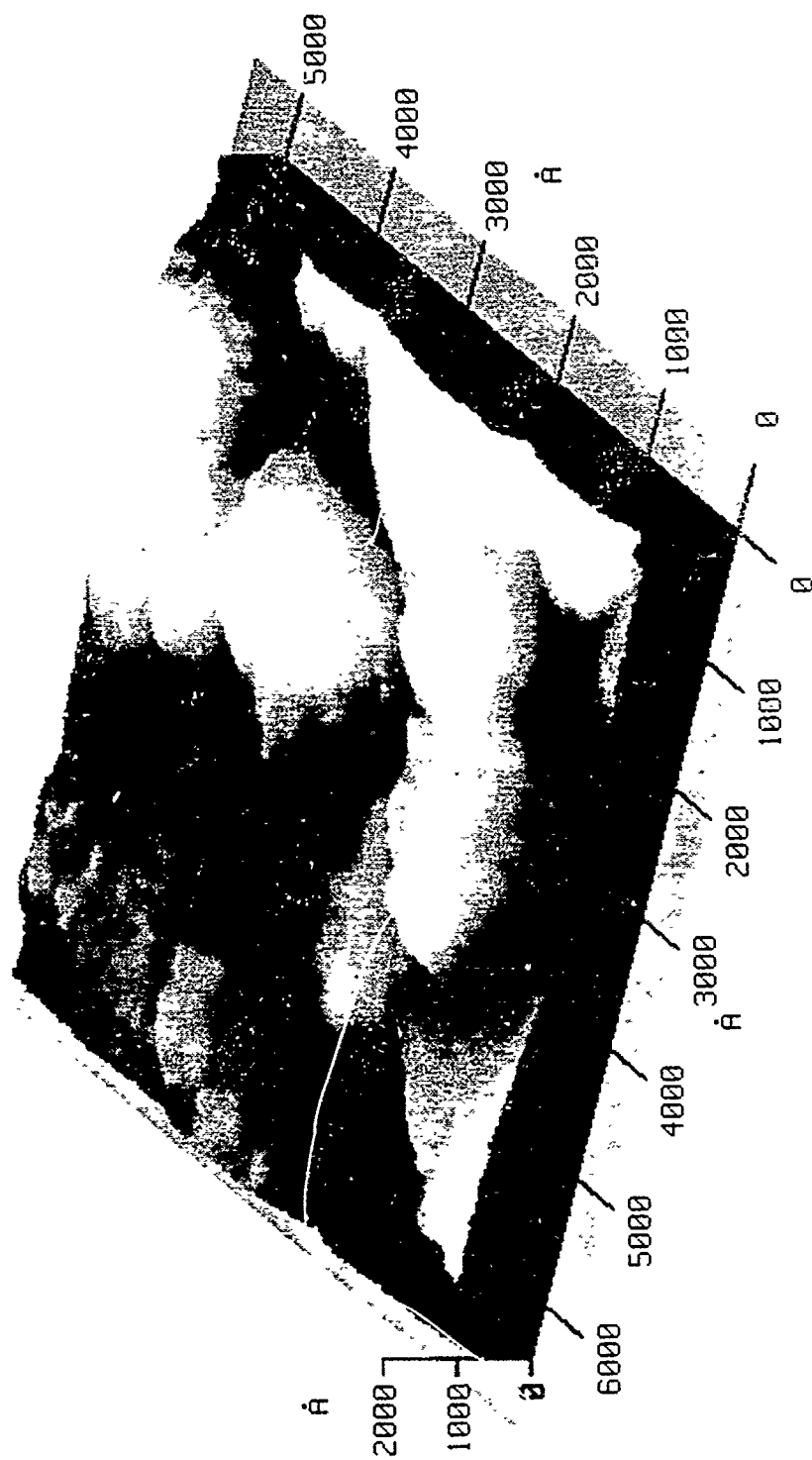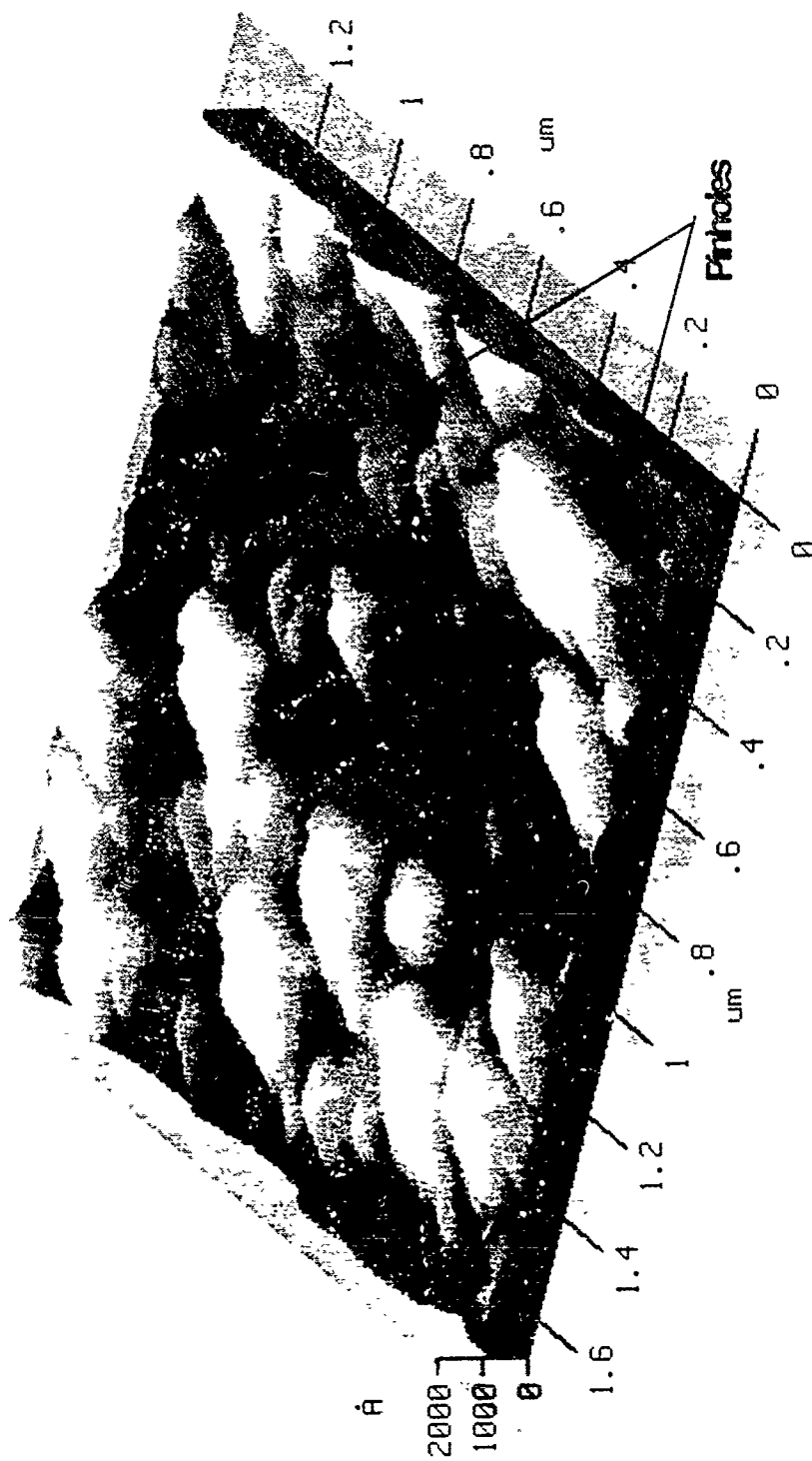
Figure 4.4 (Continued)

(b)

Figure 4.5

The surface after 6 hours of growth. There are only two regions of this scan that are not visibly covered with diamond.

"average" region was imaged of the 5 and 6 hour growth samples. This uncertainty arises because the STM can only examine a maximum area of 8μm by 8μm , and variations of nucleation density are found to occur over the entire surface of a 1" Si wafer.

IV. Growth Structures on Complete Films

For comparison, the thicker doped films used in this section were grown for ~20 hours, but this must be taken as relative, because the samples were grown in different CVD systems under similar conditions. On a large scale, the topography is exactly the same as could be discerned from a scanning electron microscope image of the surface. The more interesting structure can be found on a smaller scale.

Most of the facets of the surface domains were smooth to within 20Å, but some facets showed detectable structure. On the facets that showed structures, ridges were observed that ran parallel down the facets, and example of this is shown in Figure 4.6 (a). The line in Figure 4.6 (a) runs perpendicular to each ridge. The ridges, in this example, are separated by ~1200Å with a depth of approximately 100Å relative to the surface of the facet. On other facets, the spacing of the ridges and their relative heights are different from the above example, but in each case the heights and spacings were consistent over the entire plane of the facet. On one facet, a structure analogous to the elongated ridge structures described below was discovered. This structure is shown in Figure 4.6 (b). The length of each ridge is 800Å and each is ~25Å in height and ~ 150Å in width. It is interesting that the same structure is found on two different scales on the same surface. The possible purpose of this type of growth will be discussed below.

Figure 4.6

STM images of: (a) Ridges on the surface of a facet on the complete doped diamond film. (b) Elongated ridge structures found in one of the ridges.
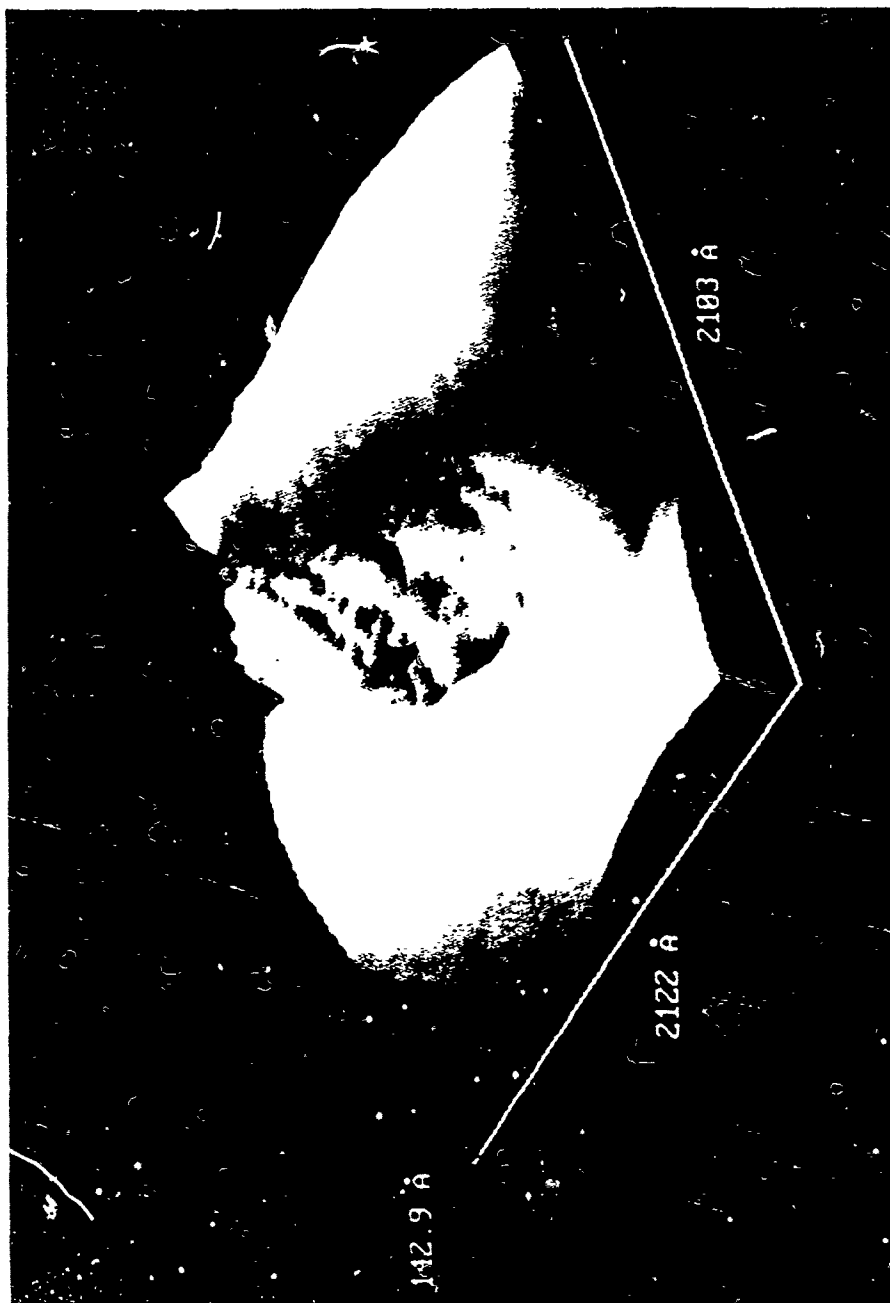
(a)

2183 Å

2122 Å

142.9 Å

(b)

Figure 4.6 (Continued)

Another aspect of the topography of the surface was the triangular shaped islands found at the intersection of domains. These structures have been observed on the flat areas between planes. These structures can be seen in Fig. 4.7. The sides of the islands are parallel to each other with the longest sides parallel to the plane of the closest facet. All three of the islands have a triangular shape roughly in the same proportions. The angles are the same to within 10° when measured from the top-down view, and the smaller islands are 10% and 30% smaller than the largest shown. The lengths of the sides of the islands range from 580Å to 240Å. The islands resemble the pyramidal nucleation that is often seen on {111} facets, but only on a much smaller scale.

The third type of areas that were examined are regions where there is growth between different domains. Elongated ridge structures have been observed between facets in areas where overgrowth has occurred. A long range view of the area that is probably formed by the re-entrant junction of two planes is shown in Figure 4.8 (a). A closer view of the elongated ridge structures is shown in Figure 4.8 (b). A cross-section of these structures is shown in Figure 4.8 (c), along the line shown in Figure 4.8 (b). The lengths of these ribbons vary from 1400Å to 500Å at the bottom of the figure. The relative height of the structures above their lowest level between the facets is between 25Å and 30Å. Their spacing varies but the larger ribbon sections are spaced ~800Å apart.

On a much larger scale, encompassing scanning regions of several microns, similar results have been reported from SEM observations [3]. The structures observed by SEM were between {111} faces and were wider and longer than the structures observed by STM here. Clausing and others identified these as regions of fast deposition and asserted that they were trian-

Figure 4.7
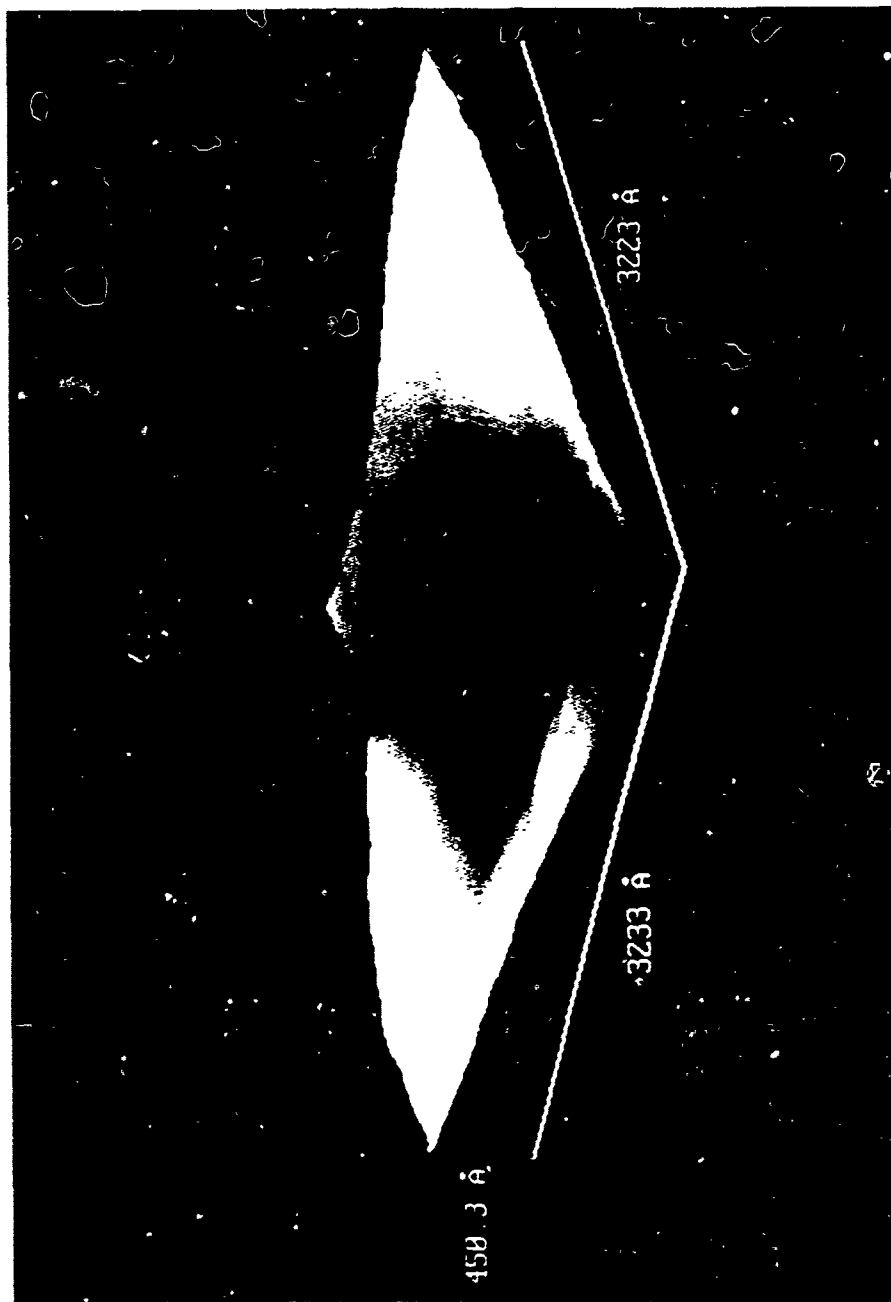Triangular islands in a region where two domains intersect.

(a)

Figure 4.8

(a) Long-range view of the intersection of two facets where there are elongated ridge structures. (b) Close-up view of the elongated ridge structures. (c) The surface topography along the line joining points **A** and **B**.
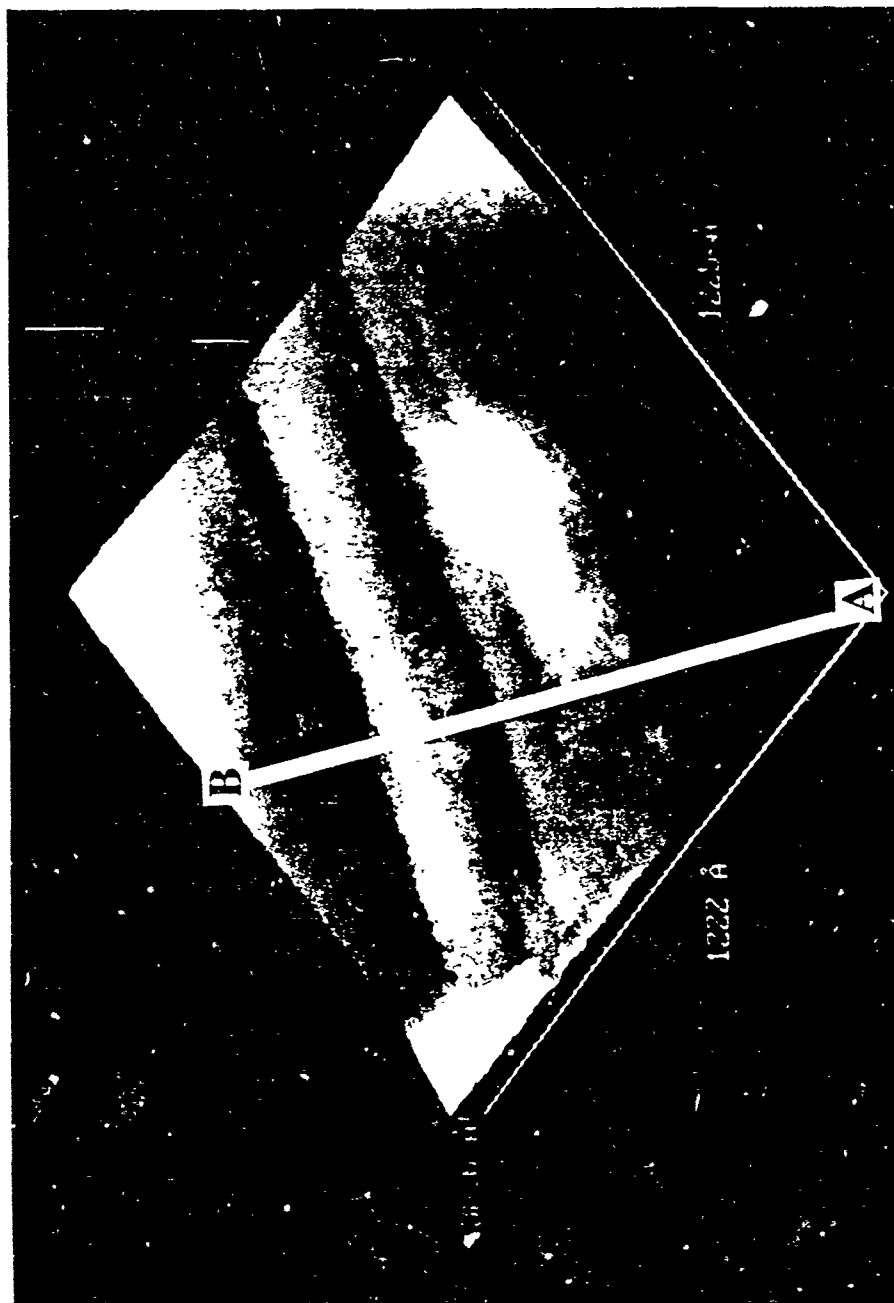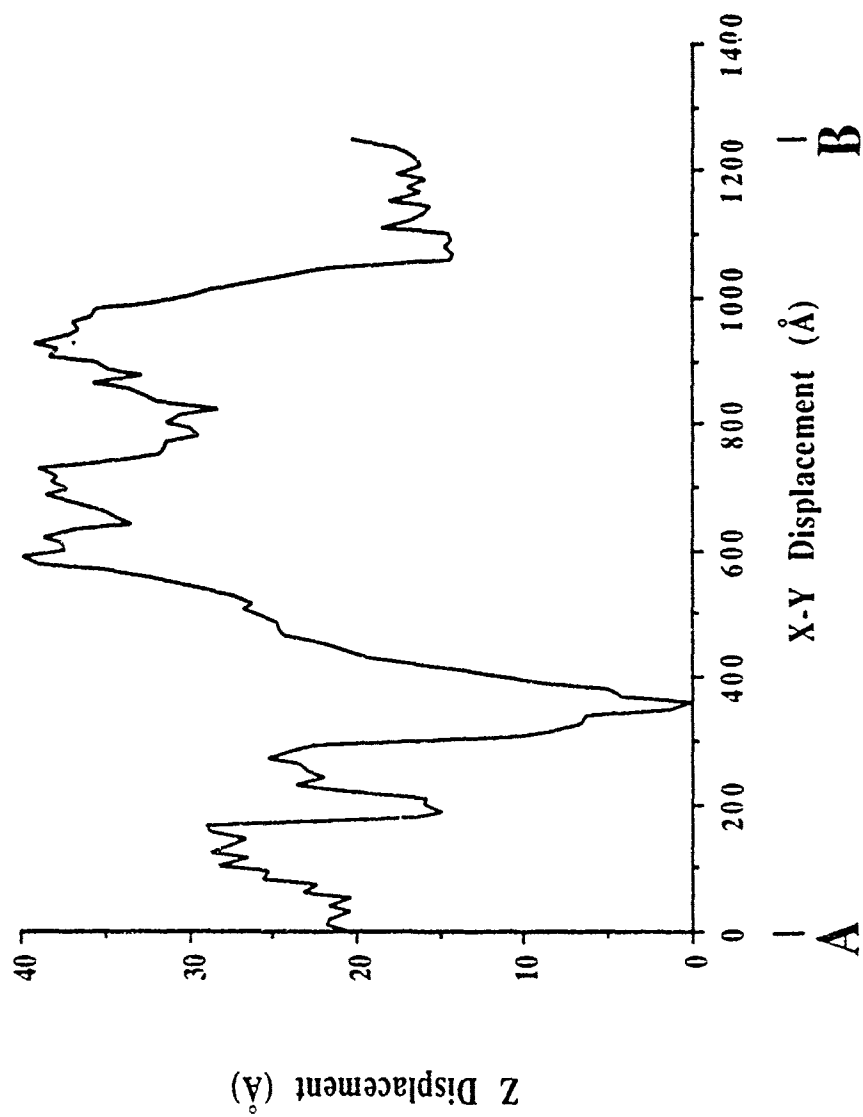
Figure 4.8 (Continued)

(b)

Figure 4.8 (Continued)

(c)

gular features of exposed {111} planes. The similar structures observed by STM may have the same functions at their respective scales, which is to provide an area of easy nucleation for species from the gas phase and to allow transfer of material to the facets to create faster growth [3].

V. The Interface Between Diamond and Silicon

The advantage of examining a freestanding thick diamond film is that it allows for characterization of the final polycrystalline surface and the interfacial properties that led to the final structure. By etching back the silicon substrate, observation of the nucleation structure and an examination of the initial growth structures is possible .

The growth surface of the thickest film is very similar to the topography observed for the complete polycrystalline diamond films, discussed in section IV. Figure 4.9 (a) shows the surface of a thinner film imaged by STM, such as those described in section IV. Figure 4.9 (b) shows an STM image of the growth surface of the freestanding film. The measured grain size is between 3 and 5μm. Like other diamond films, this surface shows evidence of growth structures and both smooth and rough facets. These results were discussed fully in the last section.

Figure 4.10 (a) shows the etched surface of the freestanding doped film. The ridges on the surface are the result of growth in and along the scratches that were made in the silicon to increase nucleation. The areas of largest height shown in the image probably represent areas of incomplete etching of the silicon. Figure 4.10 (b) shows another view of the ridges on a smaller scale.

The surface is relatively smooth, with a measured RMS roughness value of 144Å, over a 1344Å range of heights , excluding the regions which are due to

(a)
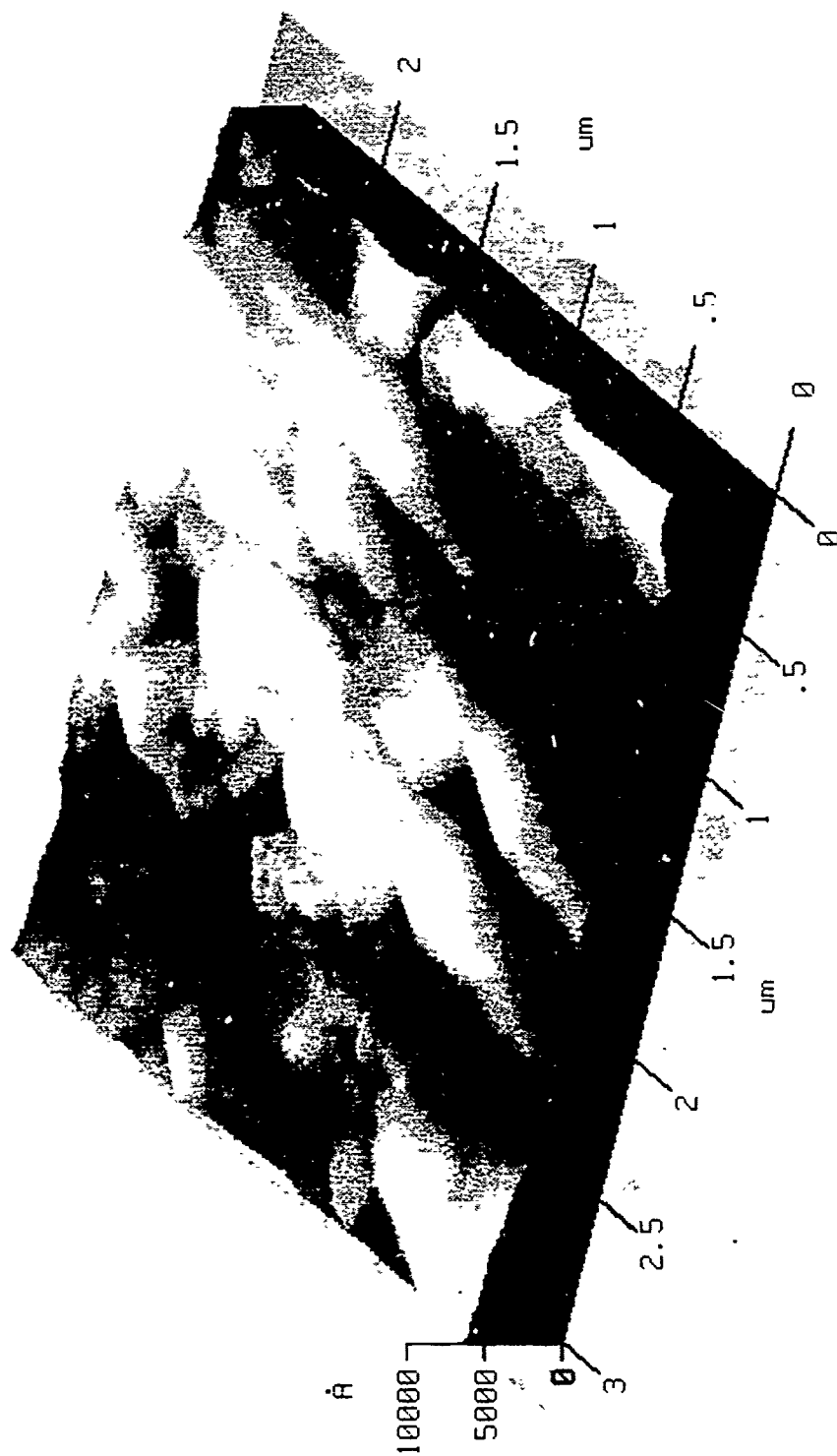
Figure 4.9

STM image of (a) the surface of a ~1.5μm thick polycrystalline diamond film deposited on Si, and, (b), an image of the growth surface of a freestanding diamond film of ~11 μm in thickness.
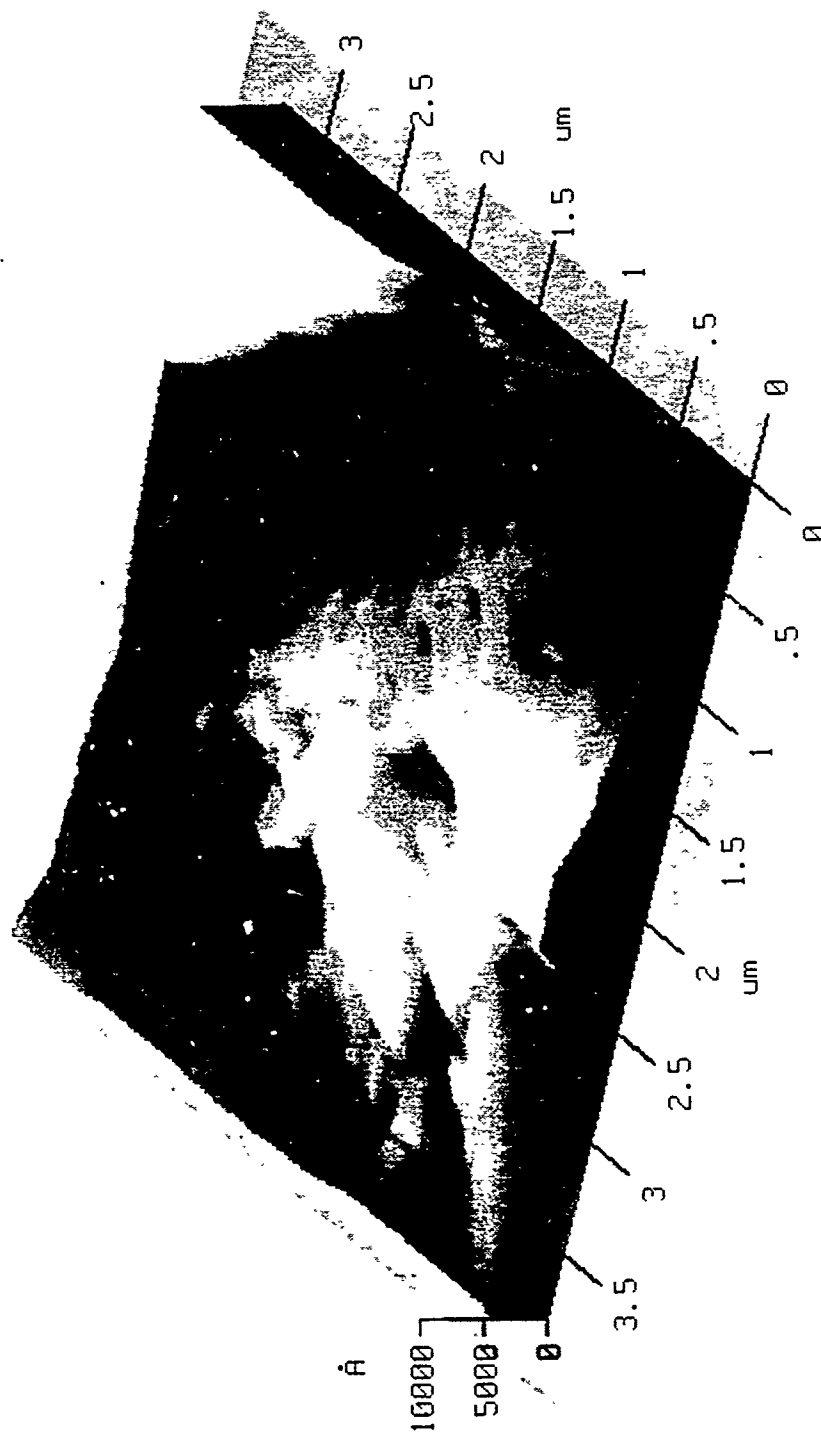
Figure 4.9 (Continued)

(b)

Figure 4.10

STM image of the etched surface of a freestanding diamond film. (a) The ridges represent regions where diamond grew in the scratches made in the Si, which was etched away. The images in (b) and (c) show the same region at smaller scan ranges.

(a)

Figure 4.10 (Continued)

(b)

Figure 4.10 (Continued)

an incomplete etch. The surface has a crystallite size of ~800Å, which is approximately equal to that of the 5 hour growth shown in Figure 4.4. This is consistent with the notion that secondary nucleation and growth perpendicular to th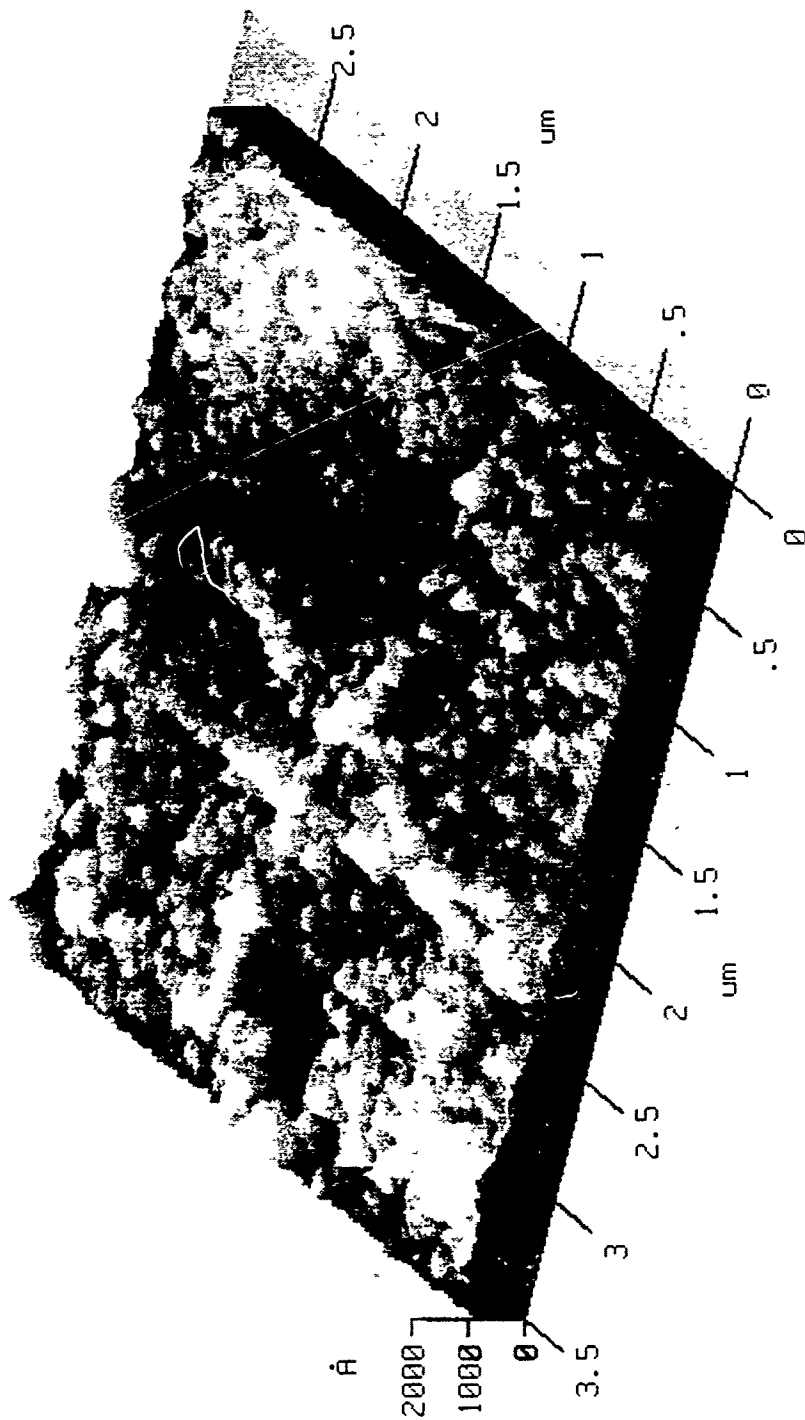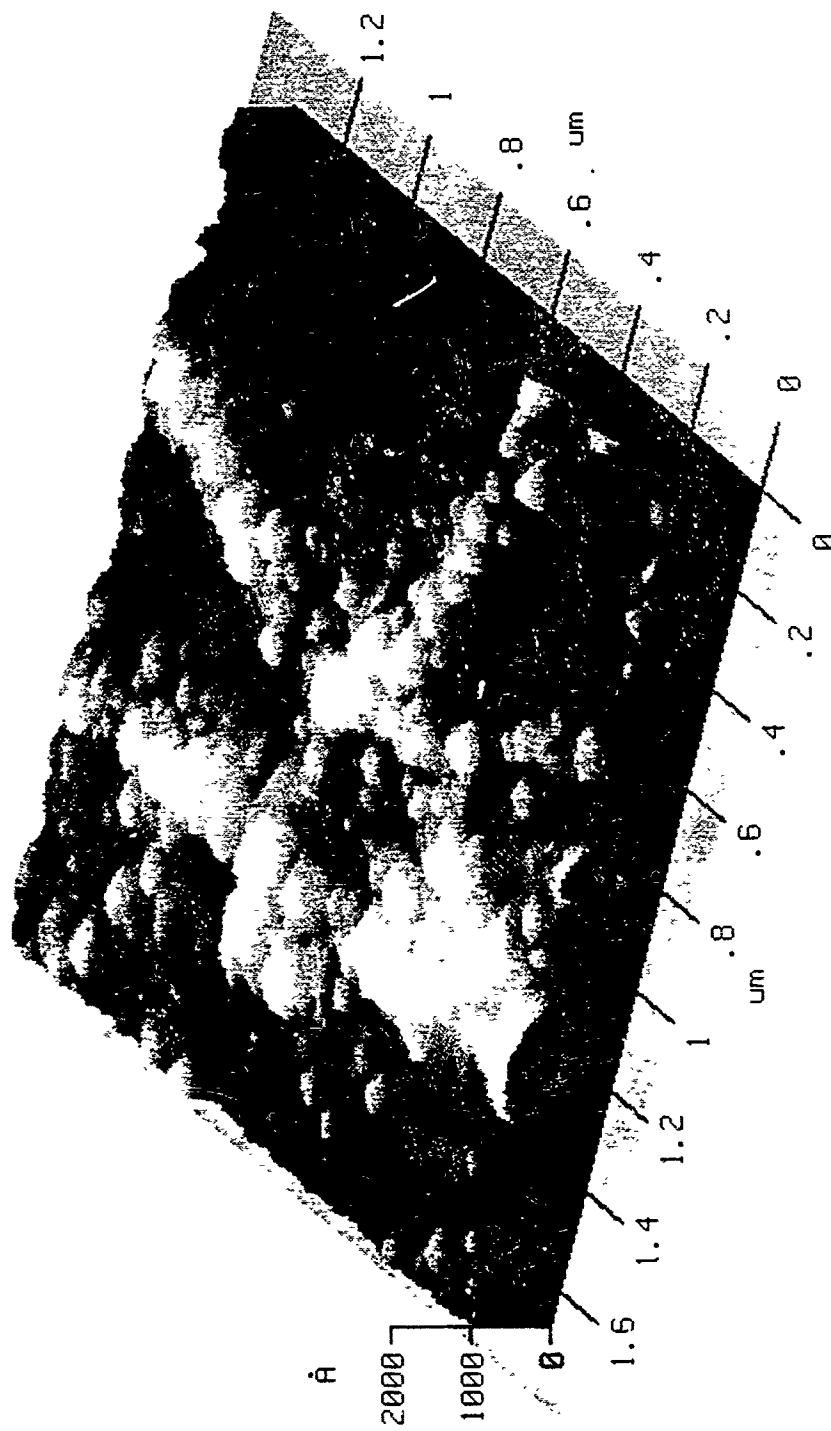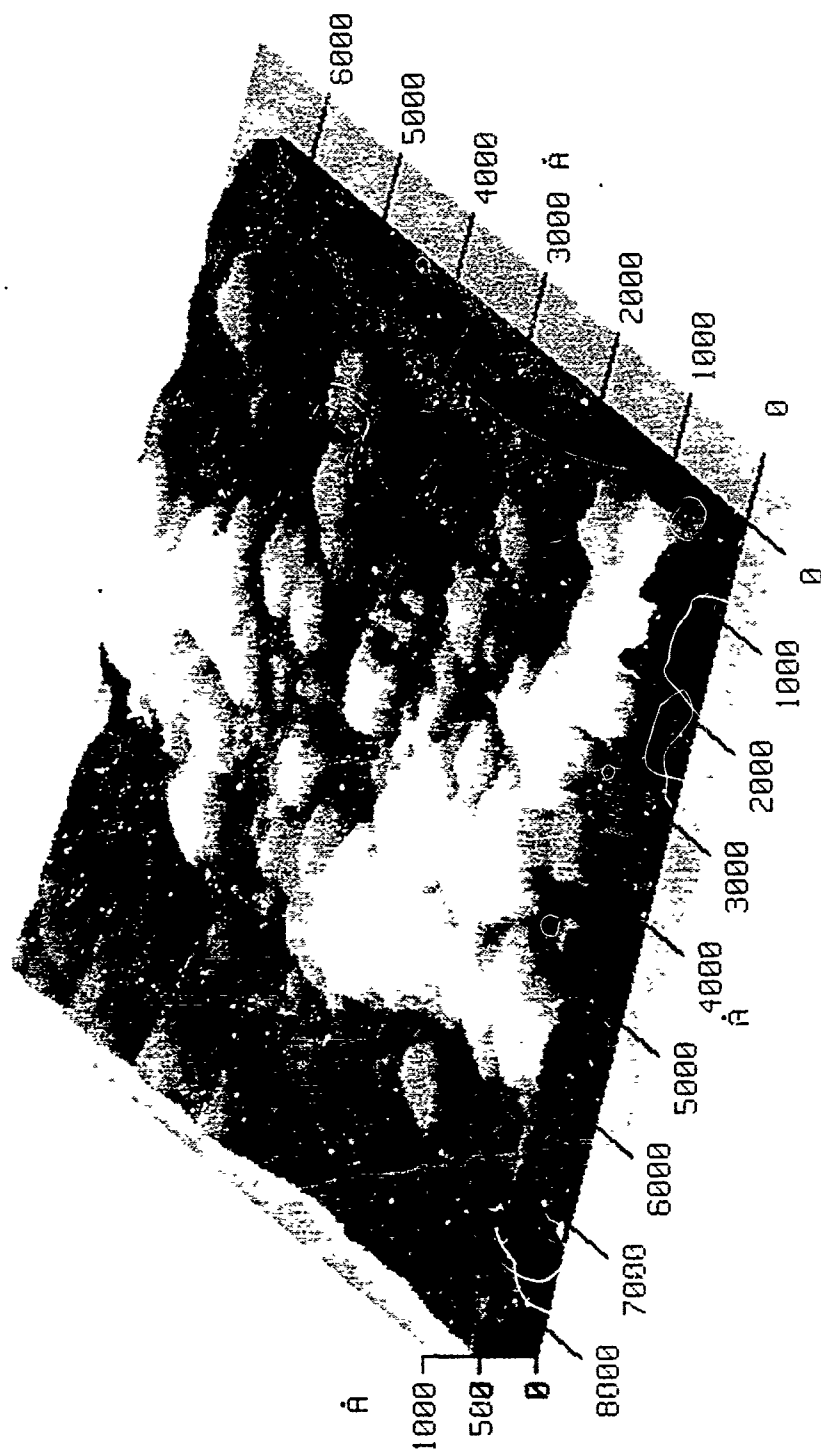e surface predominate after the surface is mostly covered by diamond. It is also consistent with changes in the grain size observed for diamond films viewed in cross-section by Graebner and others. [4] In the study cited, the authors found that the average grain size increases with increasing height above the substrate, from less than 1μm at the bottom to ~ 35μm at the top. Graebner and others note that the measurement of the average grain size at the top is actually considerably smaller than was measured, because of secondary nucleation and irregular growth morphology. With this taken into account, the results presented here are consistent with the results cited in [4].

A closer view of the criss-crossing ridges is shown in Figure 4.10 (c). This view affords a betters estimation of the observable grain size, which is ~800Å. It is difficult to observe whether there is a critical nucleus size from the this topograph. By plotting the curvature, instead of the height, as a function of position, a critical nucleus size can be estimated. A plot of this curvature versus displacement is shown in Figure 4.11. On most of the domains, a small protuberance is observed near the edge of the crystallites. On a curvature plot, a protuberance represents an area of positive concavity or a small protrusion. The size of these bumps is ~60-100Å. These bumps are more often observed on domains which are on top of the ridges.

Considering §2.2, we assume that nucleation was preceded by the formation of clusters on the surface during the initial stages of growth. We also assume that these clusters formed on the silicon substrate. As the clusters mature into nuclei, there is growth of carbon layers on the areas near the nuclei.

Figure 4.11

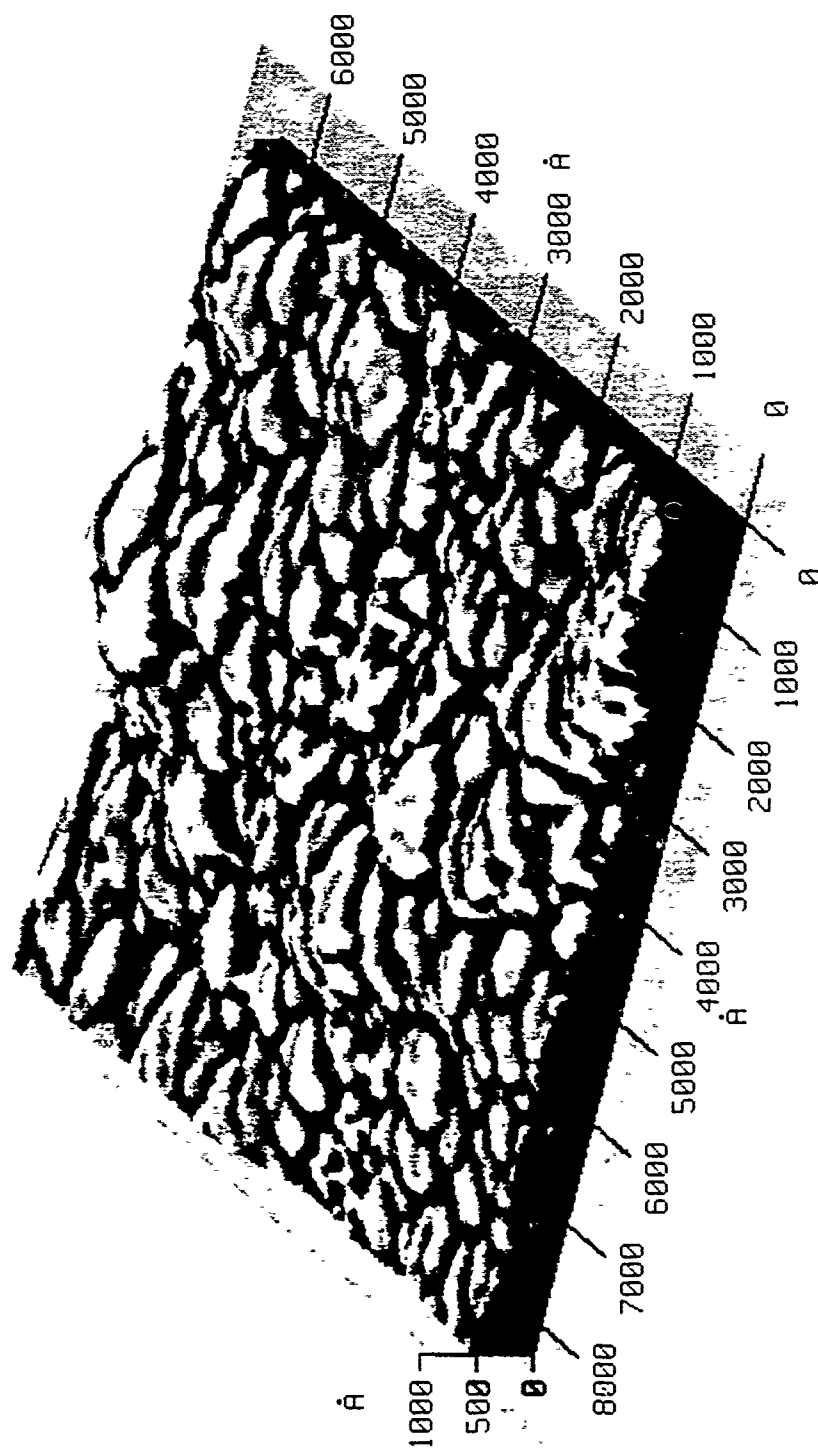Curvature plot of the etched surface of the freestanding diamond film. The curvature is the change in the height versus the change in vertical displacement for each point on the surface, and was obtained from the STM image shown in Fig. 4.10 (c)
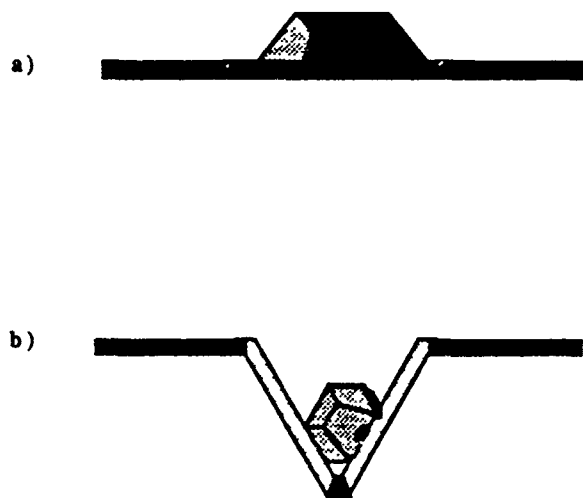
Figure 4.12

(a) Schematic showing the possible growth of a nucleus on a flat region. (b) Schematic showing the possible growth of a nucleus inside of a scratch.

This film growth on the silicon substrate was documented in §3.1. When the substrate is etched off of the thick diamond film, there will be unequal etching of the areas where the nuclei originated from and the areas where they did not. We propose that this is the origin of the bumps observed in the curvature data.

If, then, we assume that these bumps are the sites of original nuclei, which have nucleated near the bottom of a scratch, it is evident that these nuclei would grow differently than nuclei which originate on a relatively flat surface. The constraints of the topography of the scratch would limit the possible directions of growth. For a nucleus on a flat surface, further growth parallel to the surface would obscure the initial nucleus. For the case of nuclei growing in a scratch, the bumps observed may be these critical nuclei, and thus an estimation of the critical nucleus is ~60-100Å. A schematic showing these two situations is presented in Figure 4.12. This result is supported by the fact that the bumps are not at the highest points of each particle, but rather near an edge. This is consistent with a cluster nucleating on the side of a scratch, and conforming to the surface of that scratch, as the schematic in Figure 4.12 (b) shows.

VI. Summary and Conclusions

From the study of nuclei over different periods of growth we can conclude the following: A majority of the nuclei exhibit three-dimensional growth, but a minority show predominately two-dimensional growth under the same growth conditions. As in the case of undoped nuclei, the nucleation occurs in the scratches but the growth is affected by the diamond substrate interaction. There is evidence of nuclei conforming to the sides of the scratches and secondary

nucleation occurring in the scratches after 1.5 hours of growth. The growth after 6 hours shows only a few pinholes and a small observable grain size.

From examination of the surface topography of the complete boron doped diamond films on silicon, many conclusions can be drawn. Most of the facets are smooth to within 3Å. The ridges that have been observed on the facets on the surface may contribute to the growth of the facets. At the intersections of different domains, island growth occurs. Elongated ridge structures may be the regions of faster growth on the surface between different domains.

The investigation of the surfaces of the freestanding doped film provided the following results: Remnants of the scratches that were made on the silicon were observed. By examination of the curvature of the of the surface of the ridges left over from the scratches, an approximate critical nucleus size of ~60-100Å can be estimated. The growth surface of the freestanding film looks very similar to the topography imaged on the complete films grown on silicon.

References

1 J. C. Angus, Z. Li, M. Sunkara, R. Gat, A. B. Anderson, S. P. Mehandru, and M. W. Geis, in *Proceedings of the International Symposium on Diamond and Diamond Materials, Electrochemical Society Meeting, Washington, D. C.* (Electrochemical Society, New York, 1992), p.125.

2 J. V. LaBrasca, R. C. Chapman, G. E. McGuire and R. J. Nemanich, J. Vac. Sci. Technol., B. **9**, 752 (1991).

3 R. E. Clausing, L. Heatherly, K. L. More, G. M. Begun, Surf. and Coat. Tech. **39/40**, 199 (1989).

4 J. E. Graebner, S. Jin, G. W. Kammlott, B. Bacon, L. Seibles, and W Banholzer, J. Appl. Phys. **71**, 5353 (1992).

5.0 STS of Electronic Properties during Diamond Growth

I. Introduction

The possibility of growth of diamond thin films under conditions of low temperature and pressure was realized in the 1950's [1]. It has only been in the last twenty years that the process has become economically and technically feasible. More recently, the thrust of most of the diamond research has focused on the film quality and growth rates [2]. The surface chemistry involved is understood in the simplest terms [3], but the growth of high quality chemical vapor deposited (CVD) diamond has been achieved. Many different surface and bulk characterization methods have been applied to study the growth processes, nucleation, and the resulting complete diamond films [4-6].

A relatively new characterization process is scanning tunneling microscopy (STM) and its associated microscopies. One of the techniques related to STM used to identify surface electronic structure, is scanning tunneling spectroscopy (STS). The utility of STS, where current-voltage data is taken at the same time that the STM image is recorded, was first realized by Hamers et al [7]. This concurrent measurement of topographical and electronic structures allows for the correlation of the two properties. The process has been used to characterize the electronic structures of many surfaces including silicon [8-10] and germanium [11-13]. Wide band gap semiconductors have been examined less, but examples of STS applied to SiC [14,15] and ZnO [15] surfaces have been reported. In the characterization of diamond nucleation and growth, a few examples of scanning tunneling spectroscopy (STS) can be found, but most have been adjuncts to other STM work [16, 17].

The purpose of this study is to investigate the electronic structures of the doped and undoped diamond nuclei, the interface between diamond and silicon, and surfaces involved in the growth of diamond. The STS results discussed in this chapter were taken in air. This limits the resolution of the process, but does not preclude its usefulness. STS measurements in air have been used to delineate pn junctions [18] in Si and to identify defects in semiconductors [19], to name a few. As will be discussed more fully in the discussion section, STS performed in the ambient is useful as long as the limits of the technique are understood.

II. Experiment

The STM analysis of the surface was carried out over a wide range of parameters. The analysis was performed using a Park Scientific Instruments STM-SA1, which is an ambient STM. The scans of the surface covered ranges between 100Å - 10nm. The tip was scanned at rates corresponding to between 0.08 to 2 Hz and tunneling currents ranging between 0.2nA to 4nA. The parameters of the system were changed for each sample in order to enhance imaging of that particular film or substrate.

STS results were obtained in the following manner. First, the surface was imaged by STM. Regions of interest were identified and these regions were scanned over ranges between 100Å - 200Å. STS was performed over this region to identify its uniformity. If the current-voltage curves were uniform, to within a level of noise, then STS was performed over the area for eight values of the set point current, i. e. eight different tip to sample distances. Several such regions were examined for each surface. The STS spectra presented here have been averaged over all eight curves taken at the eight values of the set

point current. The STS curves were then smoothed to allow for better interpretation of the major peaks of each spectrum. All of the results presented in this work were obtained using etched or mechanically ground PtIr tips.

It has been shown that the ratio of the differential conductance (dI/dV) to the conductance gives a relative measure of the surface density of states [20, 21]. To analyze the data, derivatives of the current-voltage curves were calculated from the I-V curves. The derivatives were then divided by the conductance (I/V) to normalize the data.

One of the objectives of this work is to characterize the electronic structure of diamond nuclei. In order to accomplish this goal, many samples were needed to provide standards with which the results could be compared. The Si(100) substrate was cleaned with HF acid and examined within 10 minutes with the STM. The graphite sample was cleaved with a piece of adhesive tape to produce a clean surface.

The undoped nucleation samples were prepared by microwave plasma CVD on 1 inch diameter Si(100) substrates. The substrates were polished with 0.25 μm diamond powder for 5 minutes and then solvent cleaned. The substrates were exposed to growth conditions for 1 hour for both doped and undoped studies. In both cases, the growth occurred at a pressure of 35 Torr, a methane to hydrogen ratio of 0.5% with a total flow rate of 1000 sccm and an average substrate temperature of 800°C. Doped diamond nuclei were also grown under the same conditions as above. For the doped nuclei, diborane was included in the gas mixture at a level of 10.0 ppm. SEM micrographs were obtained from the surfaces to provide an estimate of the nucleation density.

Complete diamond films grown on Si were prepared by hot filament CVD on Si<100> substrates. The substrates were preseeded with diamond powder,

and the gas flow of 100 sccm hydrogen, 1.5 sccm methane, and 0.4 sccm oxygen were controlled to obtain diamond growth. The thickness of the film was between 1μm and 2 μm. Diborane was introduced into the gas flow to dope the sample. The film was doped with a gas phase concentration corresponding to 6 x 10^{19} per cm^3. The boron incorporation efficiency was determined to be approximately 20% by SIMS analysis.

The freestanding film used in the exploration of interfacial properties was originally grown on a Si<100> substrate. The substrate was polished with 0.25 μm diamond powder and then solvent cleaned. The sample was grown for 27 hours. The growth occurred at a pressure of 90 Torr, a methane to hydrogen ratio of 0.5% with a total flow rate of 100 sccm and an average substrate temperature of 900°C. Diborane was included in the gas mixture to dope the film and a doping concentration of 1020 atom/cm^3 was subsequently measured by SIMS. The silicon substrate was removed by chemically etching using a solution of nitric and hydrofluoric acid.

III. Electronic Structure of Single Crystal Diamond

When STS is performed under UHV conditions, the presence of surface absorbates can be eliminated, the atomic structure can be observed and a measure of the surface structure can be obtained. Without absorbates on the surface, all observed electronic structure must be ascribed to the electronic structure of the sample and the tip. Variations of the electronic structure can often be measured over the surface to an atomic scale. In some cases, STS can also be used for the determination of the presence of surface absorbates.

When STS is performed in air, the situation is more difficult. For most surfaces examined in the ambient, the presence of absorbed molecules is

almost assured. It is, therefore, not likely that every peak can be attributed to the atomic scale electronic structure of the surface. It is, however, possible to identify significant features of the electronic structure. To that end, standards were developed for several surfaces imaged in air which can be compared with suitable results taken under UHV conditions. Using these standards, the electronic states of the growth surfaces can be identified.

The (dI/dV)/(I/V) curve, referred to as a surface DOS curve, of boron doped type IIb single crystal diamond is shown in Figure 5.1. A schematic of band structure of diamond and how it is measured by STS is shown in Figure 5.2. The point of zero bias voltage corresponds to the Fermi level position (E_F), indicated as E_i in Figure 5.2. For negative applied bias voltages, states with energy greater than E_F are probed, i. e. probing empty electronic states. For positive biases, the inverse is true. We assume that the PtIr tip has a metallic density of states and does not significantly influence the surface DOS curves. There is a region of low conductivity between -3.2eV and 1.0eV. This presumably is the surface bandgap of diamond. It is consistent with the p-type character of the sample, with an increase at 1.0eV below E_F due to tunneling from the valence band.

The authors also assert that the sudden rapid increase in the DOS beginning at -3.5eV is due to Fowler-Nordheim tunneling [22]. This field-emission effect was discussed in §2.1. This sharp increase is observed, in some form or another, for almost all of the diamond samples in this study. This effect has been observed by other authors conducting STM investigations of Si and Cu surfaces [23, 24]. It is observable at bias potentials for diamond because the conduction band edge is close to the vacuum level. In fact, for some surfaces of diamond, near the onset of tunneling into the conduction

Single Crystal Diamond
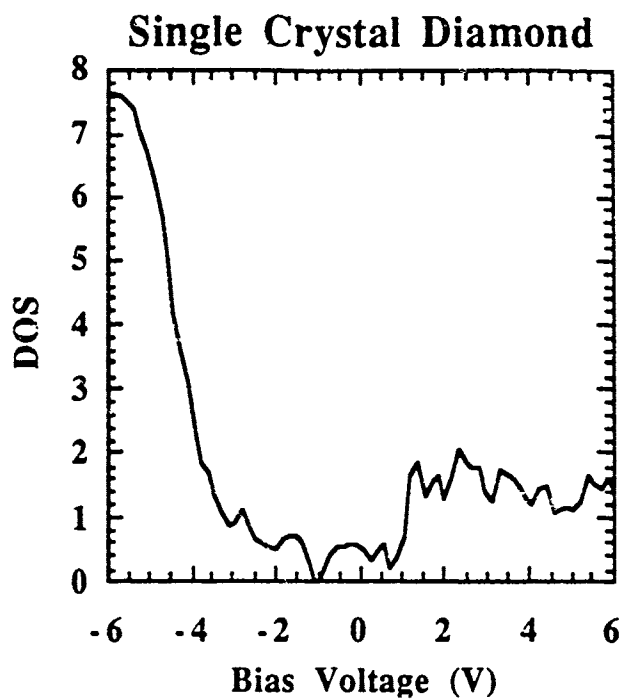

Figure 5.1

STS curve showing the surface density of states for single crystal diamond. The curve is a plot of the normalized differential conductivity versus bias voltage. In this plot, and all subsequent plots, the normalized differential conductivity is labeled as "DOS".
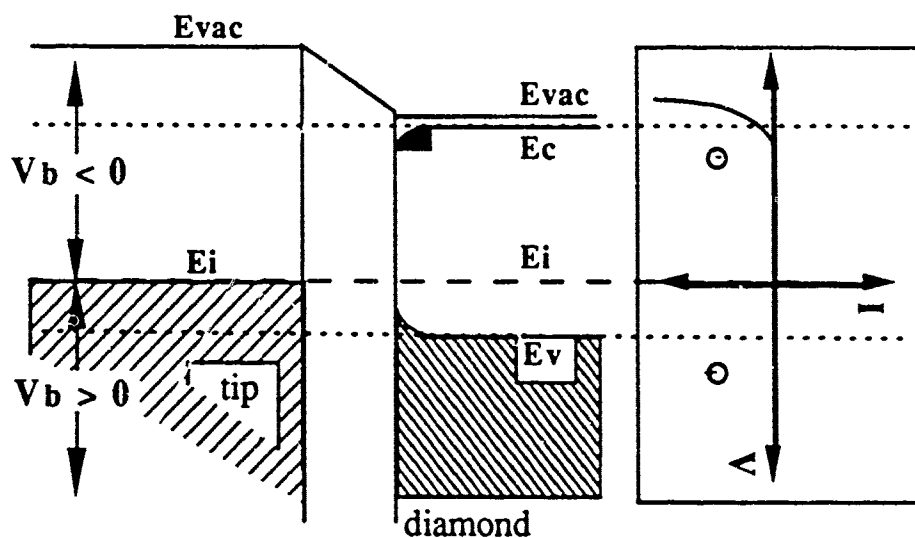

Figure 5.2

Band diagram showing the tunneling spectroscopy process in the case of single crystal diamond.

band, a small negative electron affinity has been observed [25,26]. We were not able to determine if the diamond surfaces exhibited a negative electron affinity, because the spectra presented here do not have a sufficient energy resolution. The energy resolution for all of the spectra taken over the ±6V range is 0.15eV. In principle, it would be possible to measure this effect by STS.

IV. Electronic Structure of Diamond Nuclei

In order to effectively characterize the electronic structures of the surfaces of diamond nuclei, standards need to be established for STS performed in air It is for that reason that the STS spectra are presented for silicon, graphite, silicon carbide, and doped polycrystalline diamond grown on silicon. These spectra can, in turn, be compared with spectra obtained under UHV conditions.

The spectrum shown in Figure 5.3 was obtained from a Si(100) surface which was cleaned with HF and examined immediately after. The surface should be hydrogen-terminated. [27] Through examination of Figure 5.3, a region of low conductivity can be observed between -0.5eV and 0.4eV. This probably represents the surface bandgap of the Si(100). This value for the bandgap is somewhat smaller than expected, but is still consistent with results found under UHV conditions [28, 29]. Several prominent peaks can be observed at -1.9eV, -1.4eV, 0.9eV, and 2.5eV. While several of these peaks are close to the values obtained in UHV, correspondences between peaks found in the ambient and those found under UHV conditions cannot be assured.

In Figure 5.4, the surface DOS spectrum of n-type Si terminated SiC is presented. Here, the region of low conductivity runs from 0eV to 2.0eV. This feature probably corresponds to the surface bandgap. The Si terminated surface accumulated an oxide before examination by STM, as evidenced by its
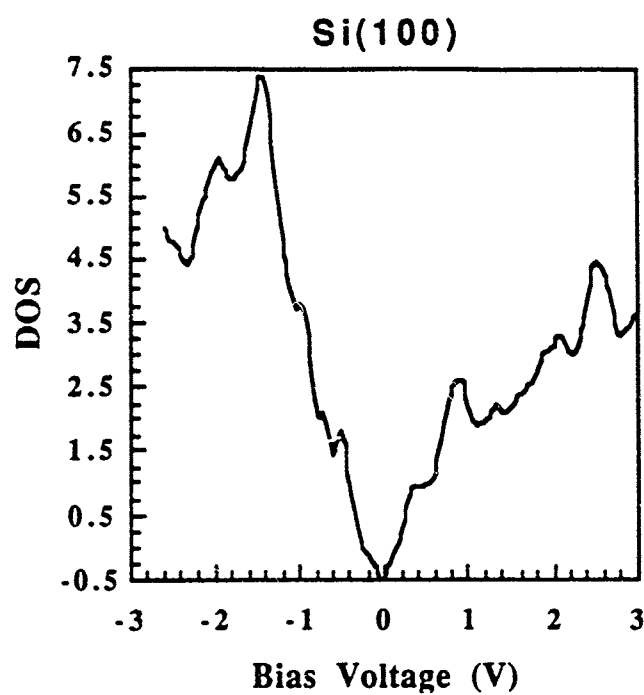
Si(100)

Figure 5.3
STS curve obtained from the Si(100) surface. The surface was prepared by cleaning with HF/
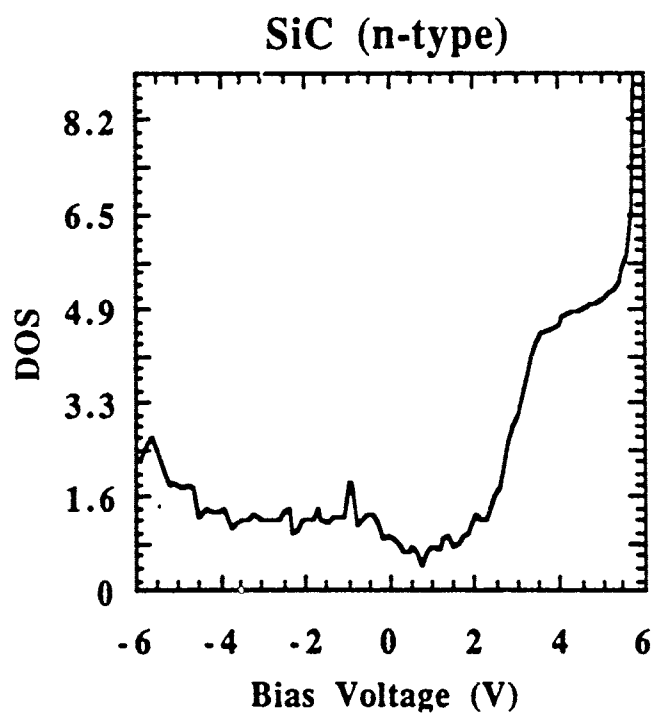
SiC (n-type)

Figure 5.4
STS curve obtained from the surface of n-type SiC.
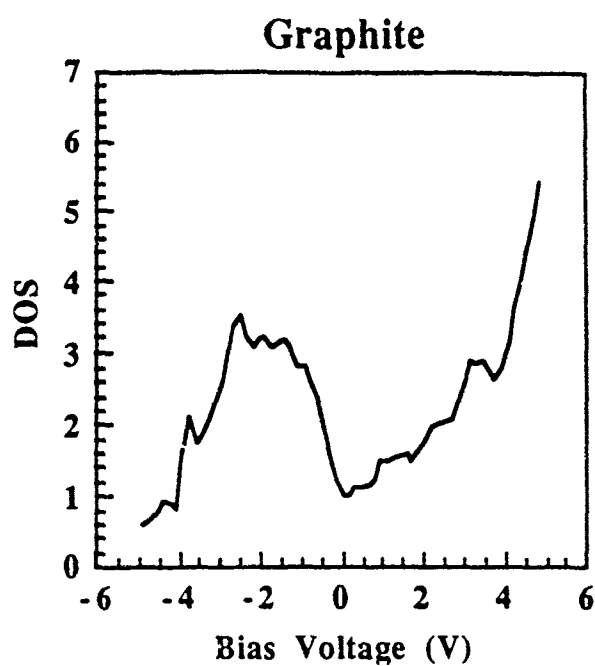
Graphite

Figure 5.5
STS curve obtained from the surface of highly-oriented pyrolithic graphite.
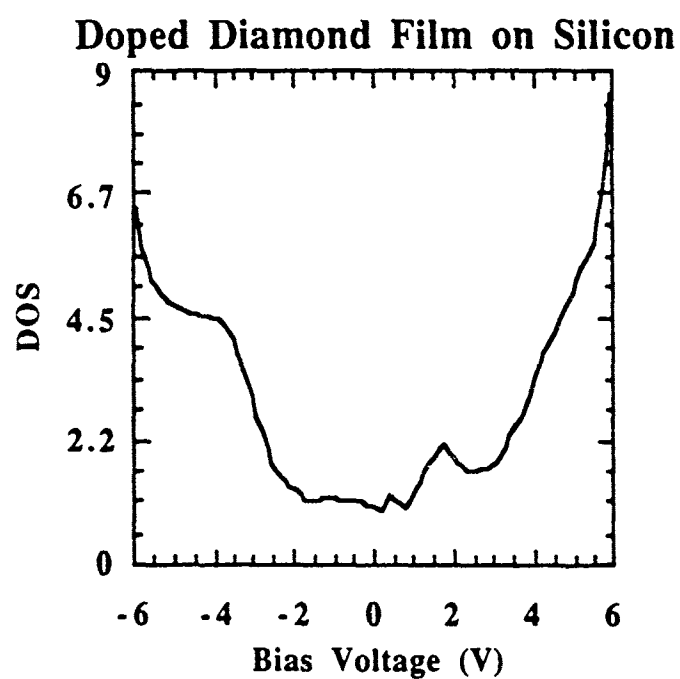
Doped Diamond Film on Silicon

Figure 5.6
STS curve obtained from the surface of a doped polycrystalline diamond film on silicon.

poor imaging quality. This also can be inferred because of the differences between these results and those obtained under UHV conditions [14]. The most prominent features that we observe are the "shoulder" extending from 2.0eV to 3.4eV, the low conductivity region mentioned above, and a peak at -1.0eV.

Figure 5.5 shows the surface DOS spectrum for highly oriented pyrolithic graphite (HPOG). Since HOPG does not readily oxidize, it is possible to identify actual bonding, antibonding, or surface states. In this case. the low conductivity regions extends between 0eV and 0.6eV. Peaks are located at +3.5eV, +1.5eV, -1.3eV, -1.7eV, -2.5eV, and -3.6eV. Comparing these results with the work of Fuchs et al. [30], and the calculations of Selloni and others [31], all of these peaks have been reported or predicted with the exception of the peak at +3.5eV. Selloni calculated that there is a state at +2.5eV and this state has been observed in other studies [31]. It is likely that the +2.5eV peak is present in the spectrum, but it is obscured by the presence of the peak at +3.5eV. The origin of the 3.5eV peak is unknown, but may be due to the presence of bsorbates on the surface.

The surface DOS of a doped polycrystalline diamond film grown on silicon is shown in Figure 5.6. A region of low conductivity is shown between -2.2eV and 1.0eV. A peak is observed at +1.8eV, a shoulder extending from -2.5eV to -3.8 eV, and an increase in the current starting at 3.0eV. It is important to note that this gap is less than the 5.4eV expected for diamond. One rationale for this change is that the actual gap ends at +2.4eV, which can be found by tracing down the sharp increase at high positive bias. In that case, the peak at +1.8eV would most likely be due to the presence of surface states, a bulk impurity level, or surface contaminants.

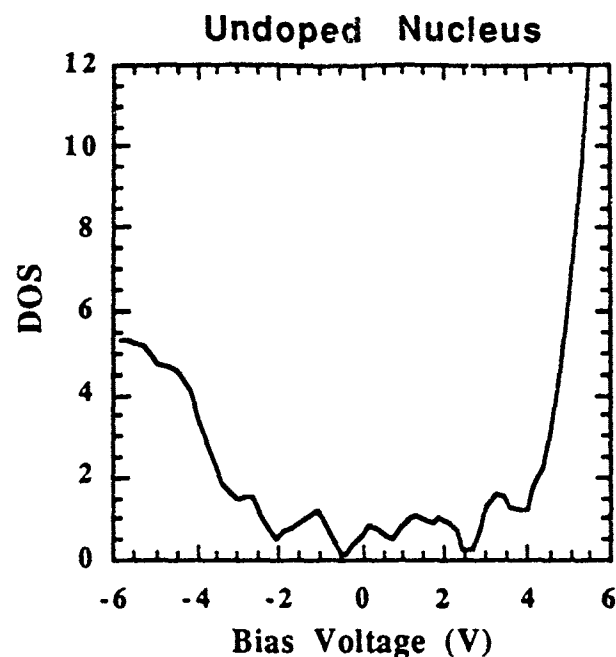## Undoped Nucleus

Figure 5.7
STS curve obtained from the surface of an undoped diamond nucleus on silicon.

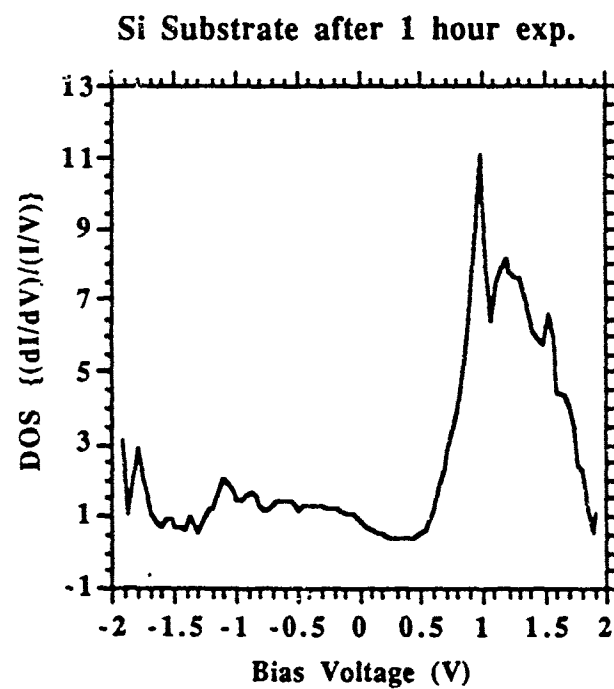## Si Substrate after 1 hour exp.

Figure 5.8
STS curve obtained from the surface of the substrate near an undoped diamond nucleus.

Figure 5.7 shows the surface DOS spectrum for a small nucleus of undoped diamond deposited on Si. We note that this is the same sample that was described in §3.1 As described in §4.2, examination of the undoped diamond nuclei by photoluminescence showed that the defect density in the nuclei was relatively large. We asserted that it was due to this large defect density that imaging of undoped nuclei by STM was possible. The surface DOS results support these results. The spectrum shows an electronic structure with a bandgap of 5.3 eV with endpoints of -2.0eV and 3.3eV. There appears to be several small peaks within the gap that may be attributed to defect levels. Note also the increase in the surface DOS for high positive bias voltages, as in the spectrum shown in Figure 6, which was also grown on silicon.

From the same sample, Figure 5.8 shows the surface DOS from a region near a nucleus on the substrate. It has been proposed that carbonaceous [32] or silicon carbide [33] layers form on the surface prior to or during diamond deposition. It is useful to compare the spectrum in Figure 5.8 with that of Si (Figure 5.3). The peaks of the spectrum of the surface DOS, which are at -1.8 eV, -1.1eV, 1.0eV, 1.2eV and 1.5eV, do not align with those found in the spectrum of Si. We can conclude that a film has formed on the surface that has altered the electronic structure. A few of the peaks in Figure 5.8 are in the same positions as peaks in the STS spectrum of HOPG, but the general shapes of the two spectra are very different. The electronic structure does not closely resemble any of the standards presented in Figures 5.1-5.6. The characterization of the electronic structure of this growth surface may require more standards than have been examined in this study.

Examination of Figure 5.9, which provides a contrast of the electronic structure of the undoped nuclei with the electronic structure of the growth sur-

Diamond Nucleus and Substrate
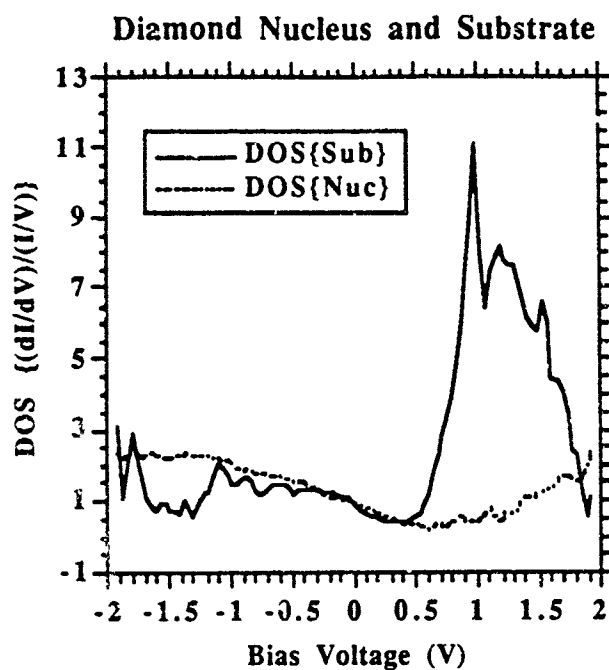
Figure 5.9
Comparison of the STS curves obtained from the surfaces of an undoped diamond nucleus on silicon and an adjoining region of the substrate.
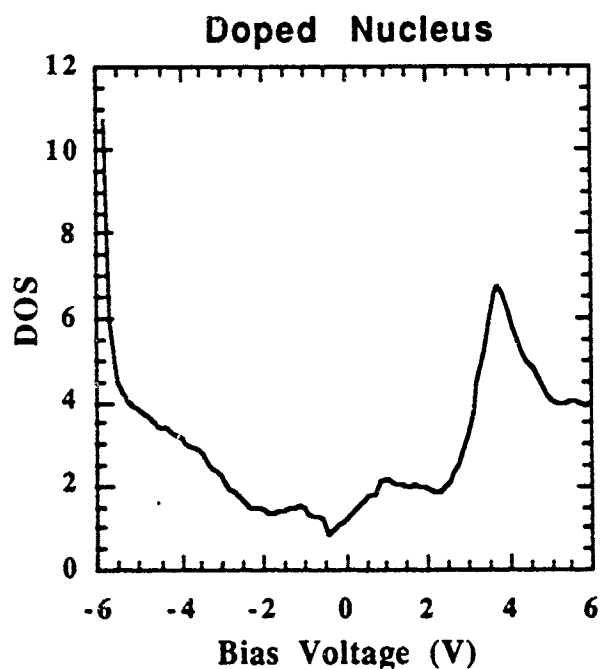
Doped Nucleus

Figure 5.10
STS curve obtained from the surface of a doped diamond nucleus on silicon.

face, may suggest an alternate interpretation. When molecules are absorbed on the surface, it has been shown that the molecules contribute discrete levels to the DOS if they are loosely bound to the surface [34]. Other studies [35] have shown that, depending on how the diamond reactor is shut down after growth, a layer of hydrocarbons may be left on the surface. If this interpretation is correct, then the spectrum shown in Figure 5.8 could show the surface DOS of a carbon layer with loosely bound absorbates on its surface.

In Figure 5.10, the surface DOS for a doped nucleus grown on silicon is presented. The most prominent feature is the peak at 3.5eV. If the slope of the line from 3.5eV to 2.2eV is extrapolated to the lowest DOS value, a region from 2.2eV to -2.1eV can be estimated to be the bandgap region. Two mid-gap states can be identified: one at +1.0eV and the other at -1.2ev.

The surface DOS from a region near a doped nucleus on the substrate is shown in Figure 5.11. Again, the peaks of this spectrum, at -0.8eV, 0.7eV, 1.0eV, 1.2 eV, and 1.5eV, do not seem to correspond to any peaks in the spectrum of silicon (Figure 5.3). Perhaps more surprisingly, all of the peaks at positive bias voltages, where filled states are being probed, have corresponding peaks in the spectrum shown in Figure 5.8. This indicates that the substrate surface for doped diamond growth is similar to the substrate surface of the undoped diamond growth. Even if the substrate surface cannot be totally characterized by attributing of the features to other known electronic structures, it still allows of differentiation of diamond materials from non-diamond materials. This differentiation makes it possible to distinguish regions which are diamond from the substrate using spectroscopic methods, even when the structures themselves cannot be imaged. This differentiation also provides

Si Substrate (Doped Growth)
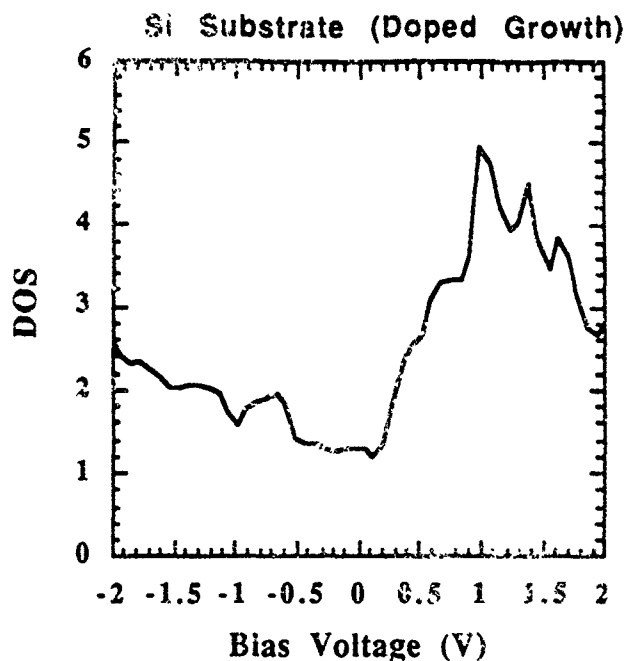
Figure 5.11
STS curve obtained from the surface of the silicon substrate near a doped nucleus after one hour of growth.
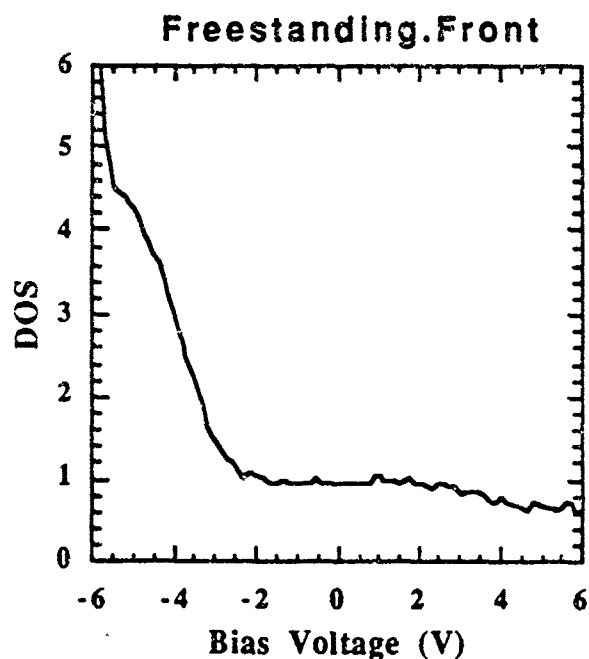
Freestanding.Front

Figure 5.13
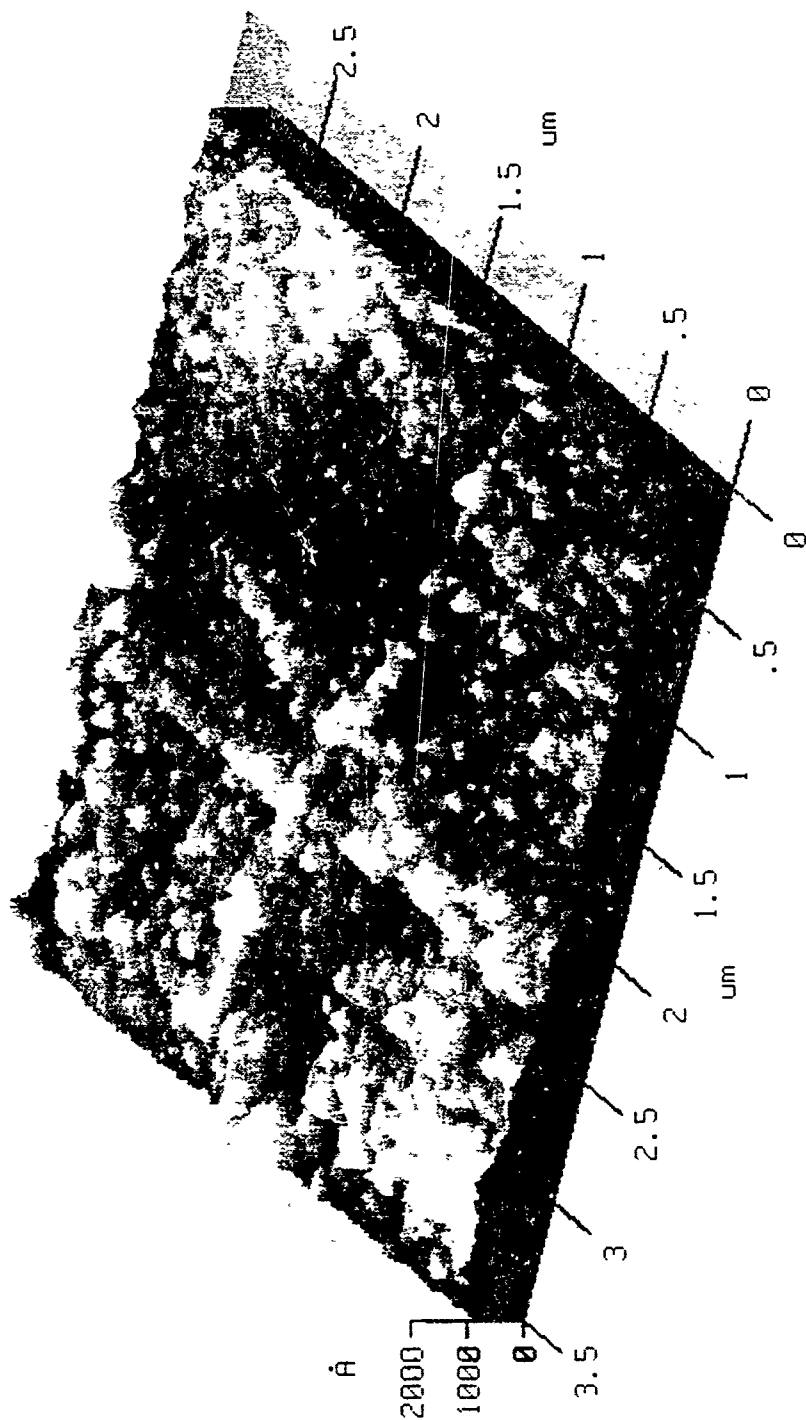STS curve obtained from the growth surface of the freestanding diamond film.

Figure 5.12

STM image of the etched side of the freestanding diamond film. This figure shows ridges caused by scratchs that were made on the silicon, which was etched away.

for the opportunity to establish the location of probable nucleation sights on the substrate prior to growth, as first suggested by Everson and others [17].

V. Comparison of the Interface and Growth Surfaces

The last sample to be examined in this study is a freestanding polycrystalline diamond film. The growth surface of this film, when examined by STM, showed typical structure for extended growth of diamond on silicon. The etched side displayed a very different type of topography and is shown in Figure 5.12. The ridges that can be seen on the surface are remnants from the scratches that were made on the silicon to increase the nucleation density. Further analysis of this surface was provided in §4.1, section V.

Figures 5.13, 5.14, and 5.15 present the surface DOS of this freestanding film. Figure 5.13 shows the spectrum taken from the growth side of the freestanding diamond film. The electronic structure most resembles that of the single crystal diamond (Figure 5.1). It is also close in structure to the doped diamond film grown on silicon but without the steep climb in the surface DOS for positive bias nor the state at 1.8eV.

One could conclude that this sudden rise for positive bias is due to the presence of the silicon substrate, because it is observed for diamond grown on silicon but not for the freestanding diamond film. This cannot be the cause, since STS measures the surface electronic structure and also because tunneled electrons that reach the Si substrate would be thermalized and would not show the electronic structure.

An alternate explanation is that the sudden rise for positive bias is due to graphitic electronic structures on the surface or in the film. Referring to Figure 5.5, there is a rise also for positive bias voltages, but it is less steep. The results

Freestanding - Etched Side
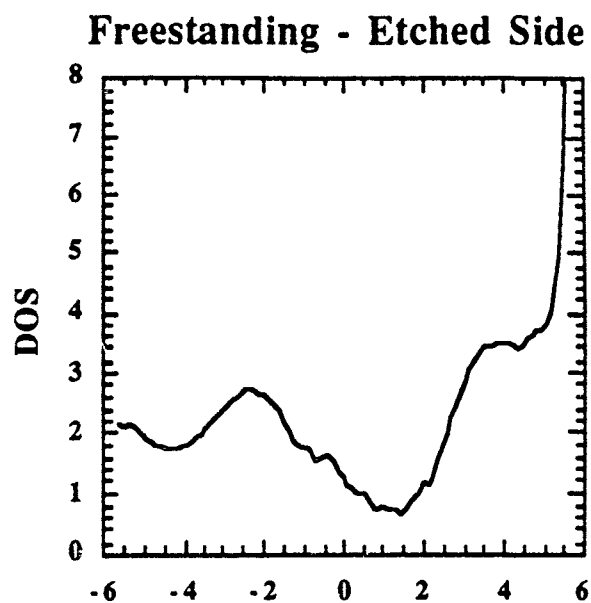

Figure 5.14
STS curve obtained from the etched surface of the freestanding diamond film.
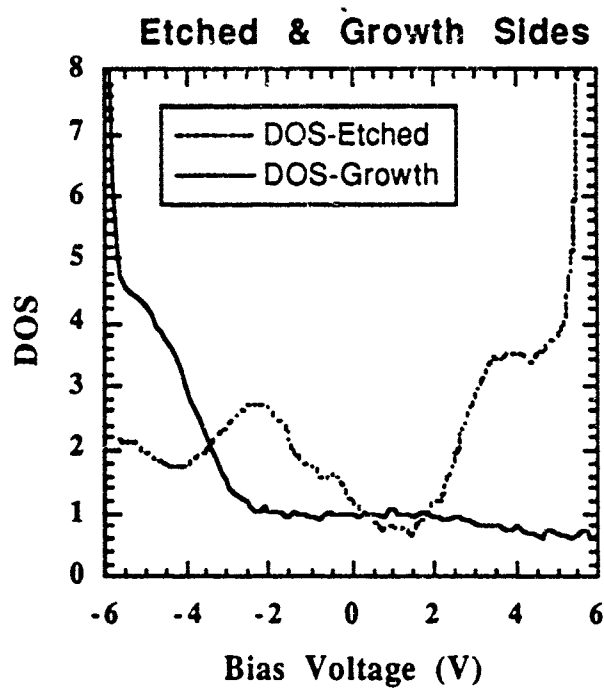
Etched & Growth Sides

Figure 5.15
Comparison of the STS curves obtained from the growth and etched sides of
the freestanding diamond film.

of Raman spectroscopy of the diamond nuclei and films show that all of the diamond has some sp^2 bonded material with the exception of the freestanding film. For the freestanding film, no sp^2 bonded material was detected. This result illustrates the utility of using STS as a measure of the sp^2 bonded material on the surface of diamond.

Figure 5.14 provides the clearest example of the utility of STS for characterization of the electronic structure of the surface. It shows the STS spectrum of the etched, back side of the freestanding film, which is pictured in Figure 11. The spectrum shows a broad peak centered at -2.2eV, a region of low conductivity between 0.5eV and 2.1eV, and a shoulder extending between 2.2eV and 3.5eV. By comparing this spectrum with those featured in Figures 5.5 and 5.6, a discovery can be made. Most of the surface DOS is made up silicon carbide-like and graphitic-like structures. In fact, if both the graphite and silicon carbide spectra are added together, the result looks remarkably like the spectrum shown in Figure 5.14. Since the Si has been etched away, only the interfacial layers remain behind. Several studies have provided evidence for the formation of silicon carbide or other carbon layer as a precursor for diamond growth [32,33,36]. This provides further evidence for the precursor being made up of graphitic and silicon carbide layers.

Figure 5.15 provides a contrast between the front and the back sides of the freestanding diamond film. It also emphasizes the surface sensitivity of the STS process. Working with a UHV STM, one could map out such an interface on both the physical and electronic levels. Working in UHV, the surface electronic structure could be separated from the structures created by absorbed molecules, and thus a finer level of characterization. Better resolution would allow for surface band structure theories to be applied and tested.

VI. Conclusions.

The structures of Si(100), graphite, single crystal diamond, and SiC were measured to serve as standards. The electronic structures of doped diamond films, undoped diamond nuclei, and doped diamond, all deposited on Si, were all charted. The three appear to be very similar in terms of their STS spectra. The structures of the layers deposited on the substrates during diamond deposition were identified. The etched and growth sides of a freestanding film were found to have different electronic structures, and the etched side provided evidence for precursor layers containing silicon carbide and graphitic carbon. In subsequent research, use of a UHV STM would allow for greater resolution, and actual identification of bonding and surface states.

References

1   W. G. Eversole, U. S. Patent 3,030,188 (1961).

2   W. A. Yarbrough and R. Messier, Science **247**, 688 (1990).

3   J. C. Angus, Z. Li, M. Sunkara, R. Gat, A. B. Anderson, S. P. Mehandru, and M. W. Geis, in *Proceedings of the International Symposium on Diamond and Diamond Materials, Electrochemical Society Meeting, Washington, D. C.* (Electrochemical Society, New York, 1992), p.125.

4   B. E. Williams and J. T. Glass, J. Mater. Res. **4**, 373 (1989).

5   A. A. Morrish and P. E. Pehrsson, Appl. Phys. Lett. **59**, 417 (1991).

6   B. R. Stoner, G. H. M. Ma, S. D. Wolter and J. T. Glass, Phys. Rev., B **45**, 11067 (1992).

7   R. J. Hamers, R. M. Tromp, and J. E. Demuth, Phys. Rev. Lett. **56**, 1972 (1986).

8   J. A. Stroscio, R. M. Feenstra, and A. P. Fein, Phys. Rev. Lett. **57**, 2579 (1986).

9   F. Iwawaki, M. Tomitori and O. Nishikawa, J. Vac. Sci. Technol., B **9**, 711 (1991).

10   J. J. Boland, J. Vac. Sci. Technol., A **10**, 2458 (1992).

11   R. S. Becker, Proc. Nat. Acad. Sci. **84**, 4667 (1987).

12   R. S. Becker, B. S. Swartzentruber, and J. S. Vickers, J. Vac. Sci. Technol. A **6**, 472 (1988).

13   R. M. Feenstra and A. J. Slavin, Surf. Sci. **251**, 401 (1991).

14   C. S. Chang, I. S. T. Tsong, Y. C. Wang and R. F. Davis, Surf. Sci. **256**, 354 (1991).

15   D. A. Bonnell, G. S. Rohrer and R. H. French, J. Vac. Sci. Technol., B **9**, 551 (1991).

16   K.F. Turner, Y.M. LeGrice, B.R. Stoner, J.T. Glass, R.J. Nemanich, J. Vac. Sci. Technol. B **9**, 914 (1991).

17   M.P. Everson, M.A. Tamor, J. Vac. Sci. Technol. B **9**, 1570 (1991).

18   J. V. LaBrasca, R. C. Chapman, G. E. McGuire and R. J. Nemanich, J. Vac. Sci. Technol. B 9, 752 (1991).

19   T. Takigami and M. Tanimoto, Appl. Phys. Lett. **58**, 2288 (1991).

20   R. M. Feenstra, J. A. Stroscio and A. P. Fein, Surf. Sci. **181**, 295 (1987).

21   N. D. Lang, Phys. Rev. B **34**, 1164 (1986).

22   R. H. Fowler and L. Nordheim, Proc. Roy. Soc. London A **119**, 173 (1928).

23   H. J. Freund, J. Ragozik, V. Dose and M. Neumann, Surface Sci. **175**, 94 (1986).

24   J. A. Kubby and W. J. Greene, J. Vac. Sci. Technol. B **9**, 739 (1991).

25   F. J. Himpsel, J. A. Knapp, J. A. VanVechten, and D. E. Eastman, Phys. Rev. B **20**, 624 (1979).

26   B. B. Pate, M. H. Hecht, C. Binns, I. Lindau, and W. E. Spicer, J. Vac. Sci. Technol. **21**, 364 (1982).

27

28   F. Iwawaki, M. Tomitori and O. Nishikawa, J. Vac. Sci. Technol., B 9, 711 (1991).

29   J. J. Boland, J. Vac. Sci. Technol., A **10**, 2458 (1992).

30   H. Fuchs and E. Tosatti, Europhys. Lett. **3**, 745 (1987).

31   A. Selloni, P. Carnevali, E. Tosatti and C. D. Chen, Phys. Rev. B **31**, 2602 (1985).

32   B. R. Stoner, G. H. M. Ma, S. D. Wolter and J. T. Glass, Phys. Rev., B **45**, 11067 (1992).

33   B. E. Williams, B. R. Stoner, D. A. Asbury, and J. T. Glass, in *Diamond and Diamond-Like Films and Coatings, NATO Advanced Study Institute, Series B: Physics*, edited by J. Angus, R. Clausing, L. Horton, and P. Koidl (Plenum, New York, 1990).

34   Ph. Avouris, I.-W. Lyo, and F. Bozso, J. Vac. Sci. Technol. B **9**, 424 (1991).

35   R. J. Nemanich, L. Bergman, Y. M. LeGrice, and R. E. Shroder, in *Proceedings of the Second International Conference on the New Diamond Science and Technology*, edited by R. Messier and J. T. Glass (Japan New Diamond Forum, Washington, D.C., 1990).

36   J. J. Dubray, C. G. Pantano, M. Meloncelli and E. Bertran, J. Vac. Sci. Technol., A. **9**, 3012 (1991).

6.0 A Comparison with Nucleation on Other Substrates

I. Introduction

In this chapter, a comparison is made between nucleation of diamond on silicon and diamond nucleated on germanium and copper. Most of the research examining the nucleation and growth of diamond on non-diamond substrates has employed silicon as the growth substrate. A search of the literature reveals that many studies ([1-3], as examples) have examined the process of nucleation and growth of diamond on Cu substrates, but no references to growth on Ge substrates could be found. Cu was chosen as an alternate substrate because its lattice constant (3.61Å) is close to the lattice constant of diamond (3.57Å) and is a good candidate for heteroepitaxial growth. Ge was also chosen as an alternate substrate because it is another group IV semiconductor.

In terms of STM/STS investigations, a large number of studies have examined the surfaces of Ge [4,5] and Cu [6,7]. This chapter will focus on the differences in the nuclei formed on these substrates and characterization of the growth surfaces

II. Experimental

Two samples were used to compare the nucleation of diamond on Si with that on other substrates. Nuclei were grown on Ge(001) and polycrystalline Cu. Both samples were prepared by microwave plasma CVD. The Ge substrate was polished with 1 μm diamond powder for 5 minutes and then solvent cleaned. The Ge substrate was exposed to growth conditions for 2 hours. The growth occurred at a pressure of 25 Torr, a methane to hydrogen

ration of 1% with a total flow rate of 200 sccm at a power of 900 Watts forward and 50 Watts reflected. The polycrystalline Cu substrate was solvent cleaned and then biased in situ at -250VDC to enhance nucleation. This process of enhancement has been described elsewhere [8]. The growth occurred at a pressure of 15 Torr, a methane to hydrogen ration of 4% with a total flow rate of 200 sccm at a power of 800 Watts forward and 260 Watts reflected.

All of the data reported in this chapter was taken with a Park Scientific Instruments STM-SA1. The parameters are the same as given in the preceding experimental sections of §4.1 and §5.0. For the STS section, a Ge(100) surface was needed to provide a standard for the investigation of growth surface. The Ge(100) substrate was cleaned with DI water and examined within 10 minutes with the STM. The spectroscopy was performed in the same manner as was detailed in the experimental section of §6.0.

Raman spectroscopy showed the presence of particles with diamond structure on the surfaces of the Ge and Cu substrates.

III. Results and Discussion

The critical result of this chapter, in the investigation of diamond nucleation on other substrates, is the difficulty in tunneling to the nuclei deposited on the substrates. For both Cu and Ge, it was possible to opitimize the tunneling parameters for imaging of the substates. The optimal conditions for the Ge substrate was at a set-point current of 1.5nA and a bias potential applied to the tip of -2.0V. The optimal conditions for the Cu substrate was at a set-point current of 0.5nA and a bias potential applied to the tip of +1.0V. For STM imaging of undoped diamond grown on Si, it was possible to slightly modify the substrate tunneling conditions to best image the diamond nuclei. For

both Ge and Cu substrates, no modification of the tunneling conditions resulted in stable imaging of the nuclei. Because of the difficulty in maintaining stable tunneling, it is not possible, in this case, to determine to any degree of accuracy, whether the particles imaged were diamond.

Some imaging, however, was possible. Figure 6.1 shows an STM image of nuclei on the surface of Ge. The image is similar to the undoped diamond nuclei presented in §3.1. In this case, however, the faceted structure of the nuclei cannot be discerned. Compared with SEM micrographs of the surface, the nuclei have the same dimensions and relative spacing. The dark regions next to each nucleus are observed for both doped and undoped diamond nuclei (see 4.1 (a), for example). It also appears that the particle to the far left in the image has nucleated on a scratch.

In Figure 6.2, nucleation on top of a polycrystalline Cu surface is shown. Optical microscopy has shown that this surface is rough, when compared to the surfaces of the Si and Ge substrates. The nuclei seem to be growing along the side of a large break in the surface. There are no scratches on the surface because the bias enhancement process was employed. These nuclei cannot be substantiated to be diamond, but from the surface topography, it is clear that they have formed on the surface during growth. The nuclei have similar topographies and the presence of small particles can be observed in the rear of the image.

The subject of nucleation of undoped diamond on Si was examined in §4.2. A similar analysis has been performed on the nuclei found on the surfaces of Cu and Ge. Micro-photoluminescence (PL) was performed on the nuclei deposited on each substrate. In both cases a weak PL peak was found at 1.68eV, which has been ascribed to defects in doped diamond. But in each
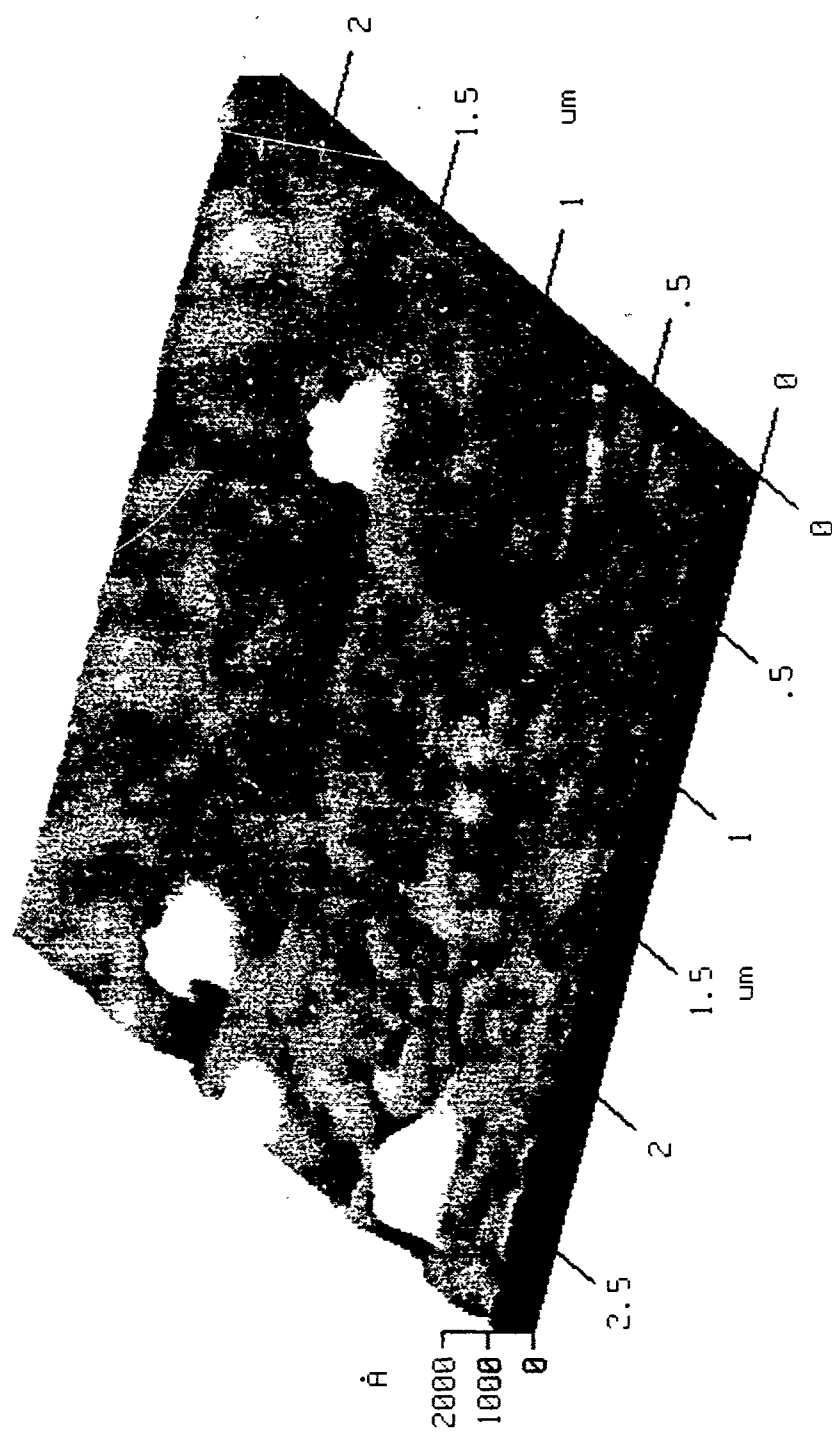
Figure 6.1
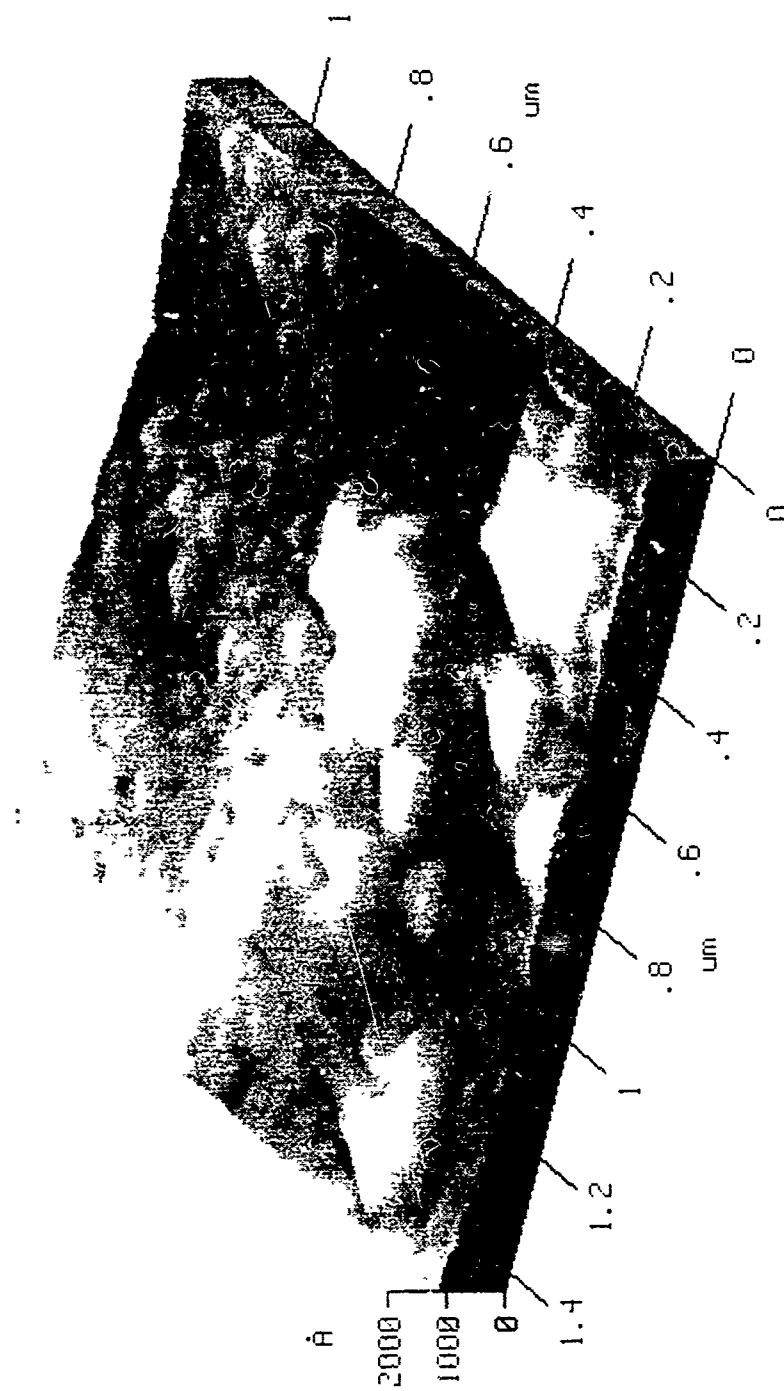STM image showing carbon nucleation on the surface of germanium

Figure 6.2

STM image showing carbon nucleation on the surface of copper

case, the relative intensity of this peak to the intensity of the diamond Raman peak was much less than for diamond nucleated on Si. As proposed in §4.2, this peak is probably due to the presence of silicon as a defect in the diamond. The etch rate for Ge and Cu by a mostly hydrogen plasma is expected to be lower than the etch rate for silicon under the same conditions. The 1.68eV peak is probably still due to the presence of Si, either residual in the chamber or from etching of the SiO_2 windows of the growth system. Therefore, it is understandable that the incorporation of substrate defects would be less. This would also mean that tunneling to that material would be more difficult without the electrically active defects. This result is important because it emphasizes that tunneling to undoped diamond nuclei is possible only for certain conditions.

The STS results obtained from the clean surface of Ge and the surface of Ge after exposure to growth conditions are shown in Figures 6.3 and 6.4 respectively. Figure 6.3 shows a gap of low conductivity between -0.65eV and 0.4eV, corresponding to a gap of 1.05eV, which is close to the value of 0.9eV found for the Ge(001) surface under UHV conditions by Kubby and others [4]. The peak that is observed at -1.2eV was also found by Kubby et al, but the peak which they reported to be at +0.9eV is not in evidence for the curve in Figure 6.3. This missing peak is probably due to absorbates on the surface. The STS spectrum of a region on the Ge substrate near the nuclei is shown in Figure 6.4. Here peaks are located at -1.05eV, -0.65, +0.05, +0.5eV, and +1.8eV. A gap is observed from -0.45eV to +0.3eV, a gap of 0.75eV, with a mid-gap peak near 0.05eV. The change in the STS spectrum, from comparison of the clean Ge(001) and the surface on Ge after growth, indicates the growth of C containing layers on the Ge substrate. As stated in §5.0 for STS results of the silicon surface after growth, the sharp peaks in Figure 6.4 may be due to the

presence of loosely absorbed atoms or molecules on the surface. In this respect, the change in the electronic structures for Si and Ge are similar.

IV. Conclusions

It is much more difficult to examine the nucleation of diamond on Cu and Ge substrates. The author was not able to tunnel in a stable manner to diamond nucleated on these substrates. This is theorized to be due to the lack of electrical defects found in the nuclei. Comparison with PL results obtained from diamond nucleated on Si with that nucleated on Ge and Cu, showed a much lower relative 1.68eV defect for diamond nuclei on both Ge and Cu. Sustained tunneling was achieved for the Ge substrate near nuclei, and the electronic structure of the growth surface was shown to be different from the electronic structure of a bare germanium substrate.
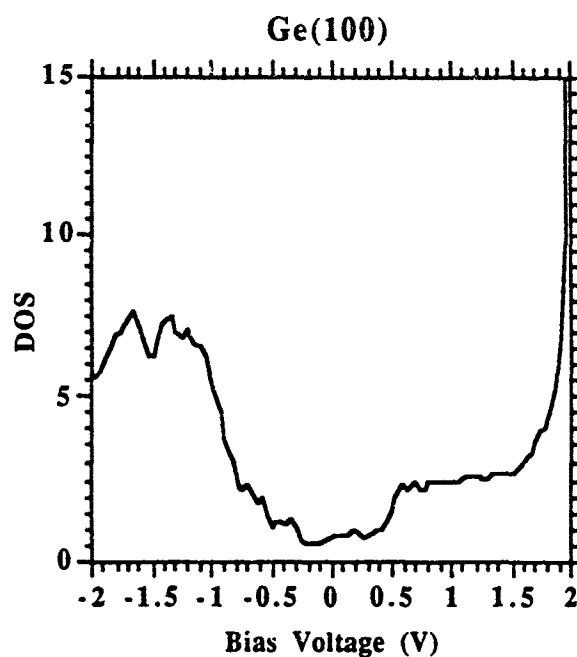
Ge(100)

Figure 6.3
STS curve obtained from the surface of germanium.
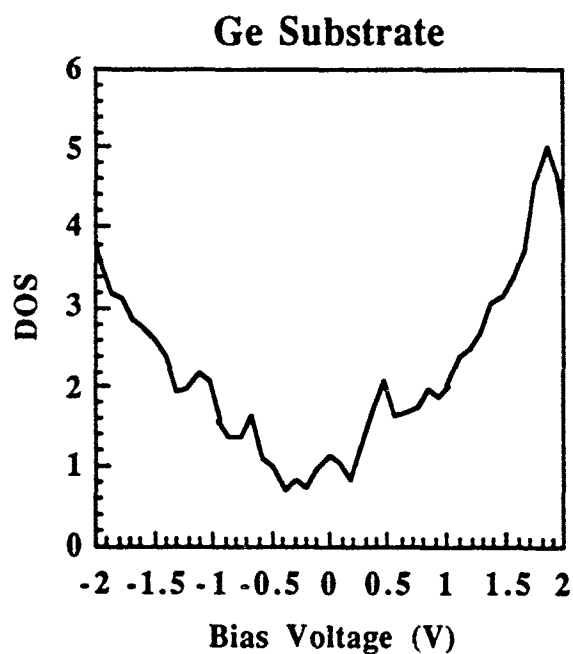
Ge Substrate

Figure 6.4
STS curve obtained from the surface of the germanium
substrate near a nucleus

References

1   A. A. Morrish and P. E. Pehrsson, Appl. Phys. Lett. **59**, 417 (1991).

2   C. M. Niu, G. Tsagaropoulos, K. Dwight, A. Wold and J. Baglio, J. Solid State Chem. **91**, 47 (1991).

3   T. P. Ong, F. Xiong, R. P. H. Chang and C. W. White, Appl. Phys. Lett. **60**, 2083 (1992).

4   J. A. Kubby J. E. Griffith, R. S. Becker, and J. S. Vickers, Phys. Rev. B **36**, 6079 (1987).

5   R. M. Feenstra and A. J. Slavin, Surf. Sci. **251**, 401 (1991).

6   A. Brodde, St. Tosch, H. Neddermeyer, J. Microsc. **152**, 441 (1988).

7   F. M. Chua, Y. kuk, and P. J. Silverman, Phys. Rev Lett. **63**, 386 (1989).

8   B. R. Stoner

9   R. S. Becker, Proc. Nat. Acad. Sci. **84**, 4667 (1987).

10   R. S. Becker, B. S. Swartzentruber, and J. S. Vickers, J. Vac. Sci. Technol. A **6**, 472 (1988).

11   R. M. Feenstra and A. J. Slavin, Surf. Sci. **251**, 401 (1991).

7.0 Thesis Summary and Future Research

In this thesis, the growth of diamond thin films has been studied by scanning tunneling microscopy and scanning tunneling spectroscopy. This investigation has examined the nucleation of diamond, the growth of diamond from nucleation to a complete film, the growth surface, and the interfacial properties between the diamond and the silicon. In this final chapter, the most important conclusions of this work will be restated and suggestions will be made for future research, which may lead to a more complete understanding of diamond growth.

7.1 Thesis Summary

In chapter three, the application of STM to explore the initial stages of undoped diamond growth was demonstrated. An increase in the surface roughness of the modified surface of the silicon with growth was observed. Nucleation of diamond was observed, and the growth was found to occur along the scratches. The growth of the nuclei was observed to occur parallel to the surface. With the nucleation occurring in the scratches, this would imply that the lateral growth of the nuclei conforms to the surface. Inspection of the nuclei revealed that they exhibited faceting and twinning. Most of the facets were found to be smooth to within the limit of the electrical noise. Other structures were found between some of the nuclei that may be precursors to intergrowth of the nuclei later on in the growth process.

Also in chapter three, an understanding of tunneling to undoped diamond was presented. It was shown that the presence of the strong PL peak at 1.68eV provided evidence of silicon impurities in the diamond. It was

asserted that this large density of silicon impurities allows for STM imaging of undoped diamond nuclei.

In chapter four, the study of doped nuclei over different periods of growth, the following conclusions were reached: A majority of the nuclei exhibit three-dimensional growth, but a minority show predominately two-dimensional growth under the same growth conditions. As in the case of undoped nuclei, the nucleation occurs in the scratches but the growth is affected by the diamond substrate interaction. There is evidence of nuclei conforming to the sides of the scratches and/or secondary nucleation occurring in the scratches after 1.5 hours of growth. The growth surface after 6 hours shows only a few pinholes and a small observable grain size.

The examination of the surface topography of the complete boron doped diamond films on silicon, presented in chapter four, allowed several conclusions to be reached. Most of the facets of the complete polycrystalline films are smooth to within 3Å. The ridges that have been observed on the facets on the surface may contribute to the growth of the facets. At the intersections of different domains, island growth occurs. It was suggested that the elongated ridge structures, observed in several places on the surface, were the regions of fast growth on the surface between different domains.

In chapter four, the investigation of the growth and etched surfaces of the freestanding doped film provided the following results: Remnants of the scratches that were made on the silicon were observed. By examination of the curvature of the of the surface of the ridges left over from the scratches, an approximate critical nucleus size of ~60-100Å can be estimated. The growth surface of the freestanding film looks very similar to the topography imaged on the complete films grown on silicon.

In chapter five the electronic structures of the diamond nuclei and the growth surfaces were examined. The structures of Si(100), graphite, single crystal diamond, and SiC were measured to serve as standards. Fowler-Nordheim tunneling was observed for single crystal diamond and in most of the other electronic structures of diamond. The electronic structures of doped diamond films, undoped diamond nuclei, and doped diamond, all deposited on Si, were all charted. The three appear to have similar electronic structures. as evidenced by their STS spectra. The structures of the layers deposited on the substrates during diamond deposition were identified. The etched and growth sides of a freestanding film were found to have different electronic structures, and the etched side provided evidence for precursor layers containing silicon carbide and graphitic carbon.

In chapter six, nucleation and growth on other substrates were examined for comparison. The difficulty in examining the nucleation of diamond on Cu and Ge substrates was observed. The inability to tunnel, in a stable manner, to diamond nucleated on these substrates was theorized to be due to the lack of electrical defects found in the nuclei. Comparison with PL results obtained from diamond nucleated on Si with that nucleated on Ge and Cu, showed a much lower relative 1.68eV defect for diamond nuclei on both Ge and Cu. Sustained tunneling was achieved for the Ge substrate near nuclei, and the electronic structure of the growth surface was shown to be different from the electronic structure of a bare germanium substrate.

7.2 Future Research

For future work, it is suggested that other methods that may be used to examine diamond growth and other areas of the growth process that warrant further

study. The most obvious continuation of this research would be to repeat many of the key experiments mentioned above under UHV conditions.

Performing STM measurements in an UHV environment allows for greater understanding of the surface chemistry. It would be possible to desorb any absorbed species from the surface before examining the sample. For the case of doped diamond nuclei, without the presence of absorbed layers, imaging of atoms on the surface of the diamond would be assured. This is not to say that a stable reconstructed surface would be uncovered, but imaging of the atoms of the diamond crystals would be guaranteed.

Under UHV conditions, it would also be possible to investigate the physical and electronic structures of the growth surface. There is evidence that, when nucleation is enhanced by use of a bias voltage, the resulting carbonaceous layers are epitaxial [1]. An UHV STM investigation of this surface would be the ideal method to substantiate the epitaxial relationship. Biasing of the substrate also allows for increased nucleation density without abrading the surface. [2] This is a major advance, since the exact nucleation mechanism could be examined without the additional variables introduced by scratching or other rough surface topography.

In tandem with this, the electronic structures of the surface DOS could be mapped, also unencumbered by atmospheric effects. This would also allow for characterization of electronic properties on an atomic scale. Through STS and other STM related spectroscopies, the bandgap, the workfunction, the electron affinity, and presence of surface defects and impurities could possibly be measured over a scale of nanometers.

Another technique that should be applied to the study of diamond growth is ballistic electron emission microscopy (BEEM) [3]. Several authors [4,5] have

used the technique to investigate the structural and electrical properties of buried interfaces between semiconductors and metal layers. This technique allows for the imaging of defects and impurities at the interface and the nature of electron or hole transport across the interface.

By applying BEEM methods to the diamond substrate interface, it may be possible to image the interface with spatial resolution. If a freestanding film, such as was used in §5.0, was adapted for this investigation, then the interface between the intermediate carbon layer, if one exists, and the nuclei could be probed. The results could provide the answer to the question of where and how nucleation occurs on the surface.

References

1   B. R. Stoner and J. T. Glass, Appl. Phys. Lett. **60**, 698 (1992).

2   B. R. Stoner, B. E. Williams, S. D. Wolter, K. Nishimura and J. T. Glass, J. Mater. Res. **7**, 257 (1992).

3   W. J. Kaiser and L. D. Bell, Phys. Rev. Lett. **60**, 1406 (1988).

4   L. J. Schowalter and E. Y. Lee, Phys. Rev. B **43**, 9308 (1991).

5   A. Fernandez, H. D. Hallen, T. Huang, R. A. Buhrman and J. Silcox, Phys. Rev. B **44**, 3428 (1991).

Appendix A: Tip Imaging Effects in the Characterization of Diamond Deposited on Silicon by STM

Scanning tunneling microscopy (STM) has developed into a powerful surface science technique because of its ability to examine surfaces with atomic scale resolution. As detailed in §2.1, STM is capable of measuring both physical and electrical properties. In most STM studies, the physical and electronic structure of the tips used is considered relatively unimportant. Some authors have dealt with the influence of tip structure on STM images [1-5], but most have ignored the possibility of tip effects. This is a serious omission, because the results of tip imaging are far from benign. It is possible for the uniformed to report STM data that does more to describe the structure of the tip than of the surface being examined. The signs that tip imaging has occurred are simple to detect if one knows what to look for. There is little literature published on the subject [6], and no data that pertains to the imaging of diamond.

All of the data reported in this appendix was taken with a Park Scientific Instruments STM-SA1. The tunneling tips were formed by chemical etching of either platinum iridium or tungsten wire.

The first example of tip imaging involves the characterization of doped diamond nuclei on silicon. The STM image is shown in Figure A.1. The sample was examined after one hour exposure to the growth conditions, as detailed in §4.0. For comparison to what the surface should look like, please refer to Figure 4.1. The first indication that tip imaging effects are occurring is the repeatability of each observed nucleus. Each nucleus is ~1 μm long and 0.5μm wide, and each nucleus is oriented in the same direction. A second indication
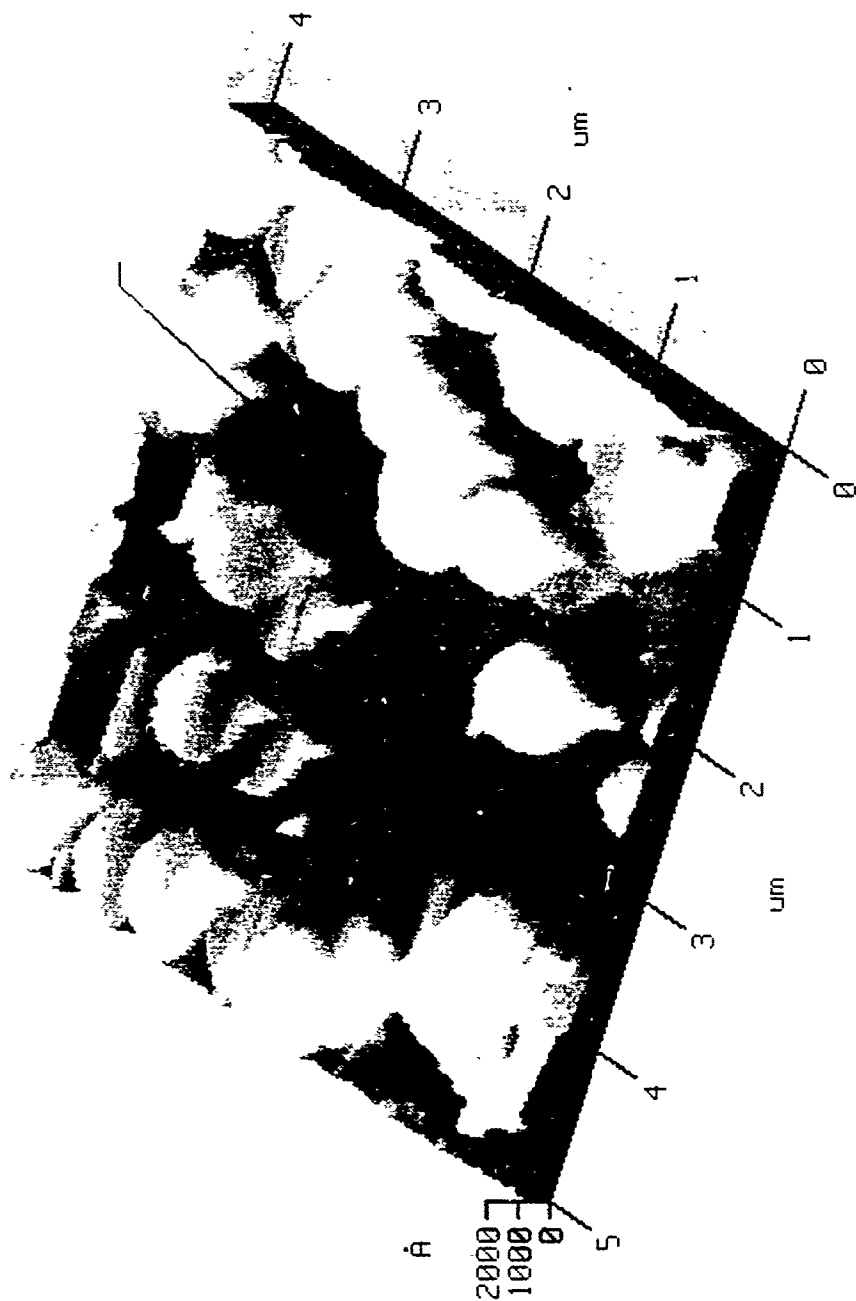
Figure A.1

An example of tip imaging for STM of doped diamond nuclei. The arrow points to a "ghost" nucleus, which is one of the signs that tip imaging is occurring.

is that several of these particles overlap. In fact, slightly away from the center of the image shown in Figure A.1, a partial nucleus is visible. Any time that an apparently smooth particle has a sudden and physically impossible change in topography, it is an indication that tip-surface interactions are occurring. Examples of other tip-surface interaction, in addition to tip imaging, are double tips and surface induced changes in tip structure.

A third indication of tip imaging effects is the presence in the image of a "ghost" nucleus, indicated with an arrow in Figure A.1. This type of "ghost" image occurs because of surface topography whose radius of curvature is smaller than that of the tip but larger than other areas on the surface. When the radius of curvature of a region is larger, this reduces the ability of the surface to image the tip, and the "ghost" image has the same lateral dimensions but a smaller vertical height.

A fourth indication that tip imaging effects are occurring, is the shape of the observed nuclei. All of the nuclei which are observed in Figure A.1 are round and flat. This structure is actually the surface structure of the tip. In this case the tip is extremely blunt. It should be noted that even a blunt tip, that gives rise to tip imaging effects, can image an atomicly flat surface [6]. This is because only a few atoms at the end of the tip are involved with tunneling, and for atomicly flat surfaces, the shortest tip to sample distance is between these atoms and atoms on the surface.

A last indication of tip imaging effects involves the conflict between what is observed from the STM image and independent knowledge of the surface topography. For the case of the STM image shown in Figure A.1, an optical scan of the surface of the nucleation sample indicates a much lower nucleation density than what could be inferred from the image.
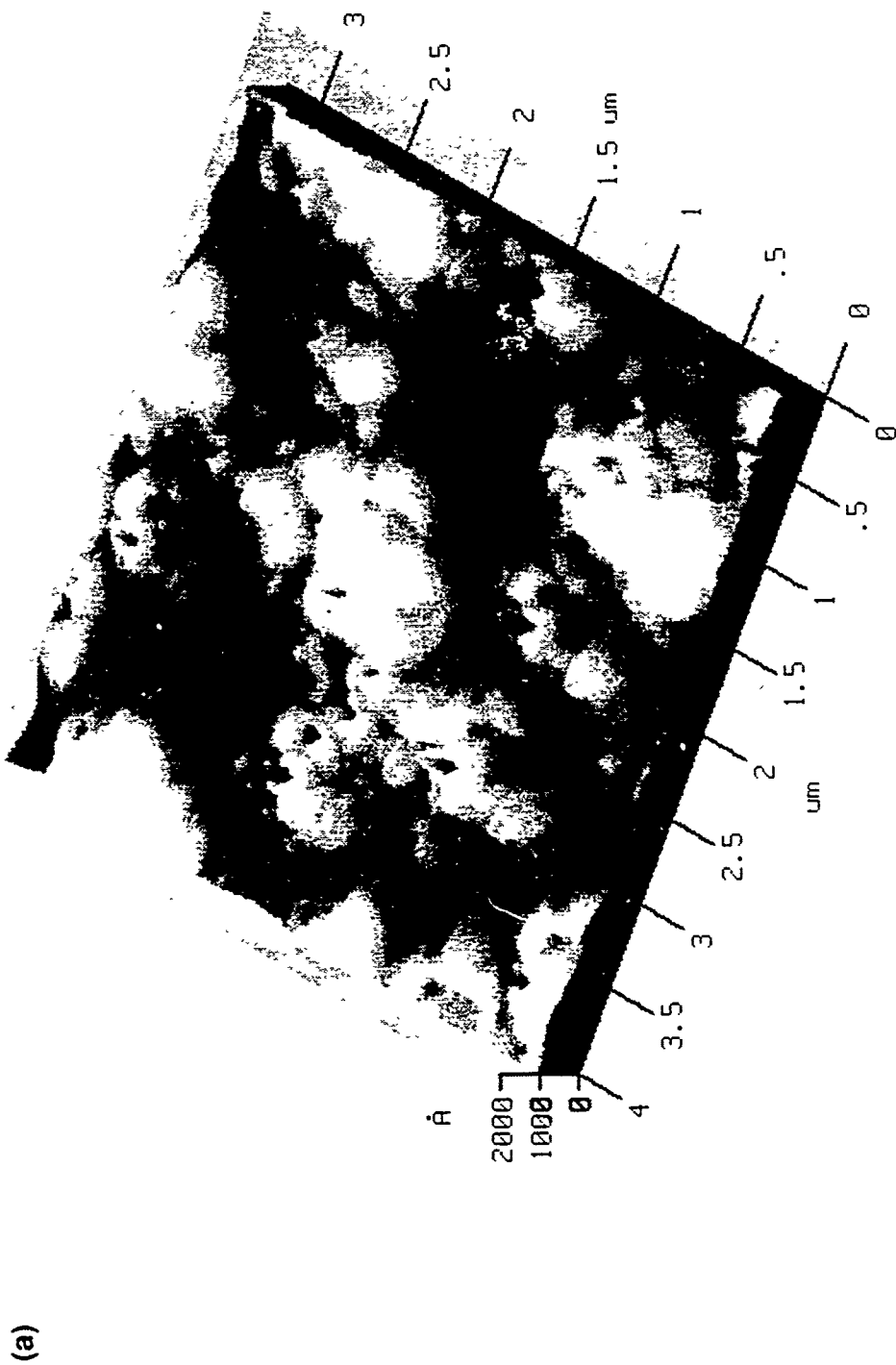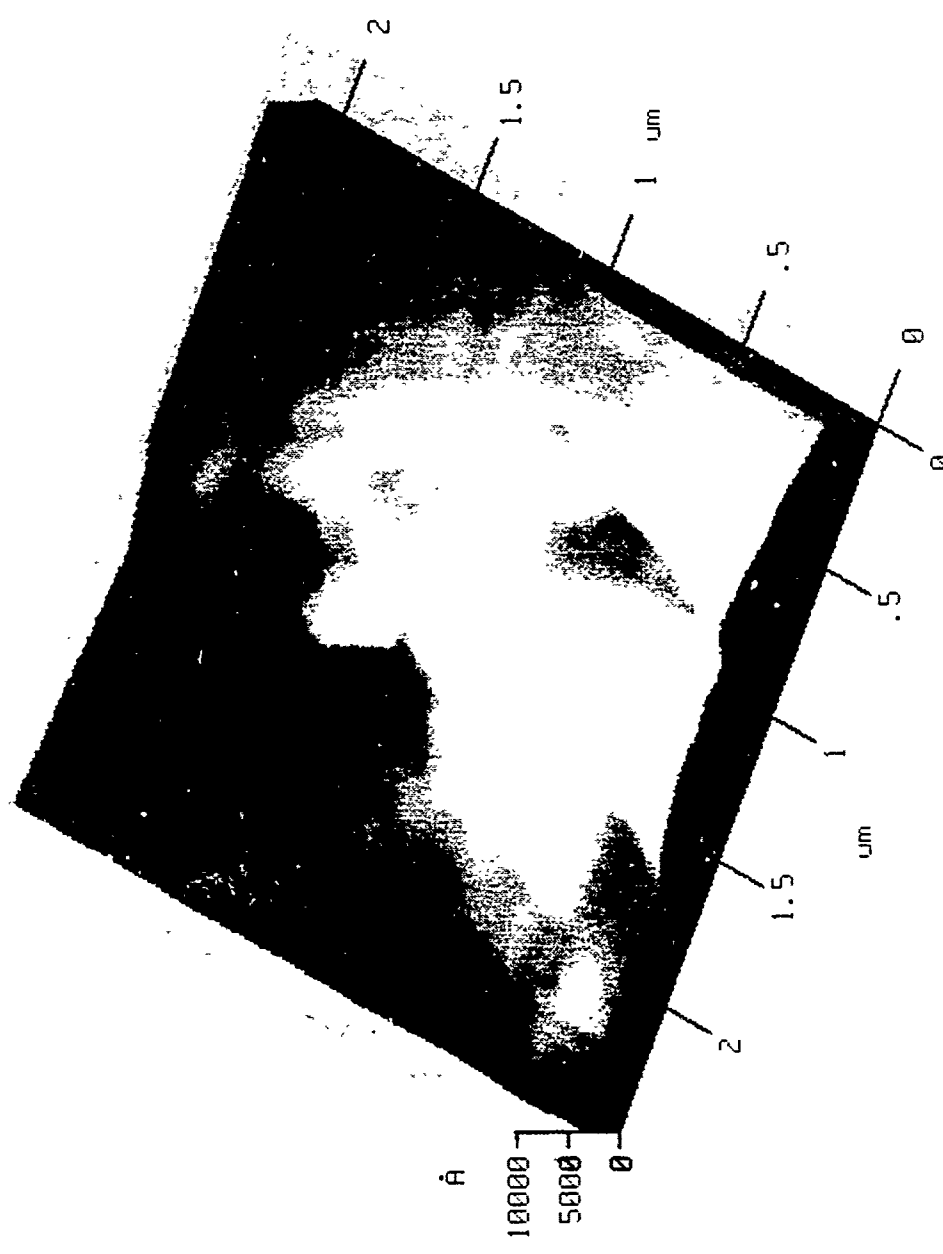
Figure A.2

STM images of the surface of doped polycrystalline diamond. The image in (a) shows the effects of tip imaging. The image in (b) was taken from the same sample as the one shown in Fig. (a), but does not show tip imaging effects.

Figure A.2 (Continued)

(b)

Some of the above observations can be used as criteria to detect tip imaging effects. These same criteria can be applied to detecting these effects for doped polycrystalline films. An example of this is shown in A.2 (a). In this example, tip imaging results from interactions between the tip and areas with very large radii of curvature which occur at the intersection of two facets of the crystalline domains. The topography that is imaged, as a result of tip imaging, has the appearance of craters on the surface. The change in the tip structure, which facilitated the tip imaging, occurred after a current - voltage curve was taken over a point on the surface. As in the case of doped diamond nuclei, the repeatability of the tip imaged topography is an indication that the effect is occurring.

A second indication is provided by previous scans of the surface before the tip imaging effect was observed. The sudden appearance of topography over various points on the surface where there had been none previously, is a clear indication. For doped diamond films, it is again possible to investigate the surface structure independently, and compare that structure with what is observed An STM image of the same surface, scanned with another tip, is presented in Figure A.2 (b), and shows the actual surface topography.

In ordinary analysis, the tip is considered to raster over the surface of the sample and then tip responds to variations of height on the surface. In order to understand the effects involved in tip imaging, it is useful to think of both the tip and the sample surfaces imaging each other. When the radius of curvature of the tip is much smaller than the radius of curvature of any feature on the surface, normal imaging will occur. Some surfaces, however, have regions where the radius of curvature is less than the radius of curvature of the tip, and this is when
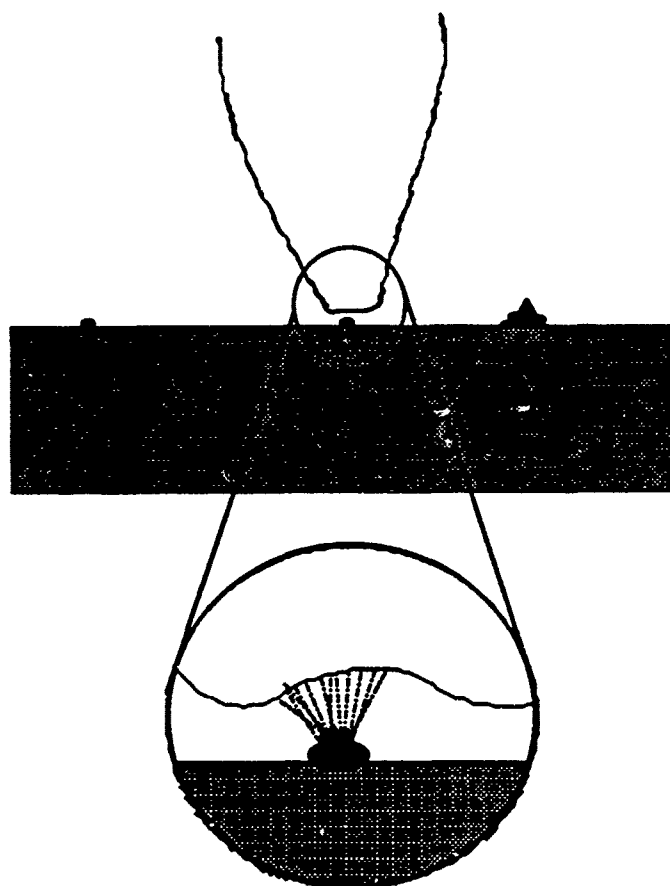
Figure. A.3
Schematic of the tunneling processes that lead to tip imaging. The effect occurs because the topography to be imaged is smaller than the tip that is imaging it. The effect could also occur when the right most particle is imaged, because it is very sharp.

tip imaging effects occurs. Figure A.3 illustrates this situation. It is important to note that if tip imaging occurs only once during a scan, it is nearly impossible to detect. It is only through the imaging of several identical tip images or independent knowledge of the shape of the tip, that tip imaging can be detected and/or prevented.

To summarize, the indications that tip imaging effects are occurring are: identical topography which is repeated over the surface, overlapping topography where none should be, the presence of "ghost" images which are similar in shape but lower in height than other images, particles that are round and flat, and topography that varies radically from that observed independently. Tip imaging is a potentially detrimental effect that can affect the validity of STM images. It can most often be readily identified as long indications that it is occurring are monitored against.

References

1 R. M. Tromp, E. J. van Loenen, J. E. Demuth, and N. D. Lang, Phys. Rev. B **37**, 9042 (1988).

2 F. F. Abraham, I. P. Batra, and S. Ciraci, Phys. Rev. Let. **60**, 1314 (1988).

3 Y. Kuk and P. J. Silverman, Appl. Phys. Lett. **48**, 1597 (1986).

4 S. I. Park, J. Nogami, and C. F. Quate, Phys. Rev. B 36, 2863 (1987).

5 E. J. van Loenen, D. Dijkkamp, A. J. Hoeven, J. M. Lenssinck, and J. Dieleman, Appl. Phys. Lett. **56**, 1755 (1990).